

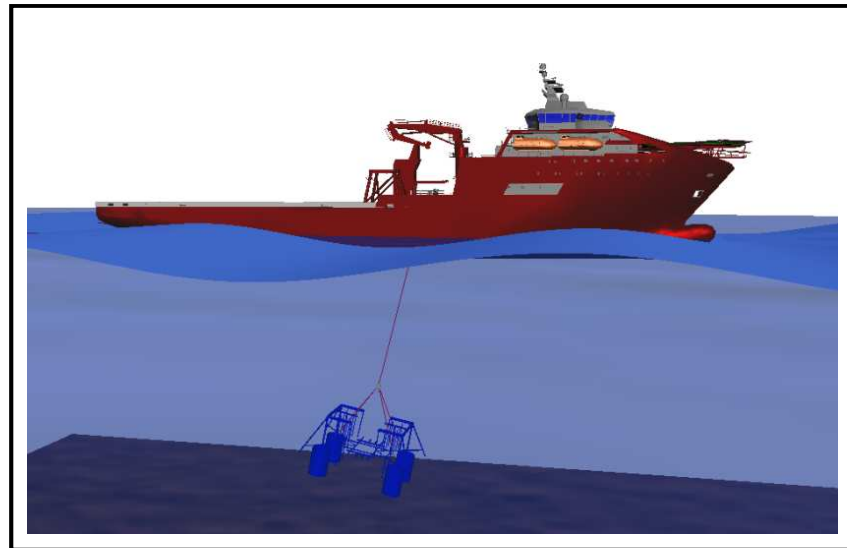
Master's thesis

Tore Jacobsen

Subsurface towing of a subsea module

Trondheim, June, 2010

NTNU
Norwegian University of
Science and Technology
Faculty of Engineering Science and Technology
Department of Marine Technology



Master Thesis, Spring 2010
for
Master Stud. Tore Jacobsen

Subsurface towing of subsea module

Undervanns tauing av undervannsmodul

The Gjøa ITS subsea template is to be towed by suspending it from Skandi Acergy's moonpool. This implies that the dynamic forces and response of the assembled system needs to be analyzed. It is also anticipated that the amount of damping in the system will play a crucial role with respect to the motion level that will occur for sea states close to the natural period.

The following subjects are to be examined in this thesis:

1. Literature review of the methods which are implemented in SIMO. In particular modelling of environmental loads, time domain simulations and various types of system elements are to be considered. A methodology for modelling and simulation of the towing operation needs to be established. Simplifications and results shall be discussed and compared to the 1-DOF of freedom mathematical model described in the project thesis by the candidate. If relevant, a parametric study should be made to determine operational limits.
2. An experimental investigation is to be performed in order to investigate the dynamic forces acting in the main lifting wire and behaviour of rigging horizontal offset of a model of the Gjøa ITS template. Horizontal offset obtained from these tests are to be compared with those obtained by the method which is outlined in the project thesis and/or SIMO.
3. A matrix of key system parameters that are to be varied, are established based on discussion with the supervisor. Parametric studies based on this matrix are subsequently performed to the extent that time allows by means of the simplified numerical method referred to in Item 1 and 2 above. It may also be relevant to perform point checks of the results by means of SIMO.

The work scope may prove to be larger than initially anticipated. Subject to approval from the supervisor, topics may be deleted from the list above or reduced in extent.

In the thesis the candidate shall present his personal contribution to the resolution of problems within the scope of the thesis work. Theories and conclusions should be based on mathematical derivations and/or logic reasoning identifying the various steps in the deduction.

The candidate should utilise the existing possibilities for obtaining relevant literature.

The thesis should be organised in a rational manner to give a clear exposition of results, assessments, and conclusions. The text should be brief and to the point, with a clear language. Telegraphic language should be avoided.

The thesis shall contain the following elements: A text defining the scope, preface, list of contents, summary, main body of thesis, conclusions with recommendations for further work, list of symbols and acronyms, references and (optional) appendices. All figures, tables and equations shall be numbered.

The supervisor may require that the candidate, in an early stage of the work, presents a written plan for the completion of the work. The plan should include a budget for the use of computer and laboratory resources which will be charged to the department. Overruns shall be reported to the supervisor.

The original contribution of the candidate and material taken from other sources shall be clearly defined. Work from other sources shall be properly referenced using an acknowledged referencing system.

The thesis shall be submitted in 3 copies:

- Signed by the candidate
- The text defining the scope included
- In bound volume(s)
- Drawings and/or computer prints which cannot be bound should be organised in a separate folder.

Supervisor: Professor Bernt J. Leira

Start: January 18th, 2010

Deadline: June 14th, 2010

Trondheim, 10 January 2010



Bernt J. Leira



NTNU
Norwegian University of Science and
Technology
Department of Marine Technology

Acknowledgment

This Master degree thesis is written by Tore Jacobsen during the spring of 2010, and is part my MSc. degree in marine structures and hydrodynamics at NTNU. The thesis is written in collaboration with Norwegian University of Science and Technology (NTNU) and Acergy Norway AS.

I would like to thank Haavard Haaskjold (Senior Project Engineer), Anton Stornes (Structural and Naval Discipline Manager), Tor-Bjørn Næss (Senior Project Engineer) and Andreas David Eilertsen (Project engineer) at Acergy Norway for providing me with hydrodynamic data, tips and experimental reports. I would also like to thank Acergy for providing me with an interesting project and master thesis topic, and also the experiment funding in the Marine Cybernetics lab at NTNU is duly acknowledged.

Next I would like to thank my supervisor Professor Bernt J. Leira for guidance and tips, and my colleagues at Tyholt who have been a constant source of motivation and help. Also Professor Sverre Steen and Torgeir Wahl have been a constant source of help.

Tore Jacobsen
Trondheim 09.06.2010



Table of contents

1	Introduction	- 10 -
2	Subsurface towing	- 12 -
2.1	The Pencil Buoy Method.....	- 13 -
2.2	Subsea 7's "Moonpool" method	- 16 -
2.3	Acergy's concept.....	- 18 -
3	Equipment	- 21 -
3.1	Vessel info	- 21 -
3.2	Template description	- 22 -
3.3	Towing lines.....	- 23 -
3.4	Tow rigging.....	- 26 -
4	Environmental loads during towing.....	- 28 -
4.1	Hydrostatic loads.....	- 28 -
4.2	Drag forces.....	- 28 -
4.3	Lift forces.....	- 33 -
4.4	Vortex induced vibrations.....	- 35 -
4.5	Effects from surface waves.....	- 38 -
4.6	Internal waves	- 40 -
5	Dynamic properties of template	- 42 -
5.1	Damping	- 42 -
5.1.1	Linear viscous damping.....	- 42 -
5.1.2	Quadratic damping	- 45 -
5.2	Added mass.....	- 46 -
6	Hand calculations of template dynamics	- 47 -
6.1	Horizontal offset.....	- 47 -
6.2	Basic 1-DOF model.....	- 50 -
6.3	1-DOF model with damping	- 53 -
6.4	Differential equation in heave.....	- 57 -
6.5	Response Skandi Acergy	- 58 -
6.5.1	Surface elevation.....	- 60 -
6.5.2	Vessel response in heave	- 61 -
6.6	Newmark's method	- 65 -
6.7	MatLab model.....	- 67 -
7	General description of SIMO	- 68 -
7.1	Program BuildUp	- 68 -
7.2	Fundamental hydrodynamic theory.....	- 69 -
7.2.1	Potential theory	- 69 -
7.2.2	Strip theory	- 70 -
7.3	SIMO theory	- 71 -
7.3.1	SIMO's objective	- 71 -
7.3.2	Environmental forces	- 72 -
7.4	Modeling capabilities	- 74 -
7.4.1	Slender elements	- 75 -
7.4.2	Coupling forces.....	- 76 -
8	SIMO modeling procedure.....	- 77 -
8.1	Environmental conditions.....	- 78 -
8.2	Skandi Acergy in SIMO	- 79 -



8.3	Gjøa ITS in SIMO	- 84 -
8.4	Rigging in SIMO.....	- 87 -
8.5	Running SIMO.....	- 88 -
8.6	Post processing in SIMO	- 90 -
8.6.1	Exclusion of regular waves.....	- 91 -
8.6.2	Inclusion of Regular Waves.....	- 92 -
9	Experiment	- 99 -
9.1	Model relationships	- 100 -
9.2	Equipment.....	- 101 -
9.2.1	Gjøa ITS model.....	- 102 -
9.2.2	Test basin.....	- 103 -
9.2.3	Oscillator.....	- 104 -
9.2.4	Towlines and slings.....	- 105 -
9.2.5	The force ring.....	- 106 -
9.3	Experimental results.....	- 106 -
9.4	Error analysis	- 109 -
9.4.1	Bias errors.....	- 109 -
9.4.2	Precision errors	- 109 -
10	Model tests vs. numerical calculations	- 110 -
10.1	Exclusion of regular waves	- 111 -
10.2	Inclusion of regular waves	- 113 -
11	Parametric study	- 118 -
12	Conclusion.....	- 122 -
13	Recommendations for further work.....	- 123 -
14	Bibliography.....	- 125 -
15	Appendix	- 128 -



List of figures

Figure 1 Accident statistics of marine operations (Lotsberg,2004)	10
Figure 2 Subsurface Towing methods (DNV H-103)	12
Figure 3 Pencil Buoy Method setup (AMC).....	13
Figure 4 Launching of pencil buoy (AMC)	14
Figure 5 Pencil Buoy Towing (AMC).....	14
Figure 6 Lowering operation with Pencil Buoy (AMC).....	15
Figure 7 Rigging configuration for Subsea 7 (Ulstein,Johnsrud)	16
Figure 8 Collection of structure from wet store location (Subsea 7)	17
Figure 9 Template pick up from location (Acergy, Haaskjold).....	18
Figure 10 Wet tow of template (Acergy, Haaskjold)	19
Figure 11 Acergy Transfer to 400 Te crane (Haaskjold).....	19
Figure 12 Skandi Acergy profile view	21
Figure 13 Gjøa ITS with hatches.....	22
Figure 14 Gjøa ITS.....	23
Figure 15 Fibre rope configurations	24
Figure 16 Dyneema rope mass-spring system	25
Figure 17 Steel wire mass-spring system	25
Figure 18 Concept sketch of moonpool configuration (Acergy Norway).....	26
Figure 19 Cross section of moonpool concept (Acergy Norway).....	26
Figure 20 Towing setup (Acergy Norway).....	27
Figure 21 Flow around a cylinder (Anderson,2007)	29
Figure 22 Viscous flow around stationary cylinder	30
Figure 23 Wake amplification factor (DNV RP H-103)	33
Figure 24 Drag and lift forces on cylinder (Journèe & Massie, 2006).....	34
Figure 25 Strouhal and Reynold's number relation (Lienhard).....	34
Figure 26 Vortex street behind 4 cylinders (Journèe & Massie, 2006).....	35
Figure 27 VIV experimental results for cylinder (Faltinsen)	36
Figure 28 Trajectories of water particles in shallow water (Groen and Dorrestein, 1958) .-	39
Figure 29 Trajectories of water particles in deep water (Groen and Dorrestein, 1958).....	39
Figure 30 Internal waves (Melville 2009)	41
Figure 31 Mass-damper system(Langen & Sigbjörnsson, 1979).....	42
Figure 32 Damping regimes (Langen & Sigbjörnsson, 1979).....	43
Figure 33 Damping in Heave Gjøa ITS (Acergy Norway).....	45
Figure 34 Added mass in heave for Gjøa ITS (Acergy Norway)	46
Figure 35 Force equilibrium in wire (FGN 2006).....	47
Figure 36 Local force equilibrium in wire (FGN 2006).....	48
Figure 37 Horizontal offset and total force in lifting wire.....	49
Figure 38 1-DOF system	50
Figure 39 1-DOF model results for damped mass-spring system.....	52
Figure 40 Real part of motion response along lifting wire	55
Figure 41 Absolute part of motion response along the lifting wire	55
Figure 42 Force Amplitude along the lifting wire.....	56
Figure 43 1-DOF system with prescribed displacement	57
Figure 44 JONSWAP spectrum	58
Figure 45 Sea state characteristics from MATLAB.....	59
Figure 46 Irregular waves in GLview	60



Figure 47 Fourier transformation of wave packet.....	- 60 -
Figure 48 Ship degrees of freedom (Faltinsen).....	- 61 -
Figure 49 Transfer function Skandi Acergy in heave	- 62 -
Figure 50 Time history of wave	- 64 -
Figure 51 Time history for heave motion Skandi Acergy	- 64 -
Figure 52 Steel mass spring system	- 66 -
Figure 53 MATLAB command window	- 67 -
Figure 54 MATLAB flowchart	- 67 -
Figure 55 Layout of the SIMO program system (SIMO manual).....	- 68 -
Figure 56 Slender element	- 75 -
Figure 57 Subsurface towing SIMVIS	- 77 -
Figure 58 Wave Conditions System Description file.....	- 78 -
Figure 59 Current Conditions System Description file	- 79 -
Figure 60 Body Location Data System Description File.....	- 79 -
Figure 61 Body Mass Data System Description File	- 80 -
Figure 62 Time Dependent Mass System Description File	- 81 -
Figure 63 Hydrostatic Stiffness Data System Description File	- 82 -
Figure 64 Transfer Functions System Description File.....	- 83 -
Figure 65 Transfer function Example System Description File	- 83 -
Figure 66 Slender element of suction anchor system description file.....	- 84 -
Figure 67 Drag coefficient for circular cylinders as function of Reynolds number (Øritsland,1989)	- 85 -
Figure 68 Template visualization in SIMVIS	- 86 -
Figure 69 Simple wire coupling system description file	- 87 -
Figure 70 Visualization files.....	- 89 -
Figure 71 Template Aerial View (Acergy).....	- 90 -
Figure 72 Horizontal offset angle for $U=5$ [knots]	- 91 -
Figure 73 Hook total force lifting wire for $U=5$ [knots].....	- 91 -
Figure 74 Maximum force in lifting wire	- 93 -
Figure 75 Force amplitude in lifting wire.....	- 94 -
Figure 76 Moonpool translation vertical direction.....	- 95 -
Figure 77 Forces in lifting wire.....	- 95 -
Figure 78 Horizontal offset angle.....	- 96 -
Figure 79 SIMO Tension in lifting wire, Regular waves analysis, $T=9$ [s], $H=5$ [m]	- 97 -
Figure 80 SIMO Tension in lifting wire, Regular waves analysis, $T=12$ [s], $H=5$ [m]	- 97 -
Figure 81 Experimental setup	- 101 -
Figure 82 Gjøa ITS model	- 102 -
Figure 83 Marine Cybernetics laboratory	- 103 -
Figure 84 Model rigging.....	- 105 -
Figure 85 Experiment picture	- 106 -
Figure 86 Sample force spectrogram.....	- 107 -
Figure 87 Horizontal offset-angle	- 107 -
Figure 88 Horizontal offset angle $H=3$ [m] , $T=12$ [s], $U=3$ [knots]	- 108 -
Figure 89 Template Aerial View (Acergy).....	- 111 -
Figure 90 Tension lifting wire Experiment vs. SIMO with no waves	- 112 -
Figure 91 Horizontal offset Experiment vs. SIMO with no waves.....	- 112 -
Figure 92 Experiment vs. SIMO vs. hand calculations for sample analysis	- 113 -
Figure 93 Normalized added mass for oscillating circular cylinder((Faltinsen,1990).....	- 114 -



Figure 94 Sample horizontal offset angle SIMO vs. Experiment vs. Hand calculations .. - 115 -
 Figure 95 Comparison tension in lifting wire, Regular Waves, T=9[s], H=5[m]..... - 116 -
 Figure 96 Comparison tension in lifting wire, Regular waves, T=12[s], H=5[m]..... - 116 -
 Figure 97 Comparison horizontal offset angle, Regular waves, H=5[m]..... - 117 -
 Figure 98 Tension in lifting wire, Irregular waves, Hs=5[m], Tp=9[s], U=5[knots]..... - 118 -
 Figure 99 Horizontal offset angle, Irregular waves, Hs=5[m], Tp=9[s], U=5[knots]..... - 119 -
 Figure 100 Tension in lifting wire, Irregular waves, Hs=5[m], Tp=9[s], U=3[knots]..... - 120 -
 Figure 101 Horizontal offset angle, Irregular waves, Hs=5[m], Tp=9[s], U=3[knots]..... - 121 -
 Figure 102 Towing with clumpweights - 123 -
 Figure 103 Towing with clump weights and buoyancy buoys - 124 -
 Figure 104 Force in lifting wire (Experiment) fullscale H=3[m] - 128 -
 Figure 105 Spectrogram force signal (Experiment) H=3[m]..... - 129 -
 Figure 106 Horizontal offset angle (Experiment) H=3[m]..... - 130 -
 Figure 107 Force in lifting wire (Experiment) fullscale H=5[m] - 131 -
 Figure 108 Spectrogram force signal (Experiment) H=5[m]..... - 132 -
 Figure 109 Horizontal offset angle (Experiment) H=5[m]..... - 133 -
 Figure 110 Scatter diagram North Sea - 134 -
 Figure 111 Conceptual hangoff structure - 135 -

List of tables

Table 1 Design criteria for wet tow operation - 20 -
 Table 2 Main dimensions Skandi Acergy - 21 -
 Table 3 Dimensions Gjøa ITS..... - 22 -
 Table 4 Rope types - 24 -
 Table 5 Horizontal offset - 49 -
 Table 6 Newmark’s β family - 65 -
 Table 7 SIMO body types..... - 74 -
 Table 8 Environment data specification - 78 -
 Table 9 Current specification..... - 79 -
 Table 10 Body location data - 79 -
 Table 11 Body mass data - 80 -
 Table 12 Time dependent mass..... - 81 -
 Table 13 Stiffness and damping reference..... - 82 -
 Table 14 Wave force transfer function - 83 -
 Table 15 Transfer function input..... - 83 -
 Table 16 Slender element description - 84 -
 Table 17 Simple wire coupling system description file - 87 -
 Table 18 Period of encounter..... - 92 -
 Table 19 Test cases..... - 99 -
 Table 20 Froude scaling table - 101 -
 Table 21 Main dimensions ITS model - 102 -
 Table 22 Vertical translation (Z-direction) of moonpool full scale - 104 -
 Table 23 Vertical translation (Z-direction) for oscillator model scale $\lambda = 25$ - 104 -
 Table 24 Model rigging setup..... - 105 -
 Table 25 Model test vs. numerical models (Aage, 1992)..... - 110 -
 Table 26 Results from SIMO with exclusion of waves..... - 111 -



Nomenclature

Latin

M Mass matrix

A frequency dependent added mass matrix

B frequency dependent potential damping matrix

K elastic stiffness matrix

d position vector

$\dot{\mathbf{d}}$ velocity vector

$\ddot{\mathbf{d}}$ acceleration vector

D diameter

C_D Drag coefficient

E modulus of elasticity

q exciting force vector

A_{ij} Added mass of structure in j-direction due to motion in i-direction

B_{ij} Added mass of structure in j-direction due to motion in i-direction

U Towing velocity/current velocity

$d\omega$ Small angular frequency increment

F_x Force in x-direction

F_k^A Added-mass force in k-direction

L length of rope

H_s significant wave height

T_p Peak period

$S(\omega)$ Wave spectrum as a function of angular frequency

E Young's modulus

λ Scale factor

C_L Lift coefficient

Greek

γ integration constant Newmarks Beta method

β integration constant Newmarks Beta method

ρ density of seawater

ω angular frequency

ξ wave amplitude

α Angle between lifting wire and z-axis

λ Scale factor

η_1 Degree of freedom, vessel surge

η_2 Degree of freedom, vessel sway

η_3 Degree of freedom, vessel heave

η_4 Degree of freedom, vessel roll

η_5 Degree of freedom, vessel pitch

η_6 Degree of freedom, vessel yaw



Abbreviations

FEA	Finite Element Analysis
FEM	Finite Element Method
ITS	Integrated template structure
MATLAB	“Matrix Laboratory” computer software
VIV	Vortex induced vibrations
JONSWAP	Joint North Sea Wave Project
DAF	Dynamic Amplification Factor
VERES	Vessel Response computer software
LCG	Longitudinal centre of gravity
FFT	Fast Fourier transformation
DNV	Det Norske Veritas
3D	Three dimensional
COG	Centre of gravity
IMR	Inspection Maintenance Repair
ROV	Remotely operated vehicle
WAMIT	WaveAnalysisMIT
AMC	Aker Marine Contractors
SIMO	Simulation of complex marine operations
DAF	Dynamic amplification factor
MBL	Minimum break load
MARINTEK	Norwegian marine technology Research institute
SWL	Safe working load
Te	Metric tonne
RAO	Response amplitude operator /Transfer function



Summary

This thesis serves as a preparatory study for a new concept in subsurface towing proposed by Acergy Norway. 3 different mathematical methods for determining the most important dynamics occurring during a subsurface towing operation is therefore discussed and compared. The 3 models examined is a simple mass-spring system with forced excitations implemented in Matlab (chapter 6), a multibody time domain simulation in SIMO (chapter 7) and a model test for verification of results (chapter 9). The accuracy of the relatively simple hand calculations is discussed and compared to experimental values in chapter 10.

The first part of this thesis includes a description of different concepts for transportation of subsea templates to installation site. Transportation by subsurface towing instead of using a barge can reduce operational costs if the dimensions of the structure require a heavy-lift vessel. Also risk related to pendulum motions in air is reduced, and subsurface towing is therefore of great interest to marine contractors.

The most significant parameters to check by hand calculations in a subsurface towing operation is natural frequencies and modes of the dynamic system, and also estimates of the maximum/minimum loads lifting wires and slings. Since simple hand calculation models are of interest in early concept studies, formulas for these values are derived in chapter 6. These formulas are also found in (DNV Recommended practice H103, 2009).

SIMO is a time domain simulation program for multibody systems, which allows export of station keeping forces and connecting force mechanism (lifting wire and slings). Based on a system description file provided by Acergy Norway, a suitable model of the Gjøa ITS subsea template is made, and positioned 50 [m] below the moonpool hangoff point. Multiple analyses with different sea conditions and towing velocities have been done in SIMO to determine the feasibility and best practice of a subsurface towing operation.

In addition, a towing tank experiment was performed in Marine Cybernetics towing tank at Tyholt in Trondheim. A detailed model of the Gjøa ITS was made in 2008, and numerous previous experiments have been conducted (e.g Solaas(2008) and Eilertsen(2008)) which provided valuable information and reduced the required amount of work in planning a model experiment. In the experiment the template was towed with a vertical oscillator to simulate the vessel translation in head sea and forces were measured in the lifting wire. These model experiments were made for various environmental conditions, and compared to the numerical models previously described.

A correct representation of the towing arrangement in SIMO provides a relatively inexpensive model for further dynamic analysis of the system. A heave compensation device can easily be implemented in SIMO when the model of the vessel and template is correctly represented and can therefore be of valuable importance when designing a new conceptual hangoff-structure.



1 Introduction

The marine industry is growing, and the tendency of going deeper and exploring more remote areas does not seem to end. Further development in the oil- and gas industry requires more complex subsea technology and new cost efficient methods for transportation of subsea modules. This also requires detailed planning of marine operations with emphasis on equipment design, and operation criteria. During temporary phases (fabrication, transport and installation), the structures and installation equipment will be subject to harsh environmental loads from waves and current, and need to be designed accordingly. Especially the transportation phase of a subsea structure is vulnerable for accidents resulting in severe damage which can be seen in the investigation performed by (Lotsberg, 2004).

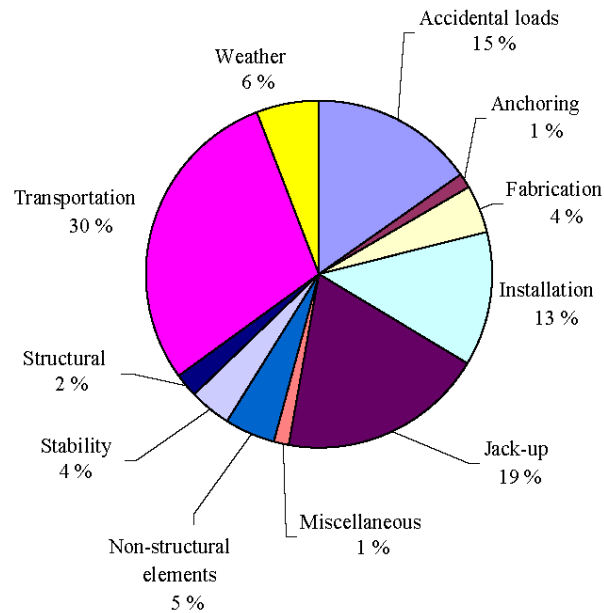


Figure 1 Accident statistics of marine operations (Lotsberg,2004)

Traditionally subsea templates are transported to site on either the deck of a crane vessel or a barge, depending on their size and shape. In both cases the template has to be lifted off from deck and lowered through the splash zone. The lift-off is a critical phase of the operation where there is imminent danger of large dynamic loads and collision between the template and vessel deck due to relative motions. During immersing, significant wave impact forces (slamming) may also be restrictive operational criteria. These hazards set the operational limits for traditional transportation operations.

Another possible way of transporting a subsea template is to perform a subsurface tow through the moonpool of an offshore service vessel. It is argued that such an operation will have a larger operational window than traditional methods and be more cost efficient. Also a subsurface towing operation of a heavy structure enables the use of the main heave compensated crane on the vessel during seabed landing, which ensures a safe installation phase.



During a subsurface tow operation, the dynamic behavior of the template and tow arrangement will depend upon the hydrodynamic loads acting on the system. The magnitude of these forces will affect the deflection angle of the towing wire in the moonpool and influence the possible outcome of slack wire. Accordingly, the forces will also set the operational limits regarding both sea state and towing velocity. The validity of the computational analysis results must be studied before such an operation can be executed, and is consequently of vital importance.

This work focuses on the dynamics in the ship-template system with varying towing velocities, and wave conditions. Since the dynamic system is similar to a simple mass spring system, the aim of the work is to investigate the accurateness of utilizing a simple 1-Degree-of-freedom (1-DOF) approach compared with a multibody time integration approach by software developed by MARINTEK (SIMO). This is done because in feasibility studies there are often lack of personnel, financial resources or time to perform advanced dynamic analyses. Hence, for practical purposes and preliminary design, there is still a need for simplified methods for determining the magnitude of dynamic loads.

The parameters of interest are the horizontal offset angle α , maximum/minimum and average dynamic loads in the lifting wire. These results are verified and compared with an experimental investigation.



2 Subsurface towing

To utilize fleet capacity and broaden acceptance criteria, marine contractors constantly try to develop new methods and technology for marine operations. Since transportation of modern subsea structures often requires a large deck space and hence expensive installation procedures, there is always a market for cost efficient marine concepts. Various methods of subsurface towing of subsea structures exist today where the most commonly used methods are:

- Subsurface tow of objects attached to towed buoy (Pencil Buoy)
- Subsurface tow of objects attached to vessel

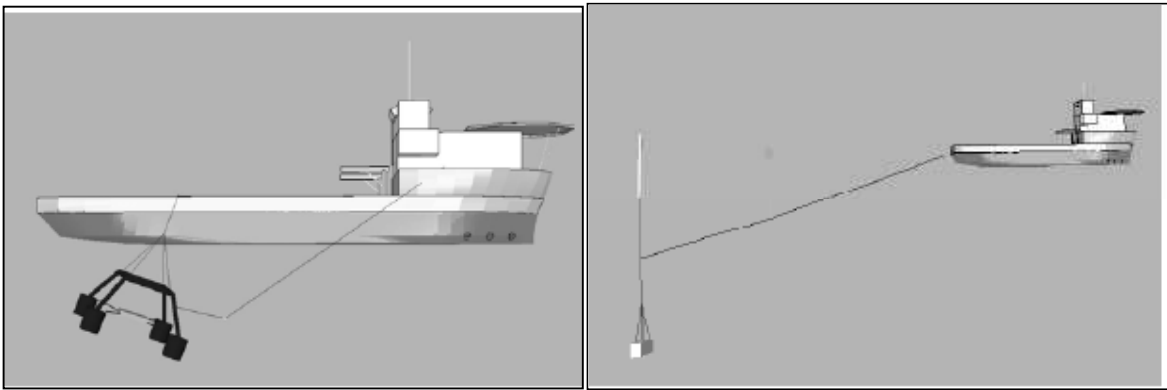


Figure 2 Subsurface Towing methods (DNV H-103)

It should be observed that wet towing of a structure is a complicated operation with several challenges. The challenges are both technical and operational, and examples of such challenges are:

- Towing velocity
- Weather restrictions (limiting wave height, currents, wind velocity)
- Routing of tow operation (depth on wet storage area, current conditions, limited space for maneuvering)
- Fatigue loading on rigging, structure and vessel
- Vortex induced vibrations (VIV)
- Directional stability of towed object
- Dynamic amplification factors (DAF)

A successful subsurface towing concept should therefore be thoroughly analyzed with respect to these challenges.



2.1 The Pencil Buoy Method

The Pencil Buoy Method is an Aker Marine Contractors (AMC) patented subsurface transportation and installation method of subsea structures (Johnsgard & Gramnaes, 2007). By use of this method the cargo is lifted through the splash zone inshore and wet towed to destination, suspended from a spare-buoy (Figure 3). The procedure of submersing the structure and fastening it to the Pencil buoy is done inshore to avoid complications due to possible harsh sea states. Normally a tow velocity of 3-5 knots is used.

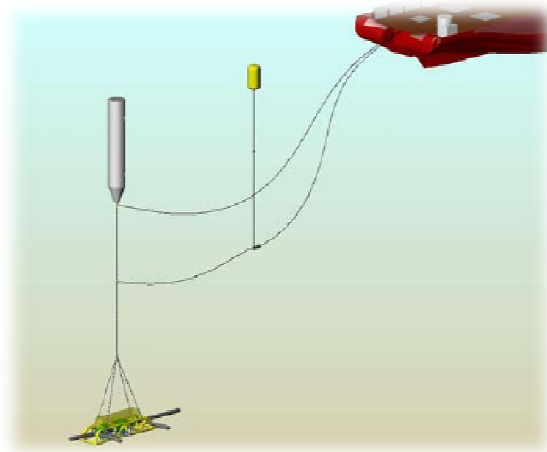


Figure 3 Pencil Buoy Method setup (AMC)

The method involves three principal steps: The first step is to transfer the weight of the subsea structure from a crane barge to a pencil buoy in calm inshore waters close to field. The pencil buoy is a cylindrical structure with an outer diameter of 5 [m] and the hull is constructed from steel plates with internal stiffeners. In the first step of the operation a crane barge lifts the structure from the transportation barge and positions itself aft of the installation vessel. The structure is then lowered through the splash zone and the load is transferred from the crane barge to the installation vessel. The different phases of operation are shown in Figure 4.

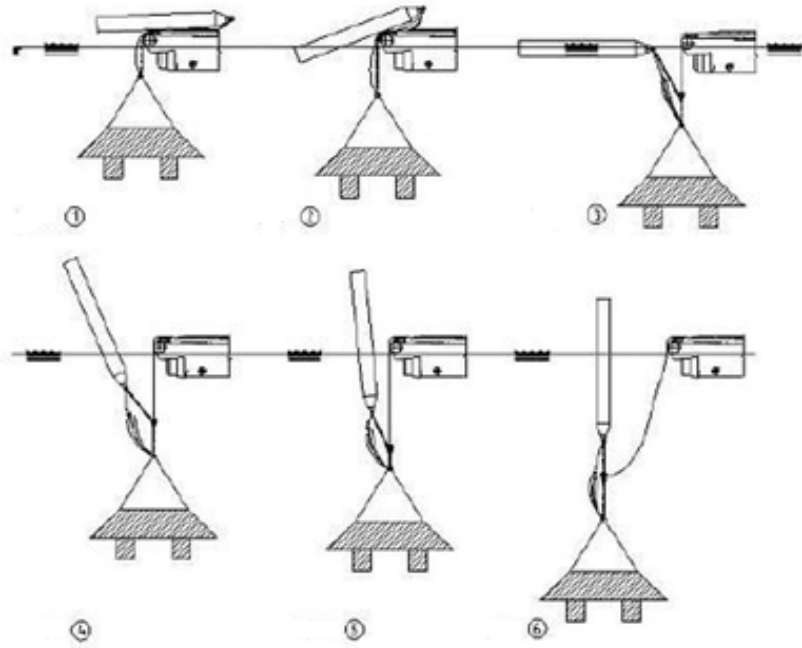


Figure 4 Launching of pencil buoy (AMC)

Step number 2 is the towing phase using the pencil buoy to carry the submerged weight of the structure and rigging to the field. Usually a 400 meter towing line is used with a helping buoy to keep the weight of the towing line from affecting the Pencil buoy, as well as directing the towing line at a normal angle of attack to the pencil buoy. This is shown in Figure 5 below.

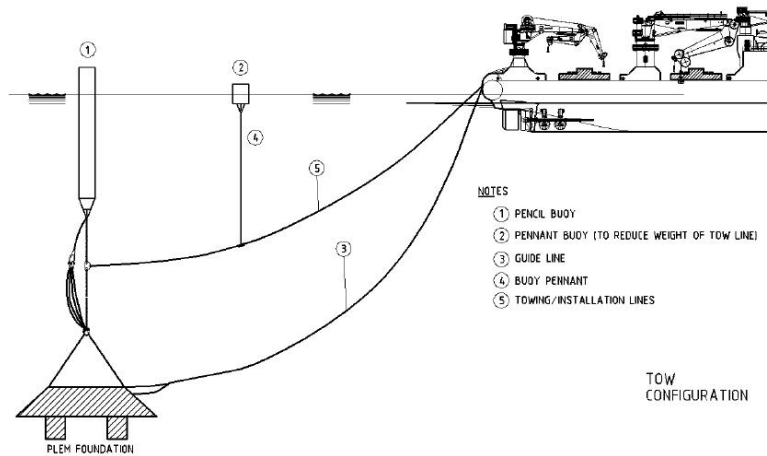


Figure 5 Pencil Buoy Towing (AMC)



At the installation site (step 3), the towing wire is winched in, and the structure weight is transferred from the Pencil Buoy back to the towing winch wire, and the buoy is disconnected. To ensure no contact between installation vessel and the Pencil Buoy, the vessel moves slowly forward during this load transfer. A passive heave compensator is then used during lowering of the structure to seabed.

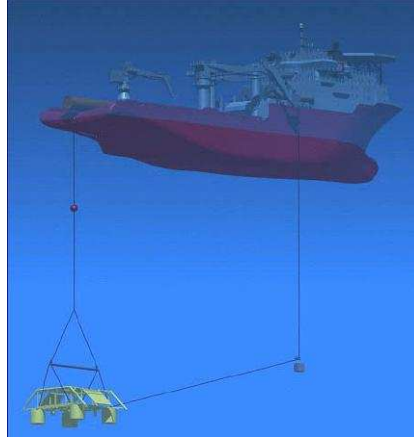


Figure 6 Lowering operation with Pencil Buoy (AMC)

Compared to traditional installation of subsea structures, e.g. wide templates, the Pencil Buoy method has several advantages. The normal situation for offshore lifts have risk elements related to pendulum motions in air and slamming loads during lowering through the splash zone. With the Pencil Buoy Method, these phases are eliminated since the lift is performed in inshore sheltered areas. Thereby less crane capacity is required and there is no need for an external offshore crane vessel. Requirements for the installation vessel are sufficient winch capacity and deck space for the Pencil Buoy and thereby a wide range of vessels are suitable for utilization of the Pencil Buoy Method. This is favorable as regards availability in the market.

Challenges using the pencil buoy method are to retrieve the buoy safely on to the vessel deck without damaging the vessel or the buoy itself, and also the limited tow velocity from 1-3 knots. For installation sites far-offshore the daily costs saved by using a Pencil buoy may be surpassed by the combined cost of a time consuming tow. Another disadvantage with the use of the Pencil buoy method is that it exposes the buoy itself, the slings, the wires and the suspended structure to dynamic loads over a relatively long period of time. Dynamic loads over time can cause fatigue in the different components of the towing system, and hence it is important to investigate dynamic loads. Also the lowering operation of the subsea structure to the seabed opposes limits regarding the heave compensation system design.

However, this method has already been used on seven projects, including a total of 17 wet tows. For the first projects a Pencil Buoy of 150 [Te] submerged capacity was used, and for the later projects a newer Pencil Buoy of 250 [Te] has been used. According to AMC, the capacity will be enhanced, and for future wet tows a buoy with the capacity of 350 [Te] will be available.



2.2 Subsea 7's "Moonpool" method

The most successful towing concept for subsurface towing through moonpool is according to (Aarset & Sinclair, 2007) Subsea 7's towing concept which was used on four templates on the Tyrihans field in 2007. Subsea7's method features a transit phase to an inshore location where a crane barge lifts the template from a transportation barge and lands it to the seabed. When the installation process commences, the installation vessel positions itself above the template and connects the rigging from the installation structure on the vessel to the template using ROV's. Using an installation structure gives major advantages with respect to safety and working conditions for the vessel crew.

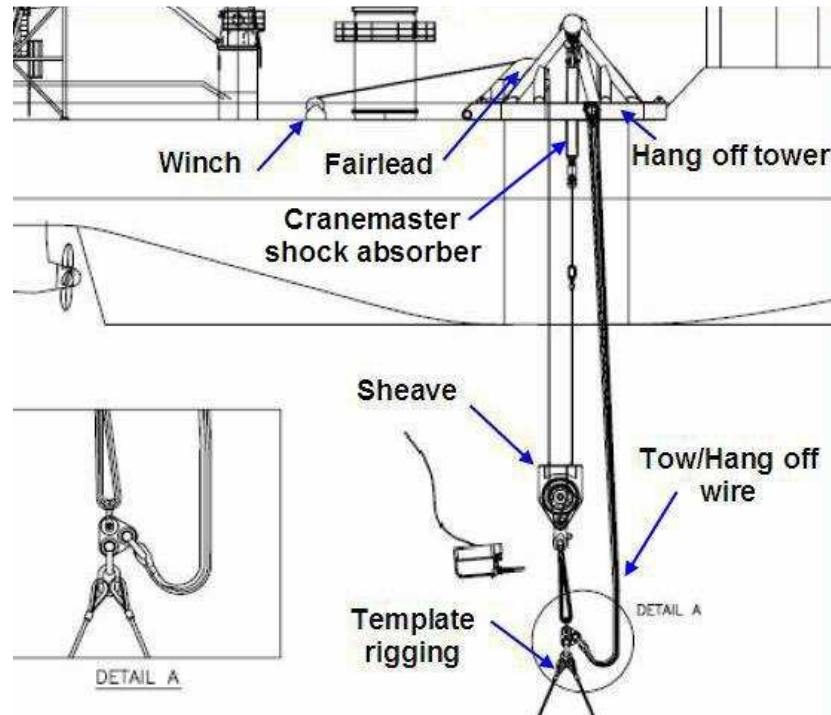


Figure 7 Rigging configuration for Subsea 7 (Ulstein,Johnsrud)

The towed installation system features a tower placed above the installation vessel's moonpool, providing hang-off points at the vessel's centerline. In addition, a 300 [Te] winch system is installed on the vessel's aft deck. The lifting wire runs from the winch, over a fairlead on the hang-off frame and down through the moonpool. The end of the lifting wire then runs up from the subsea sheave block and is connected to a cranemaster¹ overload-protection shock absorber.

Routing the rigging through the moonpool gives significant lower forced excitations on the towing system compared to routing the rigging over the vessel stern. Also the simplicity of the method is a big benefit with respect to operational and technical risk elements. However, there are some drawbacks related to the lack of heave compensation. This is due to the static configuration of the system, where there is a risk for slack and large dynamic

¹ Passive heave compensator manufactured by Ernst-B. Johansen A.S.



loads in slings as the vessel moves in waves. Thus, the operational design criteria is limited compared to other methods.

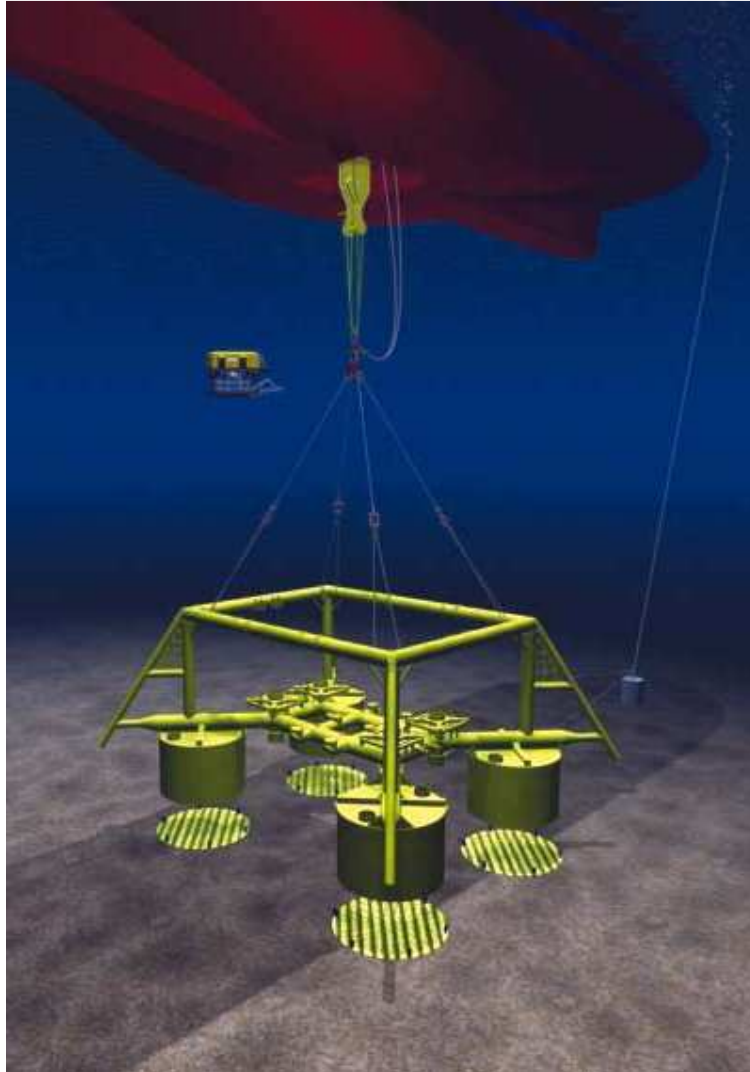


Figure 8 Collection of structure from wet store location (Subsea 7)



2.3 Acergy's concept

The main sequences in Acergy's method for subsurface towing of subsea templates are the same as in Subsea 7's method: The subsea template is wet stored inshore in sheltered waters and the installation vessel positions itself over the structure and picks it up. However, the structure load is transferred to a new conceptual hangoff structure (and not directly to the winch) positioned above the moonpool of the vessel before towing out to field.

PICK UP TEMPLATE WITH SKANDI ACERGY

NB: CRANE, FLS TOWER AND LOAD OUT SPREAD NOT SHOWN FOR CLARITY

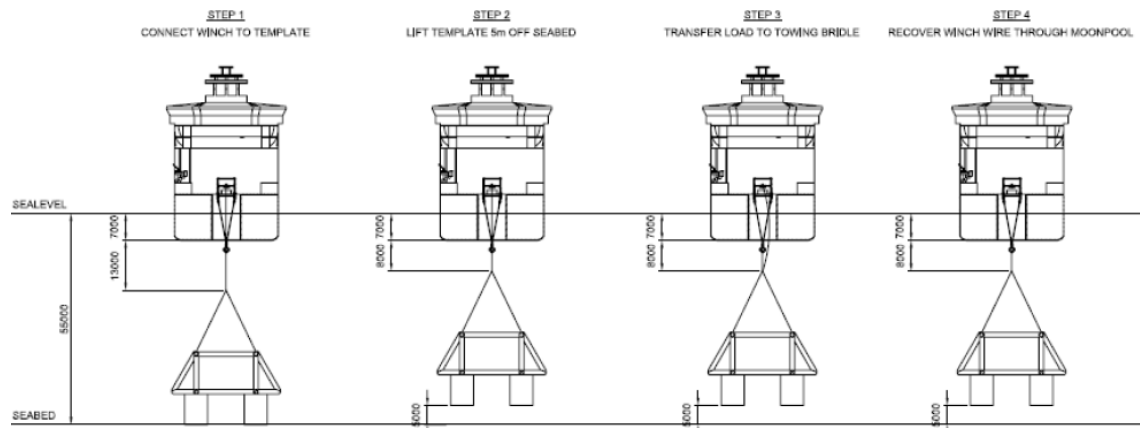


Figure 9 Template pick up from location (Acergy, Haaskjold)

Except from the new conceptual hangoff structure, the main advantage of Acergy's method compared to Subsea7's method (chapter 2.2), is that a winch is not used for landing the structure on the seabed, but the main heave compensated crane on the vessel. Once the load is fully transferred from the hangoff structure, the template is correctly oriented using a clump-weight and landed fully heave-compensated by the crane.



WET TOW OF TEMPLATE WITH SKANDI ACERGY

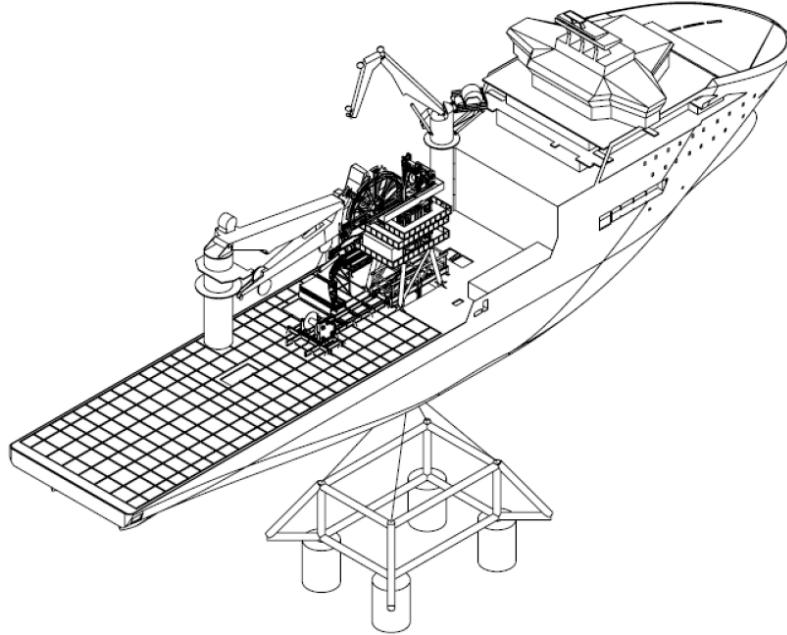


Figure 10 Wet tow of template (Acergy, Haaskjold)

As previously mentioned, to improve the weather window required for the operation, a damping or heave compensation solution is necessary. Using fiber rope and/or a heave compensated hangoff structure on the vessel deck can provide good damping alternatives for subsurface towing of large and heavy subsea modules. However, for simplicity no damping is assumed in the hangoff structure in this thesis.

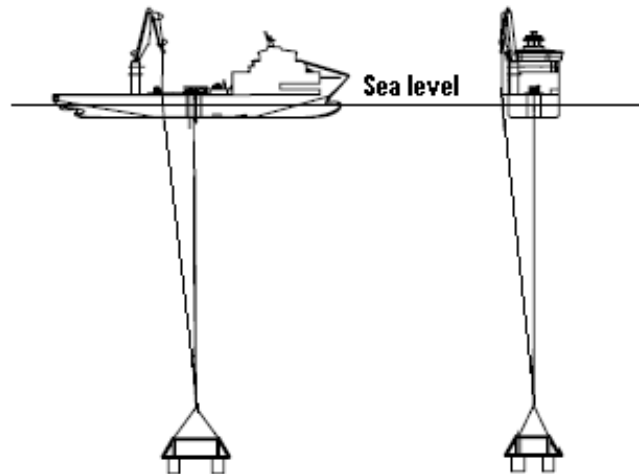


Figure 11 Acergy Transfer to 400 Te crane (Haaskjold)

During a concept evaluation phase, it is important to create design criteria which define operational limits. Usually the actual operational criteria are lower than the design values for weather restricted operations. Therefore the design criteria should be based on extreme value statistics, and this is the criteria used in this thesis.



In order to create a competitive concept, Acergy Norway require the following design criteria:

Design criteria for wet tow operation	
Towing velocity U [knots]	0-5
H _s [m]	0-5
T _p [s]	0-22
Maximum allowable horizontal offset angle α [deg]	10
Maximum structure weight [kN] in air	4000

Table 1 Design criteria for wet tow operation

The tow velocity is determined to be in the range from 0 to 5[knots] depending on weather operational criteria. These limits are declared since weather criteria and towing velocity influence the dynamic loads in the hoisting cables and on the hangoff structure on the vessel. A parameter study on alternating these parameters is therefore one of the most important aspects of this thesis, and this is done in chapter 11.

The dimensions of the moonpool are (7.2x7.2x12 m) and by assuming a hangoff point in the centre of the moonpool, the following value for the horizontal offset angle α can be obtained:

$$\alpha = \tan^{-1}\left(\frac{7.2/2}{12}\right) = 16.69[\text{deg}] \quad (2.1)$$

Determining a maximum allowable horizontal offset angle $\alpha = 10[\text{deg}]$ is therefore conservative and provides a safety factor of 1.66. This is the maximum limit allowed by Acergy in order to ensure that the hoisting wire does not make contact with the moonpool edges. If this happens, the lifting wire may be damaged and fracture.

The peak-period parameter T_p is defined for all sea states based on a scatter diagram for the North Sea (Figure 110), however only $9 \leq T_p \leq 12$ is analyzed based on “worst case” transfer functions in head sea (Figure 49).

The design criterion for the allowable structural weight in air is set to 4000 [kN] since this is limited by the heave compensator capacity on Skandi Acergy. During the landing phase of the operation, the forces in slings and towlines depend on environmental conditions and also structural properties such as damping and added mass values. This criterion is therefore not fixed and may be altered in a later design process.



3 Equipment

The main equipment of importance in subsurface towing is the vessel (chapter 3.1), the suspended load (chapter 3.2) and the rigging wire (chapter 3.3).

3.1 Vessel info

The vessel considered in this master thesis is the Skandi Acergy. The vessel, an Aker Design OSCV 06 L (Subsea Construction and Installation Work) was built at Aker Yards, Søviknes, Norway for DOF Subsea. The delivery took place in July 2008 and Skandi Acergy is chartered to Acergy.

The main activities of the vessel are ROV support, subsea construction and maintenance and installation work. Skandi Acergy's overall length is 157 [m], breadth 27 [m] and velocity is up to 18 [knots]. The vessel can accommodate up to 140 people.

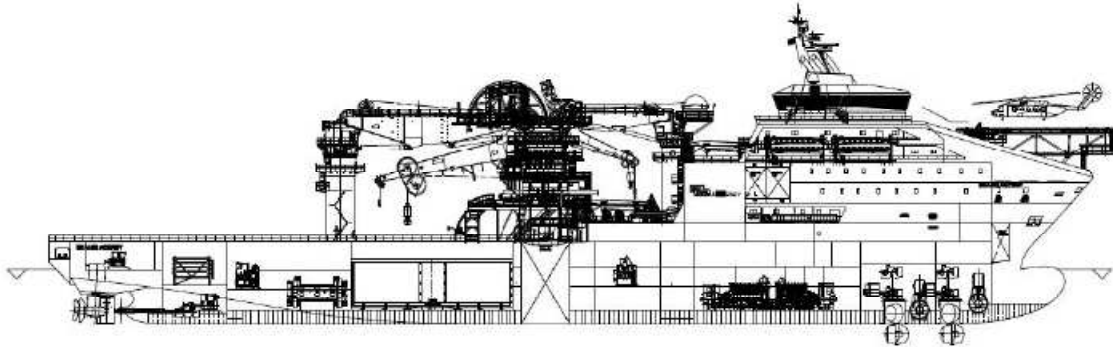


Figure 12 Skandi Acergy profile view

Skandi Acergy	
Length overall [m]	156.9
Length between p.p [m]	137.7
Depth main deck [m]	27.0
Breadth moulded [m]	12.0
Design draft midship [m]	6.5
Max scantling draft midship [m]	8.5
Gross tonnage [Te]	16230

Table 2 Main dimensions Skandi Acergy



3.2 Template description

Figure 13 and Table 3 gives an overview of the main dimensions for the template that is planned to be towed. The Gjøa ITS template is fabricated by FMC Technologies and consist of a bottom frame that shall cover 4 wellheads, which deliver oil and gas to a manifold in the middle of the frame.

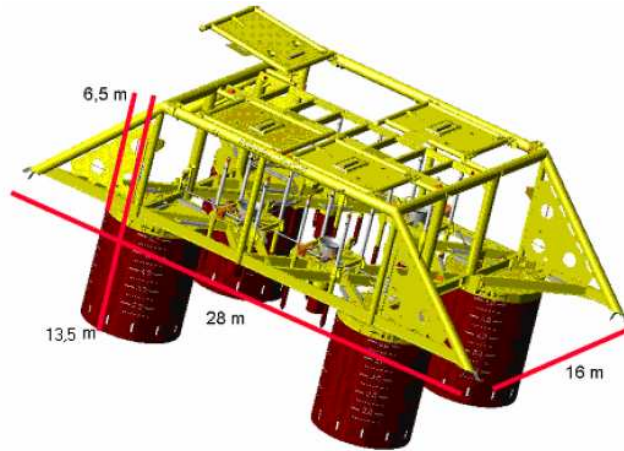


Figure 13 Gjøa ITS with hatches

A summary of main dimension is made in Table 3 below:

Gjøa ITS	
Breath top frame [m]	13.00
Length top frame [m]	19.05
Height top frame [m]	8.95
Diameter top frame [m]	0.91
Height suction anchors [m]	7.00
Diameter suction anchors [m]	5.00
Total height of template [m]	15.95
Total length of template [m]	29.20
Total width of template	21.56
Height bottom frame [m]	1.40
Breath bottom frame [m]	20.13
Length bottom frame [m]	27.35
Total weight in water [kN]	2680
Total weight in air [kN]	3073
Estimated added mass A_{33} [kg]	$1200 \cdot 10^3$
Estimated damping B_{33} (kN/(m/s))	800

Table 3 Dimensions Gjøa ITS

Since the template mainly consists of cylinders and beams; Morison's equation can be used to calculate the drag forces on the structure. However, since adding drag coefficients for different sections together is a rough estimation, this method will only give approximate results of the total drag force.

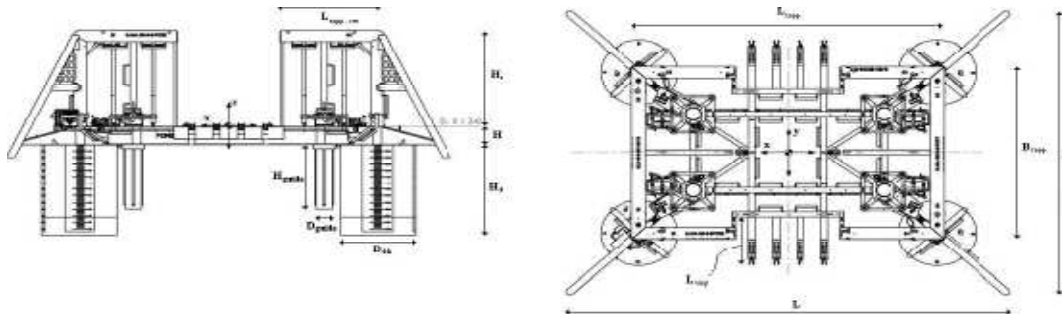


Figure 14 Gjøa ITS

The reason for this is the influence on the current profile by the interaction effects of different structural members. However using Morison theory to calculate the drag forces on the template in incident flow (chapter 6.1), can provide fairly accurate approximations and this is further investigated and compared to a more detailed SIMO model (chapter 7) and experiment (chapter 9) in this thesis.

3.3 Towing lines

Towing lines are composed of several segments with different properties. The towing line stiffness is essential to the dynamic forces, and therefore synthetic ropes are often applied (increased elasticity). Acergy has previously used the polyethylene fibre rope: Dyneema® made by DSM. This fibre is up to 15 times stronger than steel, and has high energy absorption. When using Dyneema®, Acergy has previous experience with fitting rubber inserts inside the polymer rope (Acergy Norway, 2007) which gives the rope better elastic properties. This is because when tension is applied to the rope it will compress the rubber inserts and elongate as a function of the size and shear value of the rubber. Previous tests have shown that this rope can be made to linearly expand up to 30% (Acergy Norway, 2007).

In Table 3 (Nielsen, 2007, pp. 52-56), some characteristic values for synthetic ropes and steel wires are given. Both stiffness and strength depend on material as well as rope construction. In general parallel fibre ropes are stiffer than parallel strand ropes. For synthetic ropes the stiffness depends on the load history, and the post installation stiffness is defined as (Engineers Design Guide, Deep water fibre mooring, 1999):

“The secant stiffness over the load or strain range of interest in quasi-static loading immediately after installation. It is the stiffness which corresponds to the extensibility of the mooring lines under quasistatic load once the minimum installation tensioning has been performed during installation”

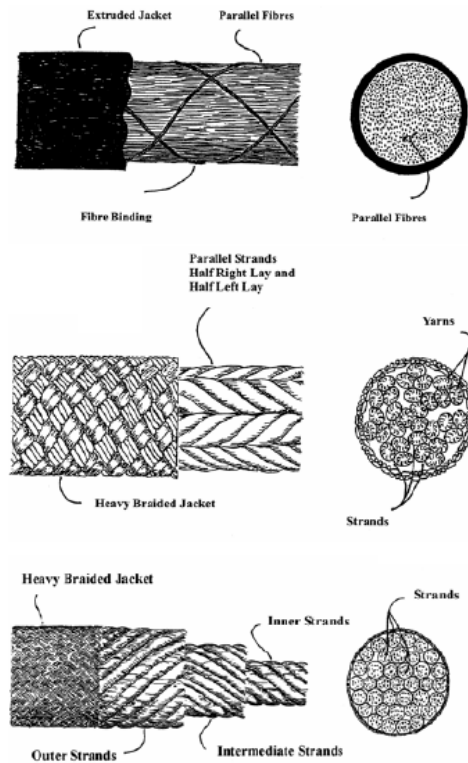


Figure 15 Fibre rope configurations

The storm stiffness is defined as:

“The maximum secant stiffness in cycles from the mean load during the maximum design storm to the cyclic strain limits predicted in the maximum design storms. This stiffness will result in the largest loads being generated in the mooring lines as the platform moves compliant in the storm”.

	POLYESTER	ARAMID	HIGH MODULUS POLYETHYLENE, DYNEEMA®	NYLON	STEEL
Dry mass [kg/m]	23	12	8	-	57
Subsurface weight[N/m]	70	30	-5	-	480
Cross sectional area[cm ²]	240	120	130	400	70
Nominal diameter[mm]	175	120	125	225	108
Post-installed stiffness[EA ₁ /MBL]	10	33	35	20-30	-
Intermediate stiffness [EA ₂ /MBL]	10-30	33-60	35-70	-	80-125
Storm stiffness[EA ₃ /MBL]	30-45	60	70	-	-

Table 4 Rope types

The choice of material depends on design criteria and wanted dynamic properties. Acergy has good operational experiences with both steel wire and Dyneema fiber rope.



In the project thesis (Jacobsen, 2009) which served as a preparatory study for this Master thesis, it was concluded that using Dyneema fiber rope with rubber inserts, a 10% reduction of relative displacements between template and vessel could be achieved (Figure 16). However, using fiber rope with rubber inserts in series complicates analytical expressions and mathematical models used for describing the dynamic system. Since one of the objectives of this master thesis is to verify simple hand calculations and more complex time-domain simulations of multi-body system with experimental results; using Dyneema fiber rope in the hoisting cable is neglected. Steel wire is therefore used for the rigging and hoisting cable in the proceeding derivations.

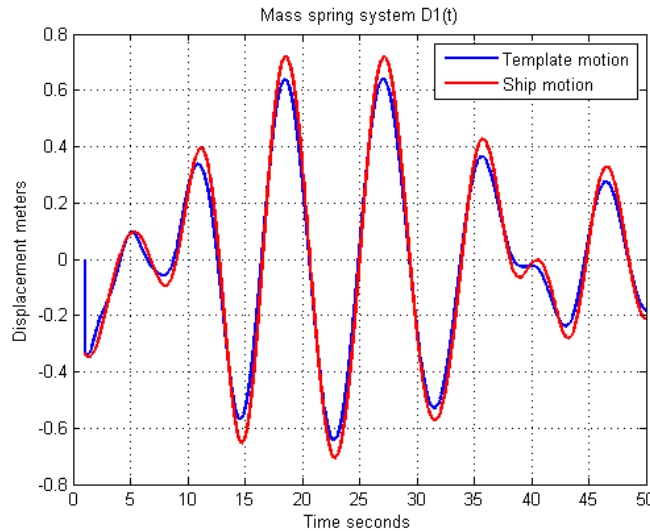


Figure 16 Dyneema rope mass-spring system

Figure 16 show that using fiber rope with rubber inserts, some level of damping is achieved. However this is not the case for steel wire shown in Figure 17. Even though the stiffness k decreases with increasing wire length, the high Youngmodulus E of steel gives a rigid body movement.

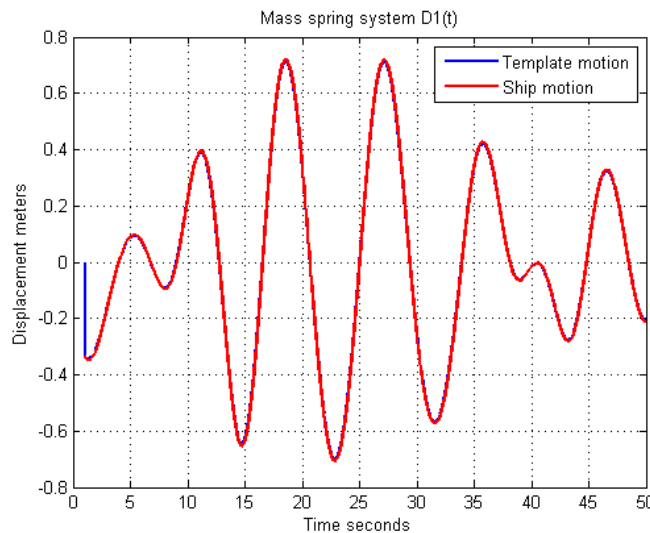


Figure 17 Steel wire mass-spring system



3.4 Tow rigging

The template bridle consists of four steel wire slings from each template corner (aft-starboard, aft-port, fore-starboard, fore-port) going up to a roundel plate via shackles. The bridle has a wire going up to the sheave located below the moonpool. The sheave's wire is then routed from the winch on deck via the fairlead, down through the moonpool to the sheave and up (through the moonpool) to a pad-eye on the moonpool frame. The proposed concept includes a towing bridle connected to the template rigging in one end and a spreader bar in the other end.

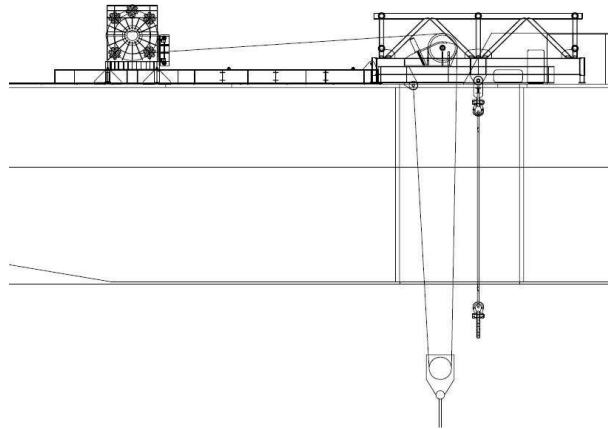


Figure 18 Concept sketch of moonpool configuration (Acergy Norway)

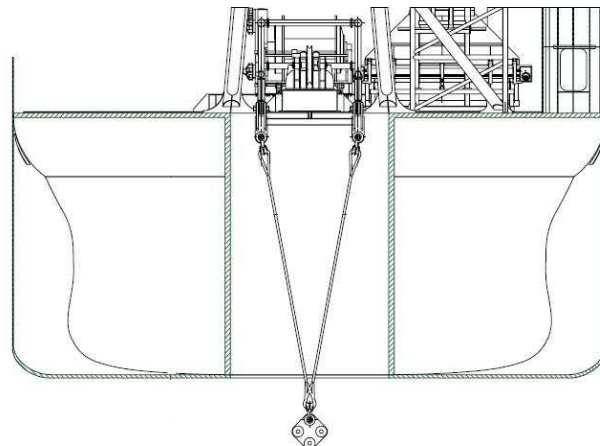


Figure 19 Cross section of moonpool concept (Acergy Norway)

Figure 18 and Figure 19 show the actual rigging configuration proposed on a tender by Acergy. For simplicity, this configuration has been simplified, and the configuration further analyzed in this thesis is shown in Figure 20.

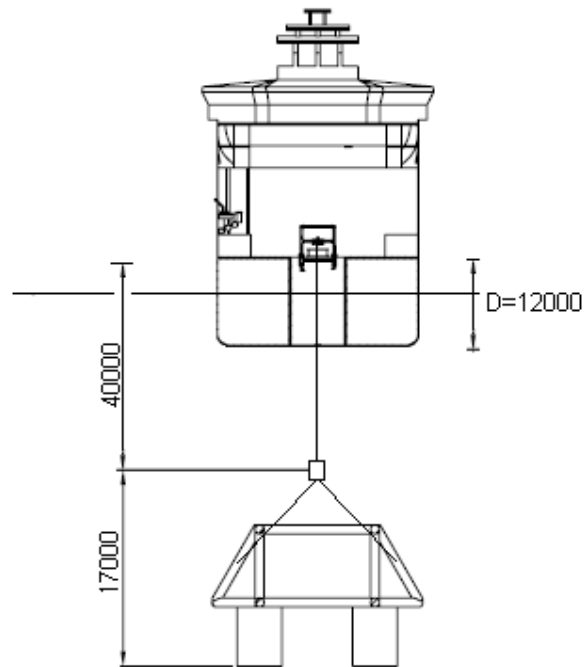


Figure 20 Towing setup (Acergy Norway)

The major difference between these two configurations is that the twin-fall configuration is replaced by a single hoisting wire, and the sheave is replaced by a hook 40[m] below deck. This is done for simplification reasons when modeling in SIMO (chapter 7) and in the experimental verification (chapter 9). Also, not having to introduce an equivalent stiffness K_{eq} caused by the twin-fall configuration reduces the chance of analysis error.

The lifting wire has a length of 40[m] and is made of steel. It has a diameter $D=122[mm]$ which is the maximum diameter allowed by the heave compensated crane on deck. The rigging consists of 4 slings of steel wire with diameter $D=90[mm]$ and length $L=17.80[m]$.



4 Environmental loads during towing

During the towing operation, various loads act on the system. These loads can be subdivided into hydrodynamic and hydrostatic loads.

4.1 Hydrostatic loads

Structures submerged in water experience a hydrostatic pressure (P_H) that depend on the depth z . Since the Gjøa ITS consists of multiple circular hollow cylinders, the hydrostatic pressure will be equal on the inside and outside of the cylinders and this pressure can therefore be neglected.

$$P_H = \rho_v \cdot g \cdot z \quad (4.1)$$

When the template is static, only the submerged weight contributes to the load:

$$W_{water} = W_{air} - B \quad (4.2)$$

where B is buoyancy force, and W_{air} is the weight of the template in air. The static weight of the Gjøa ITS in water is $W_{water} = 2680[kN]$.

4.2 Drag forces

During towing, both the template and the rigging experience drag forces. The drag forces on the rigging can be neglected since it is small compared to the drag forces on the template. These drag forces can cause a horizontal offset (chapter 6.1) which is a limiting factor during the marine operation.

Drag forces on fully submerged elements, consists mainly of friction resistance and pressure resistance. For slender elements, friction resistance is usually the dominant drag contribution.

Friction resistance force can be expressed as:

$$F_F = \frac{1}{2} \cdot C_F \cdot \rho \cdot U^2 \cdot S_v \quad (4.3)$$

where F_F is the frictional resistance on the object [N] and U is the towing velocity [m/s]. C_F is the dimensionless friction coefficient of the object which is dependent upon the Reynolds number, which again depends in turn upon the velocity U . S_v is the wet surface area of the object [m²].



The Reynolds number is defined as:

$$Re = \frac{U \cdot L}{\nu} \quad (4.4)$$

where:

L = Length of element [m]

ν = Kinematic viscosity coefficient (dependent on temperature and salinity) [m^2 / s]

Based on empirical results, ITTC (International Towing Tank Conference) established equation (4.5) for an approximation of the friction coefficient C_f .

$$C_f = \frac{0.075}{(\log Re - 2)} \quad (4.5)$$

However, for blunt bodies such as cylinders or plates, also pressure forces occur when the object is placed in transverse uniform current. The pressure distribution around the object changes depending on the tangential velocity of the current. From potential theory (no friction), the tangential velocity and radial velocity component on the surface of a cylinder can be expressed as:

$$\begin{aligned} v_r &= 0 \\ v_\theta &= -2U_\infty \sin\theta \end{aligned} \quad (4.6)$$

where:

U_∞ = Undisturbed ambient flow velocity magnitude (m/s)

v_r = Radial velocity component (m/s)

v_θ = tangential velocity component along cylinder wall (m/s)

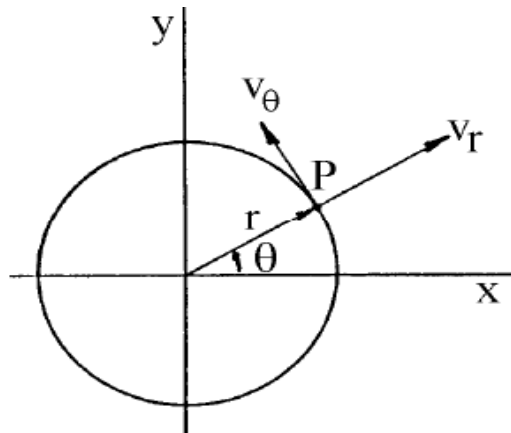


Figure 21 Flow around a cylinder (Anderson,2007)



Equation (4.6) gives the tangential velocity, which is the full magnitude of velocity on the surface of the cylinder, that is, $U = v_\theta$. The minus sign in equation (4.6) is consistent with the sign convention in polar coordinates that v_θ is positive in the direction of increasing θ .

The pressure distribution on the cylinder can be found by Bernoulli's equation:

$$P = p_0 + \frac{1}{2} \rho_v U^2 - 2 \rho_v U^2 \sin^2 \theta \quad (4.7)$$

If the pressure distribution is integrated, the net force can be calculated to be zero. The result of zero drag makes no sense, and this paradox between the theoretical result of zero drag, and in real life finite drag was encountered in the 1744 by the Frenchman Jean Le Rond d'Alembert- and it has been known as d'Alembert's paradox ever since.

Today it is known that the drag is due to viscous effects which generate frictional shear stress at the body surface. This frictional shear stress causes the flow to separate from the surface on the back of the body and create a large wake downstream. Moreover this wake destroys the symmetry of the flow around the vertical axis through the cylinder and thereby causes drag forces.

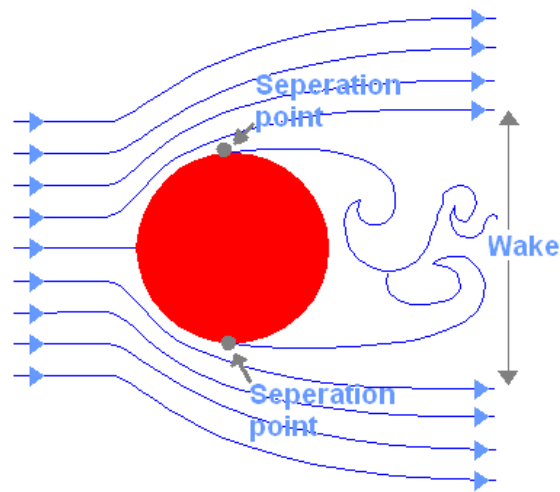


Figure 22 Viscous flow around stationary cylinder

As previously mentioned, the drag force of an object in steady uniform current consists of pressure forces and friction forces where each contribution is geometrical dependent. The drag forces on a cylinder in an unsteady viscous flow can be determined by using Morison's Equation. Morison's Equation consists of a combination of an inertia term and a drag term:

$$dF = \rho \pi \frac{D^2}{4} C_M a + \frac{\rho}{2} C_D D |U| U \quad (4.8)$$



where:

dF = force per unit length of the cylinder [N/m]

D = Diameter of cylinder [m]

ρ = density of fluid [kg/m^3]

C_M = mass coefficient []

a = acceleration [m/s^2]

C_D = drag coefficient []

The first term in equation (4.8) is the inertia term and this is dependent on the acceleration of the fluid. The last term is the drag term and this is dependent on the drag coefficient C_D , and the velocity of the fluid U . The drag coefficient C_D is a coefficient that includes friction forces and pressure forces which is described in the previous chapters. The drag coefficient C_D therefore depends on:

- Geometry
- Reynold's number
- Keulegan-Carpenter number
- Surface roughness

The Keulegan-Carpenter (KC) number is a dimensionless quantity that describes the relative importance of the drag forces over inertia for objects in an oscillatory fluid. For small KC-numbers the inertia term dominates, while for large numbers the drag forces are important. This number is defined as:

$$KC = \frac{U \cdot T}{L} \quad (4.9)$$

where U is the amplitude of the flow velocity oscillation [m/s], T is the period of the oscillation and L is a characteristic length scale of the object, for example the diameter of a cylinder [m].

In the case of subsurface towing, the towing velocity is usually constant without any oscillation frequency, and therefore the inertia dependent term in Morison's Equation may be neglected. Equation (4.8) can therefore be reduced to equation (4.10)

$$dF = \frac{\rho}{2} C_D D |U| U \quad (4.10)$$

As previously mentioned; the templates main components are multiple cylinders and beams. It is complicated to predict a value of the drag coefficient C_D that is valid for the entire structure, but the drag forces can be calculated by summation when using different C_D values for different element types. Using this method will only give approximate results, since all the structural elements influence each other (VIV, vortex shedding, shielding effects).



The most efficient way of determining total drag resistance is using model tests. Since the template is not symmetric, different values for C_D can be found depending on the towing direction. A more general form of equation (4.10) can be written as:

$$F_{D,i} = \frac{\rho}{2} C_{D,i} A_i |U_i| U_i \quad (4.11)$$

where:

$C_{D,i}$ = Dragcoefficient in direction i

A_i = Projected area in direction i

If the total drag resistance is measured in model tests, $C_{D,i}$ can be calculated from equation (4.11) when the projected area is approximated. It should be noted that the projected area depends on the dynamics occurring in the system, and thus $C_{D,i}$ will vary with time.

Empirical approximations for drag coefficients for circular cylinders can be found in (DNV Recommended practice H103, 2009, p. 26). DNV states that the drag coefficient is strongly dependent on the surface roughness of the cylinder. For high Reynolds numbers ($Re > 10^6$) and large KC numbers, the steady flow drag coefficient can be taken as:

$$C_{DS}(\Delta) = \begin{cases} 0.65 & ; \Delta < 10^{-4} \text{ (smooth)} \\ (29 + 4 \cdot \log_{10}(\Delta)) / 20 & ; 10^{-4} < \Delta < 10^{-2} \\ 1.05 & ; \Delta > 10^{-2} \text{ (rough)} \end{cases} \quad (4.12)$$

where $\Delta = k / D$ is the non-dimensional surface-roughness []. Also, the variation of the drag coefficients with Keulegan-Carpenter numbers can be approximated by;

$$C_D = C_{DS} \cdot \psi(KC) \quad (4.13)$$

where C_{DS} is the steady drag-coefficient presented in (4.12). $\psi(KC)$ is the wake amplification factor which varies with KC. Experimental results for these values are presented in Figure 23.

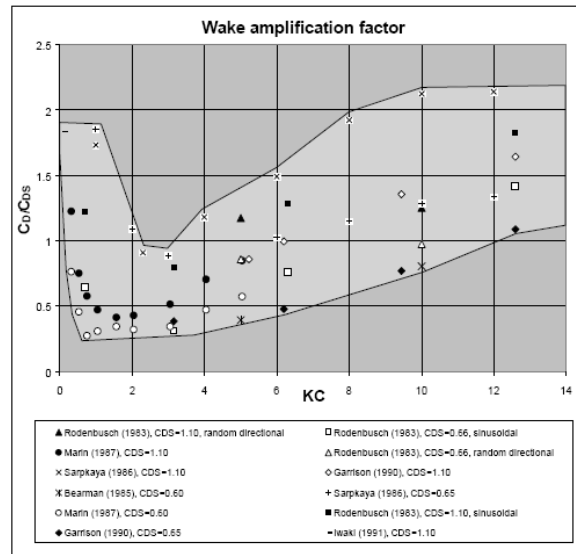


Figure 23 Wake amplification factor (DNV RP H-103)

The shaded area in Figure 23 shows the variation in the wake amplification factor ψ from various experiments. It can be observed that there is no uniform correlation between the experimental results and as a result the recommended practice is to use coefficients between the shaded areas.

4.3 Lift forces

Usually one is not too concerned about lift forces on static offshore structures. This is because of the drag forces always act in the direction of the current and add up nicely when integrated over the entire structure. On the other hand lift forces on a cylinder segment may be acting in one direction; while at the same time the lift force nearby may be acting in the opposite direction. The resultant of lift forces is usually allot smaller than the drag forces and hence often neglected. Still, for a subsurface towing operation of a subsea template, the lift forces especially acting on the suction anchors can be of great importance. These forces can impact the horizontal offset angle α and also the dynamic forces acting in the lifting wire.

Lift forces are generated when a cylinder is subject to viscous flow and according to (John D. Anderson, 2007) a lift force is defined as a force component acting perpendicular to the undisturbed flow velocity. It is therefore also perpendicular to the drag force component. In the case of a cylinder in steady, uniform flow, wake flow patterns will remain symmetrical and thus there will be no lift forces. However, when vortices are generated and shedded behind the cylinder, there will be a cyclic pressure variation in the wake. This leads to a resulting force directed toward the vortex. This effect is illustrated in Figure 24.

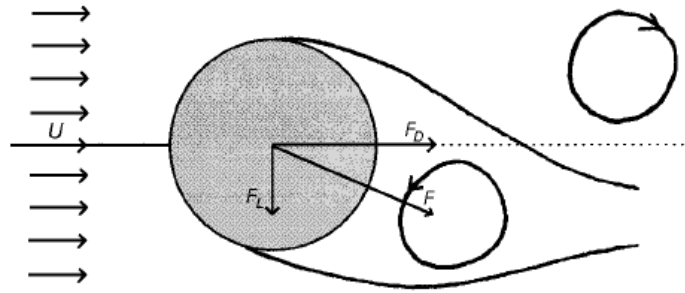


Figure 24 Drag and lift forces on cylinder (Journ e & Massie, 2006)

Because vortices are shed alternately, this lift force will alternate in direction. Its magnitude will vary sinusoidal with a frequency corresponding to the vortex shedding frequency, f_v .

$$F_t = \frac{1}{2} \rho \cdot U^2 \cdot D \cdot C_L \cdot \sin(2\pi f_v t + \varepsilon_{FT}) \quad (4.14)$$

where:

F_T = lift force per unit cylinder length [N/m]

f_v = vortex shedding frequency

D = cylinder diameter [m]

U = Undisturbed flow velocity [m/s]

C_L = dimensionless lift coefficient [-]

t = time[s]

ε_{FT} = phase shift [rad]

Given the vortex shedding frequency, the dimensionless Strouhal number can be defined as:

$$S_T = \frac{f_v \cdot D}{U} \quad (4.15)$$

As previously mentioned, this number depends on the Reynolds number as shown in Figure 25 taken from (Lienhard, 1966).

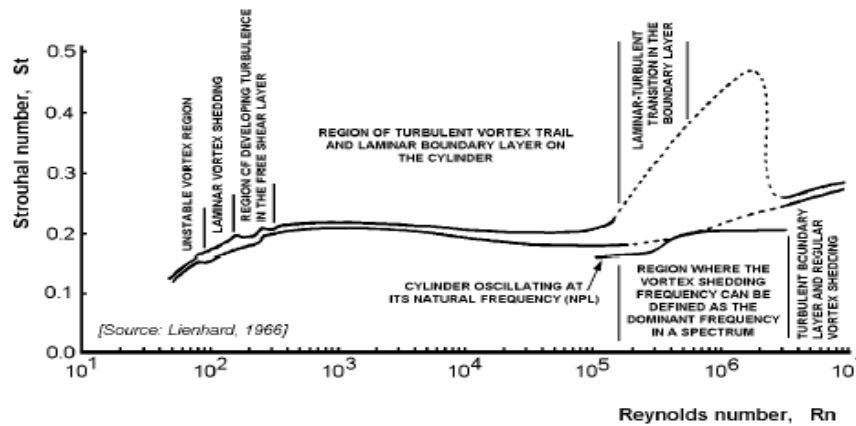


Figure 25 Strouhal and Reynold's number relation (Lienhard)



4.4 Vortex induced vibrations

Figure 26 shows the vortex street behind a cylinder at four time instants during a flow from left to right.

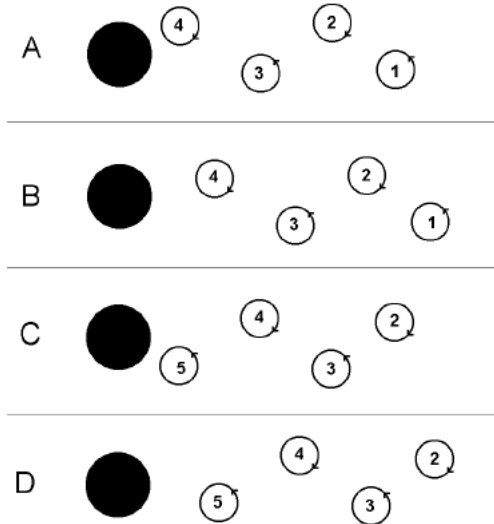


Figure 26 Vortex street behind 4 cylinders (Journée & Massie, 2006)

- A. In this vortex configuration, there is a vortex close behind the cylinder and above the flow axis. Since the velocities are high in the vortex; pressures are low. Both the upward lift force and the drag force will be maximum.
- B. Here the vortices have separated from the cylinder a bit. At this instant the pressure field will be rather uniform. The lift force will be zero and the drag force will be slightly lower than in A.
- C. This is a reflection of configuration A. The lift force will now be directed downward and reach a maximum value together with the drag force.
- D. This is a reflection of configuration B; the lift force is zero and the drag is low. This pattern keeps repeating itself. The lift force is oscillating with a frequency f_v , while the drag force varies only slightly with a frequency $2f_v$.

When the vortex shedding frequency f_v coincides with the natural frequency f_n of a element; resonant vortex-induced vibration occur. This resonance can be predicted by calculating the reduced velocity U_R (dimensionless):

$$U_R = \frac{U}{f_n D} \quad (4.16)$$

Resonance occurs when the vortex shedding frequency f_v approaches the natural frequency f_n . By using the definition of the Strouhal's number and manipulating equation (4.16) the limiting reduced velocity can be found.

$$f_v = \frac{St \cdot U}{D} \rightarrow f_n \quad (4.17)$$



$$U_R = \frac{1}{St} \approx 5 \quad (4.18)$$

In other words; when the reduced velocity U_R approaches 5, resonance oscillations and lock-in may occur on a structural element. Thus, once the natural oscillation frequency of a structure is known, the reduced velocity U_R can be calculated to forecast the dangers from resonant vortex-induced vibration.

This also applies for a fixed cylinder in a uniform current; the vortex-induced oscillation may cause elastic transverse resonance oscillations. Experimental results by (Feng, 1968) with a lightly damped circular cylinder in a current are presented in Figure 27 as a function of the reduced velocity U_R .

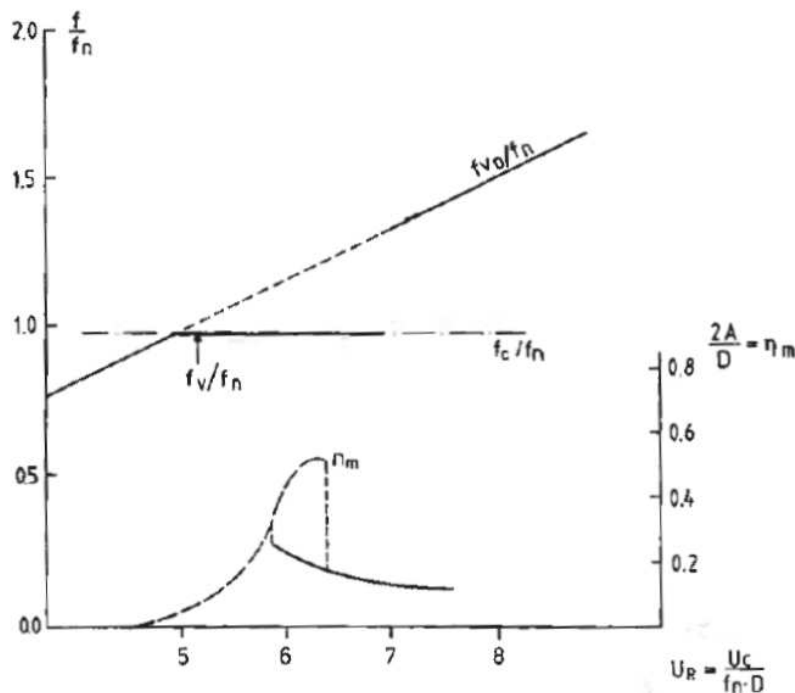


Figure 27 VIV experimental results for cylinder (Faltinsen)

When the reduced velocity is low enough (but high enough to create vortex shedding), the cylinder will remain relatively still in the flow and the vortices will be randomly distributed in the cylinder wake. As U_R reaches a value of ≈ 5 it can be observed that the cylinder begins to oscillate significantly crosswise to the flow. This is because the vortex shedding frequency f_v reaches the natural frequency f_n .

When the cylinder oscillates, it disturbs the local flow pattern, making it more attractive for vortices to be shed behind the cylinder. This happens for reduced velocities $5 \leq U_R \leq 7$ and this is referred to as the “lock-in region”. In the lock-in region the drag forces on the cylinder increase dramatically.



According to (Journèe & Massie, 2006) there are two main reasons why the drag forces increase in the lock-in region: Since drag forces acting on a cylinder can be written as:

$$F_D = \frac{1}{2} \rho U^2 C_D D \quad (4.19)$$

1. The cylinder is oscillating crosswise to the flow, it's wake becomes wider. This effect is similar to that of an increasing cylinder diameter D . However, usually the effect is expressed by increasing the value of the drag coefficient C_D .
2. The cylinder moves with velocity dY/dt , and the instantaneous incident flow of the cylinder can be written as:

$$\bar{U} = -\frac{dY}{dT} \bar{y} + U \bar{x}$$

so that

(4.20)

$$U^2 = \left[\frac{dY}{dt} \right]^2 + U^2$$

Since the instantaneous incident flow velocity is increased, this also increases the drag forces on the cylinder.



4.5 Effects from surface waves

During the towing operation, the template and rigging experience dynamic wave forces. Since the magnitude of the wave-induced forces decay exponentially with increasing depth, the influence on the template will be small if the submerged depth is large. However, wave forces will influence the motions of the installation vessel and these effects are therefore described in this thesis. From ocean wave theory (Faltinsen, 1990, p. 16) the following wave parameters in finite water depth can be derived:

$$\begin{aligned}
 \phi &= \frac{g\zeta_a}{\omega} \frac{\cosh k(z+h)}{\cosh kh} \cos(\omega t - kx) && \text{Velocity potential} \\
 \zeta &= \zeta_a \sin(\omega t - kx) && \text{Wave profile} \\
 p_D &= \rho g \zeta_a \frac{\cosh k(z+h)}{\cosh kh} \sin(\omega t - kx) && \text{Dynamic pressure} \\
 u &= \omega \zeta_a \frac{\cosh k(z+h)}{\cosh kh} \sin(\omega t - kx) && \text{x-component of velocity} \\
 a_1 &= \omega^2 \zeta_a \frac{\cosh k(z+h)}{\cosh kh} \cos(\omega t - kx) && \text{x-component of acceleration} \\
 w &= \omega \zeta_a \frac{\cosh k(z+h)}{\cosh kh} \cos(\omega t - kx) && \text{z-component of velocity} \\
 a_3 &= -\omega^2 \zeta_a \frac{\cosh k(z+h)}{\cosh kh} \sin(\omega t - kx) && \text{z-component of acceleration}
 \end{aligned} \tag{4.21}$$

Equation (4.21) simplifies to equation (4.22) when $z+h$ is large. This is because $\frac{\cosh k(z+h)}{\cosh kh} \approx e^{kz}$.

This relation is true when the relation between the water depth h and wavelength λ is greater than 0.5.

$$\frac{h}{\lambda} > 0.5$$

$$\begin{aligned}
 \phi &= \frac{g\zeta_a}{\omega} e^{kz} \cos(\omega t - kx) && \text{Velocity potential} \\
 \zeta &= \zeta_a \sin(\omega t - kx) && \text{Wave profile} \\
 p_D &= \rho g \zeta_a e^{kz} \sin(\omega t - kx) && \text{Dynamic pressure} \\
 u &= \omega \zeta_a e^{kz} \sin(\omega t - kx) && \text{x-component of velocity} \\
 a_1 &= \omega^2 \zeta_a e^{kz} \cos(\omega t - kx) && \text{x-component of acceleration} \\
 w &= \omega \zeta_a e^{kz} \cos(\omega t - kx) && \text{z-component of velocity} \\
 a_3 &= -\omega^2 \zeta_a e^{kz} \sin(\omega t - kx) && \text{z-component of acceleration}
 \end{aligned} \tag{4.22}$$

This is called “infinite water depth” and is simplifications of the “finite depth water” wave equations.

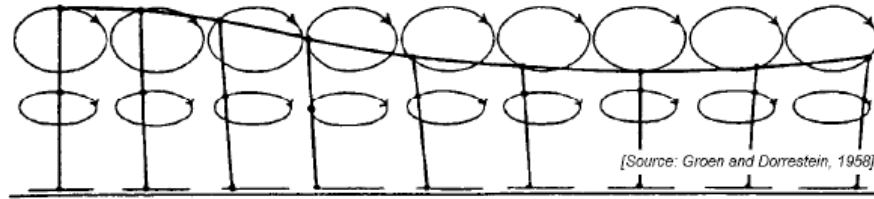


Figure 28 Trajectories of water particles in shallow water (Groen and Dorrestein, 1958)

From Figure 28, it can be observed that the effect of the sea bottom influences water particle trajectories. In infinite water depth, the water trajectory radii decrease exponentially with increasing distance below the free surface. This can be seen in Figure 29.

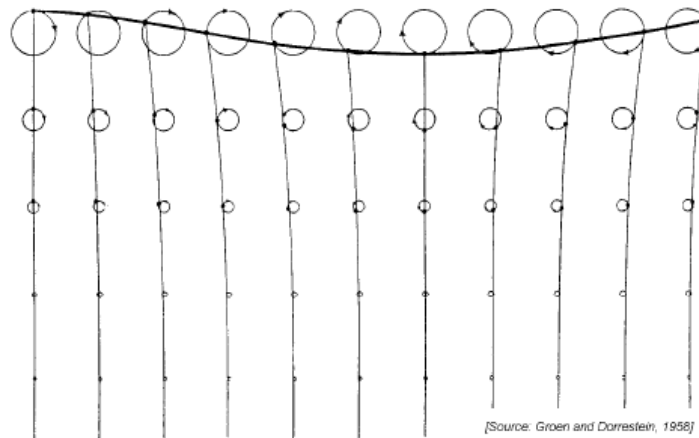


Figure 29 Trajectories of water particles in deep water (Groen and Dorrestein, 1958)

This is the main effects equation (4.21) and equation (4.22) represents: the dynamic pressure changes with increasing distance below the free surface. For infinite water depth, also the dynamic pressure will decrease exponentially.

During the subsurface towing operation, the template will be located approximately 50 [m] below the free water surface. In a conservative estimate; the limiting sea states for the operation will approximately be waves with wave height $H = 5[m]$ and $T = 10[s]$. The dynamic pressure p_D , acceleration a_1 and velocity u at a depth of $z=50(m)$ is therefore equal to:

$$p_{D,max} = \rho g \zeta_a e^{kz} \sin(\omega t - kx) = 3.4 \text{ [KPa]}$$

$$u_{max} = \omega \zeta_a e^{kz} \sin(\omega t - kx) = 0.21 \left[\frac{m}{s} \right]$$

$$a_{1,max} = \omega^2 \zeta_a e^{kz} \cos(\omega t - kx) = 0.13 \left[\frac{m}{s^2} \right]$$

These values will vary over the template and are quite small. The limiting dynamic forces acting on the template are the dynamic forces on the system caused by the vessel's heave excitation. If the heave motion of the vessel reaches the natural frequency of the system, large excitation loads will occur. Wave induced loads on the template may therefore be neglected.



4.6 Internal waves

According to (Melville, 2009), the ocean is stratified by temperature and salinity with the density varying by a few parts in a thousand over the ocean depth. However, the density gradient is not uniform over the total depth and is typically characterized by regions of larger temperature/salinity gradients. Sea water is a solution of dissolved salts, so its intensity is a function of the thermodynamic variables pressure p , temperature T and salinity S ; where salinity is the mass of dissolved solids per unit mass of water.

$$\rho = \rho(p, T, S) \quad (4.23)$$

The mathematical theory behind internal waves is very tedious and complex, so only general results will be presented here. According (Pedlosky, 2008) surface waves are constrained to propagate in horizontal direction while internal waves can propagate in any direction. The dispersion relationship for internal waves is therefore different (equation (4.24)):

$$\omega = \frac{kN}{\sqrt{k^2 + m^2}} = N \cos \theta \quad (4.24)$$

In which k, m are components of the wave vector \mathbf{K} . θ is the angle between the wavenumber vector \mathbf{K} and the horizontal direction. N is called the buoyancy frequency (or Brünt-Vaisala frequency) and can be compared with the frequency of surface waves. However, internal waves differ from surface waves also in other ways: For example, in internal waves the group and phase velocities are perpendicular, so that energy is transported parallel to the wave crests; in contrast for surface waves the group and phase velocities are parallel and energy propagates normal to the wave crests.

$$\mathbf{c} \cdot \mathbf{c}_g = 0 \quad (4.25)$$

In (Pedlosky, 2008) it follows that the average potential energy per unit volume can be written as:

$$\bar{E}_p = \frac{\rho N^2}{4\omega^2} \hat{\omega}^2 \quad (4.26)$$

where $\hat{\omega}$ is the amplitude of particle displacement velocity. According to (Melville, 2009), it can be shown that the average kinetic energy can be expressed as:

$$\bar{E}_k = \frac{1}{4} \rho_0 \left(1 + \frac{m^2}{k^2}\right) \hat{\omega}^2 \quad (4.27)$$

and the total average wave energy is given by:

$$\bar{E} = \frac{1}{2} \rho_0 \left(1 + \frac{m^2}{k^2}\right) \hat{\omega}^2 \quad (4.28)$$

These equations are only valid for small fluid elements, and are hard to implement into a simplified mathematical model to calculate resultant hydrodynamic forces on a structure



influenced by internal waves. However to be aware of internal waves is of vital importance during a wet-tow operation. According to (L.R.M,2006) the effect of increased drag caused by internal waves on for example a ship entering density-stratified water (e.g. a Norwegian Fjord/inshore waters) can be up to a factor of 5. The increase in drag is due to the fact that the ship generates internal gravity waves on the interface between two layers. This effect is called “dead water” and can be observed by the movie attached in the CD attached to this report.

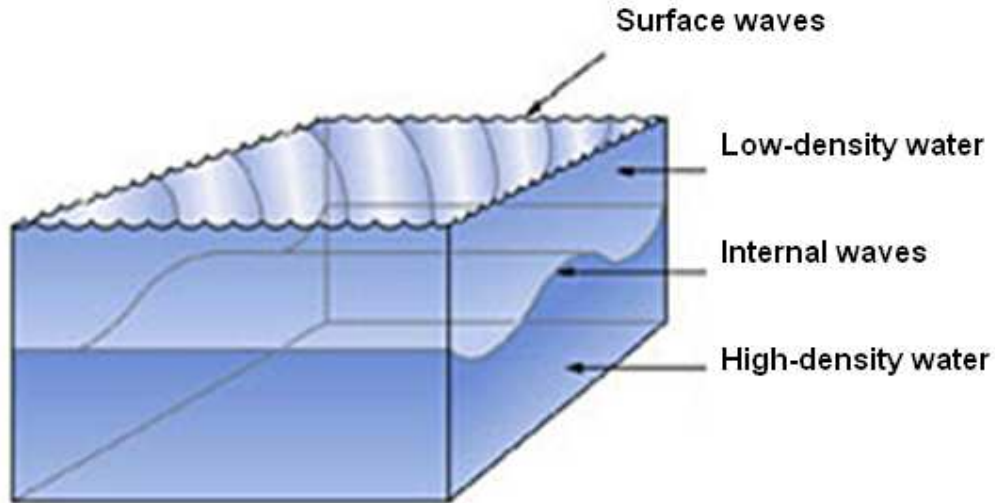


Figure 30 Internal waves (Melville 2009)



5 Dynamic properties of template

The most important parameters in a dynamic analysis for a subsurface towing operation of a subsea template are damping (5.1) and added-mass (5.2).

5.1 Damping

Damping is a construction's ability to dissipate kinetic energy, which means transforming energy to different lower order energy form. In a structure, damping will always be present and therefore a system's kinetic energy will decay with time if new energy is not added.

Modelling damping can often be very difficult, and hence simplified mathematical models are used. Examples of commonly used models are:

- Linear and nonlinear viscous damping (velocity-dependent damping)
- Structural damping (displacement-dependent damping)
- Coulomb damping (constant damping)

Linear and nonlinear viscous damping by the template is the most important parameter and will be further discussed in the following chapters.

5.1.1 Linear viscous damping

According to (Langen & Sigbjörnsson, 1979), linear viscous damping is the damping-model that is usually implemented into the equation of motion. This simplification gives simple mathematical solutions and is a good first approximation of the system damping. Physically it can be described by a mass-damper system (Figure 31).

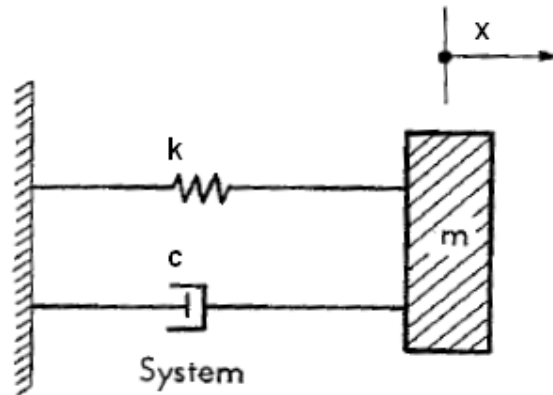


Figure 31 Mass-damper system (Langen & Sigbjörnsson, 1979)

The force magnitude is proportional to the damping coefficient and the time derivative of displacement \dot{x} [m/s].

$$F^D = C \cdot \dot{x} \quad (5.1)$$

where C is the damping coefficient [N/(m/s)].



Linear viscous damping can be examined by observing the solutions of the equation of sinusoidal motion (5.2):

$$m\ddot{x} + c\dot{x} + kx = 0 \quad (5.2)$$

where the solution of the equation of motion is:

$$x = D_1 e^{S_1 t} + D_2 e^{S_2 t} \quad (5.3)$$

And S_1 and S_2 is defined as:

$$\left. \begin{matrix} S_1 \\ S_2 \end{matrix} \right\} = -\frac{c}{2m} \pm \sqrt{\left(\frac{c}{2m}\right)^2 - \omega^2}, \quad \omega^2 = \frac{k}{m} \quad (5.4)$$

D_1 and D_2 are integration constants dependent on initial value conditions and 3. different cases for these constants are shown in Figure 32.

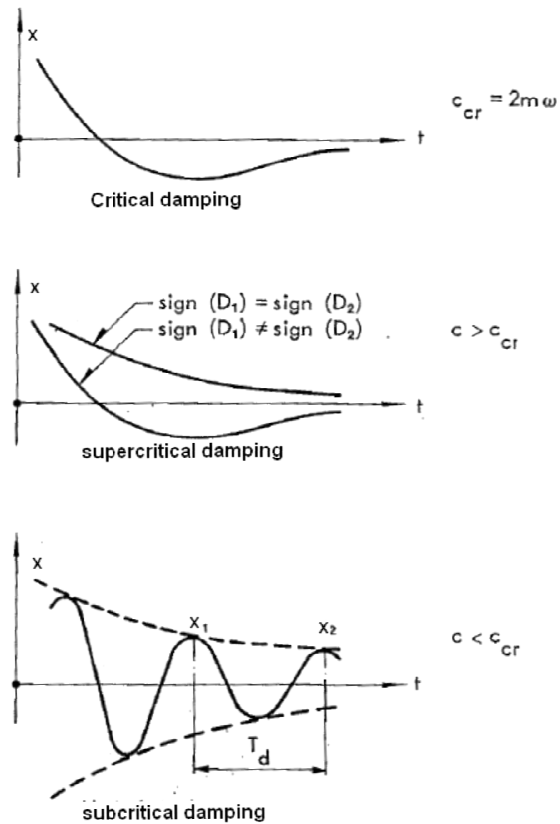


Figure 32 Damping regimes (Langen & Sigbjörnsson, 1979)



Critical damping

$$c = c_{cr} = 2m\omega \quad (5.5)$$

When the damping is equal to $2m\omega$, its defined as critical damping. This means that the system returns to equilibrium as quickly as possible without oscillating which is often desired for the damping of systems such as doors. In practical purposes, marine structures usually never reach this level of damping. A useful parameter when characterizing a structures damping is therefore the damping ratio λ .

$$\lambda = \frac{c}{c_{cr}} = \frac{c}{2m\omega} \quad (5.6)$$

Supercritical damping

In supercritical damping, the damping values are greater than the critical damping. The system reaches equilibrium quickly with no oscillations.

$$c > c_{cr} \quad (5.7)$$

Subcritical damping

This is the most usual form of damping for most marine structures. The roots of equation (5.4) are:

$$s = -\lambda\omega \pm i\omega_d \quad (5.8)$$

Where the damped circular frequency ω_d is given by:

$$\omega_d = \omega_0 \sqrt{1 - \lambda^2} \quad (5.9)$$

This means that the solution of equation (5.2) is:

$$x = e^{-\lambda\omega t} (A \sin \omega_d t + B \cos \omega_d t) \quad (5.10)$$

The integration constants A and B can be explicitly determined when the initial conditions are known. The logarithmic decrement δ is used to find the damping ratio of an under-damped system in the time domain. It's defined as the natural-logarithm of the amplitudes of any two successive peaks.

$$\frac{x_t}{x_{t+T_d}} = \frac{e^{-\lambda\omega t}}{e^{-\lambda\omega(t+T_d)}} = e^{\lambda\omega T_d} \quad (5.11)$$

$$\delta = \ln \frac{x_t}{x_{t+T_d}} = \lambda\omega T_d = 2\pi \frac{\omega}{\omega_d} \lambda \quad (5.12)$$

Linear damping during a wet tow operation of a subsea template is due to the generation of waves (potential damping) and material damping. Since the template is deeply submerged, almost no surface waves will be generated and the linear damping contribution can be neglected. The most dominant is therefore quadratic damping.



5.1.2 Quadratic damping

Quadratic damping is generally caused by drag forces, vortex shedding and viscous effects on the system. This type of damping has a force magnitude which is proportional to the square of the velocity \dot{x} .

$$F^D = c_N \dot{x} |\dot{x}| \quad (5.13)$$

Where c_n is the quadratic damping coefficient with unit $[Ns^2 / m^2]$ or $[kg / m]$.

To describe the mathematical properties of a damping model, hysteretic damping curves is often used. The energy loss during each load cycle is the curve area of the hysteretic curve.

$$W_d = \oint F^D dx \quad (5.14)$$

The energy loss in each work cycle in this hysteretic damping model is:

$$W_d = \frac{8}{3} C_N \omega^2 x_0^3 \quad (5.15)$$

Where the equivalent damping coefficient can be expressed as:

$$C_{eq} = \frac{8}{3\pi} C_N \omega \quad (5.16)$$

In MARINTEK report 550147.00.02 (Solaas, 2008) the damping values for the Gjøa ITS are obtained by hysteretic curves, so no mathematical approximations needs to be made. This data will therefore be used in the hand calculations (chapter 6) of natural frequencies, calculation of modes and dynamic forces.

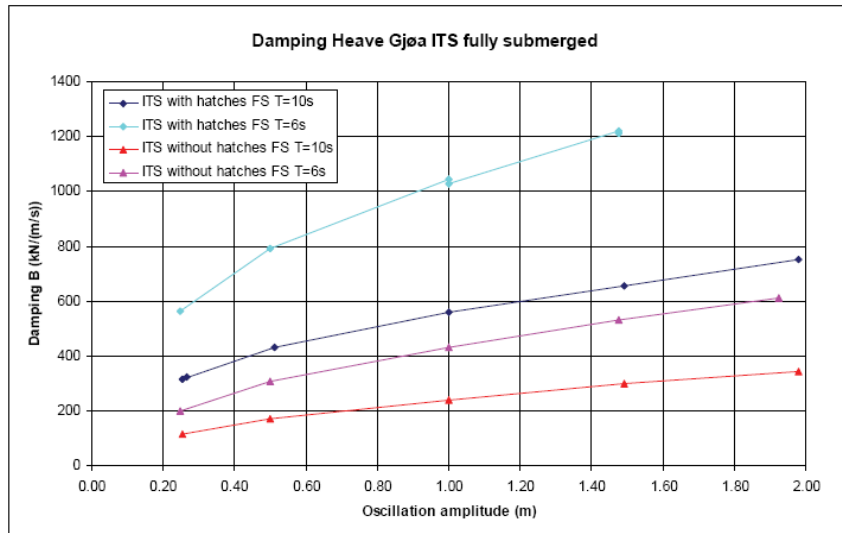


Figure 33 Damping in Heave Gjøa ITS (Acergy Norway)

A conservative damping value in heave (B_{33})=800 (kN/m/s) is further assumed in the hand calculations.



5.2 Added mass

According to (Faltinsen, 1990, p. 41) added mass loads are defined as steady-state hydrodynamic forces due to forced harmonic rigid body motions. The term added mass may be misleading since not all of the 36 added mass coefficients A_{kj} in the added mass matrix have dimension mass. It can be shown that A_{kj} is a function of body form, frequency of oscillation, forward velocity and other factors like finite water depth.

Added mass force F_A in direction k is defined as:

$$F_k^A = -A_{kj} \frac{d^2 \eta_j}{dt^2} \quad (5.17)$$

Added mass values for templates are of importance when evaluating the dynamic forces during subsea installations. Ideally all added mass values should be accurately found from free decay or forced oscillation model tests. Such values are obtained for the Gjøa ITS template in heave and can be found in Marintek report 550147.00.02 (Solaas, 2008).

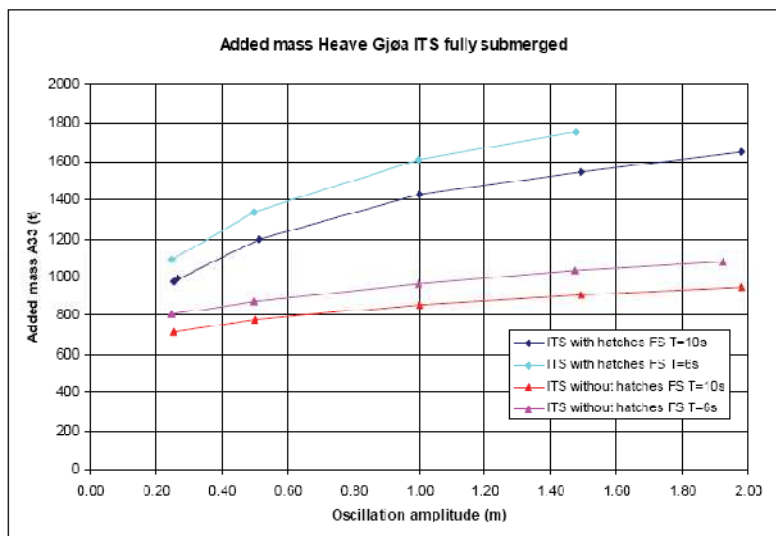


Figure 34 Added mass in heave for Gjøa ITS (Acergy Norway)

The added mass values for the fully submerged ITS without hatches is relatively independent of both the amplitude and the period of oscillation. The values for the ITS without the hatches is between 700 and 1100 tonnes, which is nearly half of the added mass of the ITS with hatches. A constant value of added mass in heave (A_{33})=1100 tonnes is assumed in the hand calculations (chapter 6).

It should be noted that during the operation, the most dominant added mass coefficients are the values obtained in heave. Yet, the dynamics occurring during towing is coupled and all 36 values in the damping and added mass matrices should ideally be identified.



6 Hand calculations of template dynamics

The main parameters that have to be examined according to (DNV Recommended practice H103, 2009) in subsurface towing are the horizontal offset, and the vertical oscillations of the vessel-template system (with emphasis on dynamic forces).

6.1 Horizontal offset

During the towing operation, the template will be subject to a current acting in the horizontal direction as indicated in (DNV Recommended practice H103, 2009, pp. 45-48). This current will cause a horizontal offset, and an angle α to the vertical plane. To derive the formulas for the angle α , small deflections are assumed and the wire is assumed to have infinite stiffness in the axial direction, and zero bending stiffness. The top of the lifting wire is located at the hangoff point of the structure ($z=0$), and $\eta(z)$ is the horizontal offset measured from the vertical plane ($x=0$). The subsurface weight of the template is denoted as W_0 .

At any vertical position z , the following equilibrium conditions have to be satisfied (Nielsen, 2007).

$$T_w \cos(\alpha) = W_0 + \rho_w g A z_b + m g s(z) - \int_0^{s(z)} q \sin \alpha ds \quad (6.1)$$

Where T_w is the wall force in the wire and q is the drag force per unit length. Also, at an arbitrary level z along the wire, equilibrium of horizontal forces can be found from the following figure:

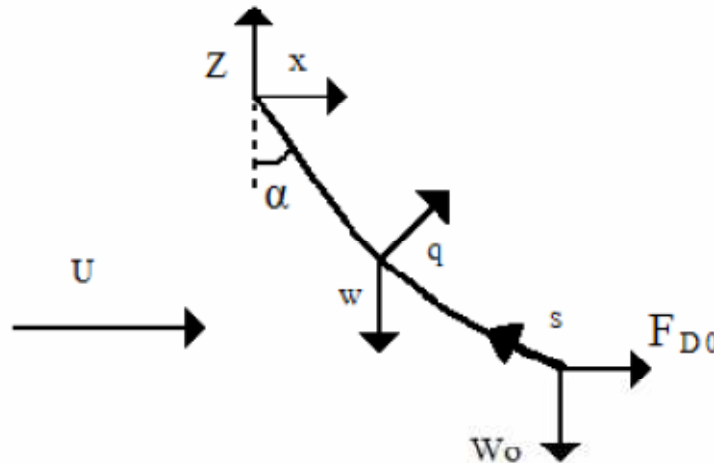


Figure 35 Force equilibrium in wire (FGN 2006)

$$T_w(z) \sin(\alpha) = F_{D0} + \int_0^z q \cos(\alpha) ds - \rho_0(z) A \sin(\alpha) \quad (6.2)$$

The first term on the right hand side of equation (6.2) is the drag on the body connected to the end of the wire, and the second term is the integrated effect of the drag force (drag from wire). The last term on the right side is the horizontal component from the hydrostatic



pressure. Assuming horizontal current acting in the positive x-direction, the drag force F_{D0} can be expressed as:

$$F_{D0} = \frac{1}{2} \rho v^2 C_D A \quad (6.3)$$

The integrated effect of the drag force and hydrostatic pressure caused by the wire is neglected since this term is small compared to the drag of the template.

Assuming small angles:

$$(T_w(z) + p_0(z)A) \sin \alpha = F_{D0} + \int_0^{s(z)} q ds \quad (6.4)$$

And using that the effective tension can be expressed as: $T_E = T_w + p_0 A$ and neglecting small terms:

$$\alpha = \sin^{-1} \left(\frac{F_{D0}}{T_E} \right) \quad (6.5)$$

Figure 36 shows that the effective tension can be written as:

$$T_E = \sqrt{W_0^2 + F_{D0}^2} \quad (6.6)$$

In the calculations presented here, only the horizontal movement of the ship is considered. In the towing operation however, the ship will also be subject to vertical forces F_3 caused by heave and the effective tension in the wire will change as a function of time. If heave motion is taken into account the horizontal offset can be written as (Nielsen, 2007, p. 150):

$$\alpha = \sin^{-1} \left(\frac{F_{D0}(v)}{F_{D0}(v)^2 + F_3^2} \right) \quad (6.7)$$

This may also lead to horizontal oscillations of the template, and in order to be safe of the dynamic response caused by drag; a SIMO analysis (chapter 8.5) of the systems and preferably an experimental investigation (chapter 9) need to be done.

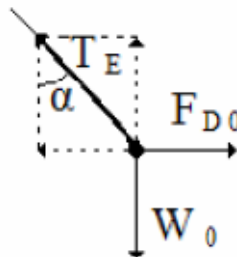


Figure 36 Local force equilibrium in wire
(FGN 2006)



Assuming drag coefficients for a cylinder and beam of $C_D = 1.0$ and $C_D = 2.0$ respectively, and subdividing the template into 4 Morison elements (equation (6.5) and (6.6)), the offset angle α and drag force F_{DO} of the template can be plotted versus towing velocity.

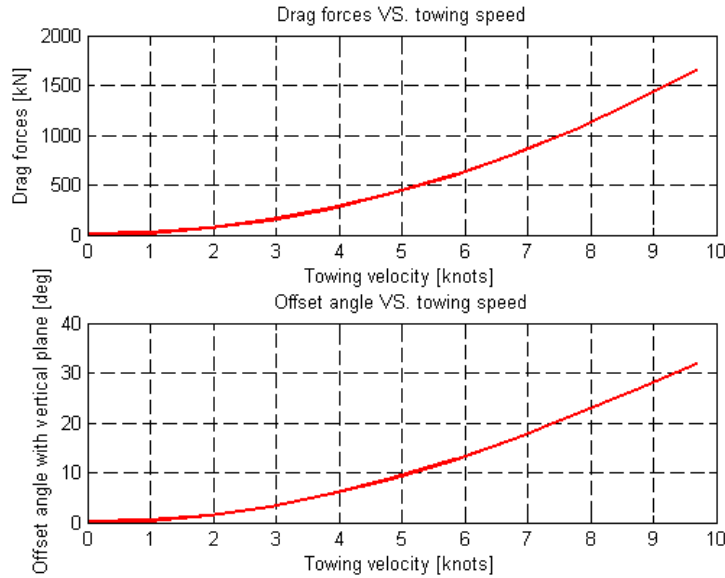


Figure 37 Horizontal offset and total force in lifting wire

The exact values of some of the values in Figure 37, are given in Table 5 below.

Towing velocity [knots]	Offset angle with vertical plane [deg]	Drag forces [kN]
0	0.0	0
1	0.3	17
2	1.0	66
3	2.2	150
4	3.8	265
5	5.8	414

Table 5 Horizontal offset

In the calculations presented here, only the horizontal translation of the vessel is taken into account. As seen from Figure 37, the offset angle with the vertical plane is reasonable for towing velocities between 1 and 5 knots which is as previously mentioned in the design criteria chapter (chapter 2.3) the maximum allowable offset angle α is 10[deg].

When the offset angle with the vertical plane and the drag forces on the template plane is known, the total force in the lifting wire can be calculated by simple trigonometric expressions. Nevertheless, these simplified calculations for lifting wire tension and horizontal offset will need to be compared with a more detailed SIMO model (chapter 7) and experimental results (chapter 9).



6.2 Basic 1-DOF model

In wet-towing of a structure, the elasticity and the mass of the wire are important parameters to consider when determining the dynamic loads. To understand the dynamics of the system, we consider a vertical wire of length L with a constant mass distribution m and stiffness EA per unit length. At the bottom end of the wire, a template with mass M is suspended. The top end of the wire that is connected to the ship is oscillating with an amplitude η_a and frequency ω . For simplicity, damping and dynamic elongation of the wire is ignored. This 1-DOF model will therefore be a rough hand calculation model of our marine operation.

According to (Nielsen, 2007, p. 160), the static elongation of a wire may be written as:

$$L - L_s = \eta(L) = \frac{L}{EA} \left[\frac{wL}{2} + Mg - \rho gV \right] \quad (6.8)$$

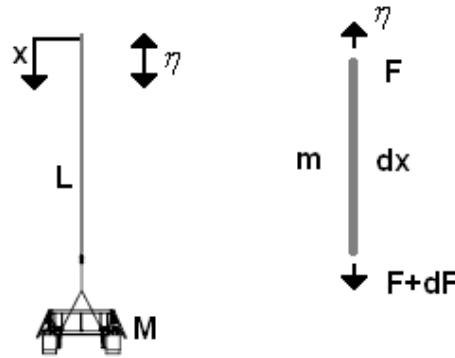


Figure 38 1-DOF system

And by considering the dynamic equilibrium of the element in Figure 38:

$$F + dF = F - w \cdot dx + m \cdot dx \cdot \frac{\partial^2 \eta}{\partial t^2} \quad (6.9)$$

$$\frac{dF_d}{dx} = m\ddot{\eta} \quad (6.10)$$

The symbol w in equation (6.9) is the mass of the wire per meter, and the last term describes the forces due to vertical oscillations by the ship.

As previously mentioned, damping has been ignored but will be introduced later in chapter 6.3. F_d is the dynamic force and $\ddot{\eta}$ is the vertical acceleration of the ship.

The stress-strain relations for the element can be written as:

$$EA \frac{d\eta}{dx} = F \quad (6.11)$$

Combining this with (6.10) yields:

$$EA \frac{\partial^2 \eta}{\partial x^2} = m\ddot{\eta} \quad (6.12)$$

This partial differential equation is valid for all x and t , and using the separation of variables technique (Kreuzig, 2006, p. 540), this equation can be solved.



This gives:

$$\begin{aligned}\eta(x,t) &= X(x) \cdot T(t) \\ \frac{\partial^2 \eta}{\partial x^2} &= X''(x) \cdot T(t) \\ \frac{\partial^2 \eta}{\partial t^2} &= X(x) \cdot \ddot{T}(t)\end{aligned}\quad (6.13)$$

Rearranging (6.13) gives:

$$\frac{X''(x)}{X(x)} = \frac{m}{EA} \frac{\ddot{T}(t)}{T(t)} = C \quad (6.14)$$

Where C is a constant value.

Since at the top of the wire ($x=0$), the top excitation can be described as:

$$\begin{aligned}T(t) &= \cos(\omega t) \\ \eta(0,t) &= \eta_a \cdot \cos(\omega t)\end{aligned}\quad (6.15)$$

And hence the constant C is:

$$C = -\omega^2 \frac{m}{EA} \quad (6.16)$$

When this constant is known, the displacement $X(x)$ can be solved:

$$X(x) = A \cos(kx) + B \sin(kx) \quad (6.17)$$

Using the boundary condition at the top of the wire in equation (6.15) gives : $A = \eta_a$.

This also gives the second constant necessary to solve the differential problem:

$$\frac{X''(x)}{X(x)} = -\omega^2 \frac{m}{EA} = -k^2 \quad (6.18)$$

At the lower end of the wire, the dynamic tension must equal the inertia force M.

$$M \ddot{\eta}(L,t) = -EA \eta'(L,t) \quad (6.19)$$

This is the last boundary condition needed in order to solve the partial differential equation. Inserting (6.19) into (6.13), the constant B may be solved:

$$B = -\eta_a \frac{\omega^2 M \cos(kL) + AEk \sin(kL)}{-\omega^2 M \sin(kL) + AEk \cos(kL)} = \eta_a \frac{1 + \frac{m}{k} \cdot \tan(kL)}{\frac{m}{kM} - \tan(kL)} \quad (6.20)$$

The dynamic displacement and force in the wire is therefore:



$$\eta(x,t) = [\eta_a \cos(kx) + B(\sin kx)] \cdot \cos(\omega t) = \left[\eta_a \cos(kx) + \eta_a \cdot \frac{1 + \frac{m}{km} \cdot \tan(kL)}{\frac{m}{kM} - \tan(kL)} \cdot \sin(kx) \right] \cdot \cos(\omega t)$$

$$F_d(x,t) = EA \frac{d\eta(x,t)}{dx} = EAk\eta_a \left[-\sin(kx) + \eta_a \cdot \frac{1 + \frac{m}{km} \cdot \tan(kL)}{\frac{m}{kM} - \tan(kL)} \cdot \cos(kx) \right] \cdot \cos(\omega t)$$

(6.21)

These equations are quite comprehensive, and the basic dynamics is hard to understand. However, from equation (6.21), we can see that $F_d(0,t) \rightarrow \infty$ when $\tan(kL) - \frac{m}{kM} = 0$. The values of k that fulfil this equation are the eigenvalues of the system, and the values of ω corresponding to k are the natural frequencies of the un-damped system.

Equation (6.21) is implemented for a fixed position x in the MATLAB code in the enclosed CD. As can be seen from Figure 39, the system reaches its natural frequencies near $\omega_0 \approx 4.8$ (rad/s).

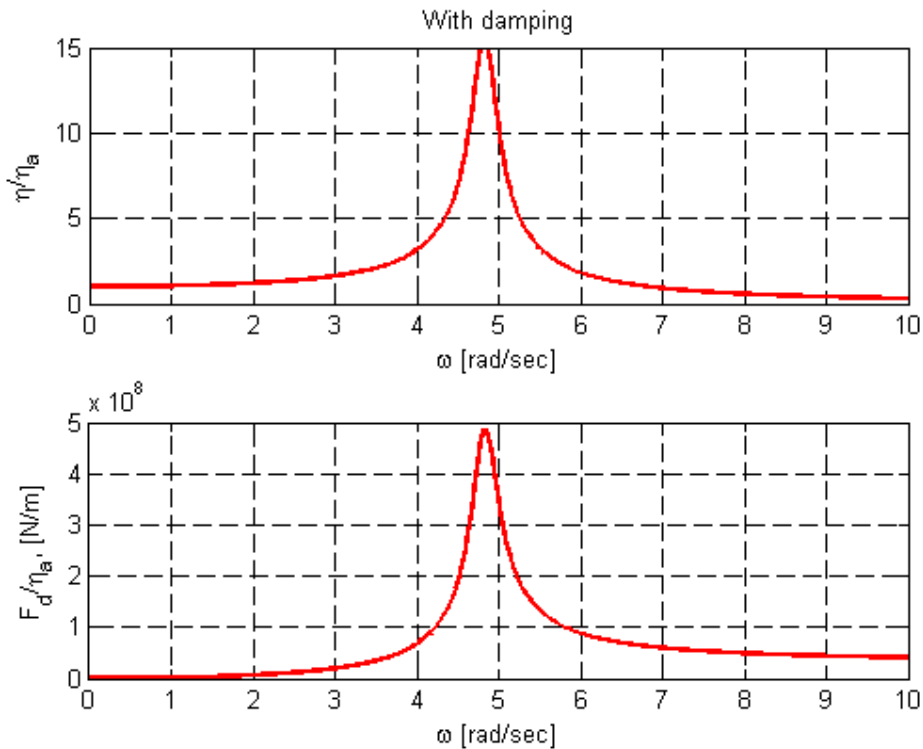


Figure 39 1-DOF model results for damped mass-spring system

Figure 39 shows that the dynamic load factor is separated into 3 distinct areas. For frequencies between 0 and 4 [rad/s] the system is stiffness dominated, while for frequencies



between 4 and 6 [rad/s] we have resonance. For frequencies higher than 6[rad/s], the system is inertia dominated. Figure 39 also shows that when the angular frequency increases, both the dynamic force F_d and the response η reach stationary values.

A quick check of the un-damped natural frequency can be made using (C.M.Larsen, 2007, p. 25):

$$\omega_0 = \sqrt{\frac{k}{m + A_{33}}} = \sqrt{\frac{3 \cdot 10^7}{1100000}} = 5.22 \text{ [rad / s]} \quad (6.22)$$

The result obtained in (6.22) seems to be similar to the natural frequencies in Figure 39 and is correct for a system where damping is neglected. The reason why the comprehensive equations for the 1-DOF system are used is because of the ability to calculate mode shapes, which is further explained in chapter 6.3.

6.3 1-DOF model with damping

To include damping in the differential equation, a velocity dependent force has to be included in (6.9). The equation can then be expressed as (Nielsen, 2007):

$$F + dF = F - w \cdot dx + mdx \frac{d^2\eta}{dt^2} + c \frac{d\eta}{dt} dx \quad (6.23)$$

$$\frac{dF_d}{dx} = m\ddot{\eta} + c\dot{\eta} \quad (6.24)$$

The dynamic equilibrium of the wire then becomes:

$$EA \frac{d^2\eta}{dx^2} = m\ddot{\eta} + c\dot{\eta} \quad (6.25)$$

Using the technique of separation of variables as before (Kreyzig, 2006, p. 540), the equation can be written as:

$$\frac{X''(x)}{X(x)} = \frac{m}{EA} \frac{\ddot{T}(t)}{T(t)} + \frac{c}{EA} \frac{\dot{T}(t)}{T(t)} = const \quad (6.26)$$

Assuming that the time dependent function $T(t)$ is harmonic in time:

$$\begin{aligned} T(t) &= T_0 \cos(\omega t) \\ \dot{T}(t) &= -\omega T_0 \sin(\omega t) = -i\omega T(t) \\ \ddot{T}(t) &= -\omega^2 T_0 \cos(\omega t) = -\omega^2 T(t) \end{aligned} \quad (6.27)$$

And hence (6.26) becomes:



$$\frac{X''(x)}{X(x)} = \frac{m \ddot{T}(t)}{EA T(t)} + \frac{c \dot{T}(t)}{EA T(t)} = \frac{m_c \ddot{T}(t)}{EA T(t)} = const \quad (6.28)$$

This equation has two new variables where m_c and M_c are “complex masses”.

$$\begin{aligned} m_c &= m + i \frac{c}{\omega} \\ M_c &= M + i \frac{C}{\omega} \end{aligned} \quad (6.29)$$

Using the assumption of linear damping, we can see that the effect of the complex mass is reduced when the frequency ω increases. However since damping is quadratic in water (Langen & Sigbjörnsson, 1979), the damping force F_d can be written as:

$$F_d = C_v \dot{\eta} |\dot{\eta}| \quad (6.30)$$

If η is harmonic with amplitude η_o , the linear damping coefficient C_e is according to equation (9.21) in (Langen & Sigbjörnsson, 1979, p. 273):

$$C_e = \frac{8\omega}{3\pi} C_v \eta_o \quad (6.31)$$

And the “complex masses” can then be written as:

$$\begin{aligned} m_c &= m + i \frac{8}{3\pi} C_v \eta_o(x) \\ M_c &= M + i \frac{8}{3\pi} C_v \eta_o(x) \end{aligned} \quad (6.32)$$

The frequency dependence has now disappeared, and the linearized damping is only dependent on the motion amplitude. The response $\eta(x,t)$ and force $F(x,t)$ can then be expressed as:

$$\begin{aligned} \eta(x,t) &= \left[\eta_o \cos(kx) + \eta_o \cdot \frac{1 + \frac{m}{kM} \cdot \tan(kL)}{\frac{(m + i \frac{c}{\omega})}{kM} (1 - i \frac{c}{\omega M}) - \tan(kL)} \cdot \sin(kx) \right] \cdot \cos(\omega t) \\ F_d(x,t) &= EA \frac{d\eta(x,t)}{dx} = E A k \eta_o \left[-\sin(kx) + \frac{1 + \frac{m}{kM} \cdot \tan(kL)}{\frac{(m + i \frac{c}{\omega})}{kM} (1 - i \frac{c}{\omega M}) - \tan(kL)} \cdot \cos(kx) \right] \cdot \cos(\omega t) \end{aligned} \quad (6.33)$$



Equation (6.33) is implemented in the MATLAB code in the enclosed CD. Using MATLAB's surf and mesh functions, 3D plots of the displacement $\eta(x,t)$ and the force $F_d(x,t)$ can be shown at arbitrary positions along the lifting wire for different oscillation frequencies. The results can be seen in Figure 40, Figure 41 and Figure 42.

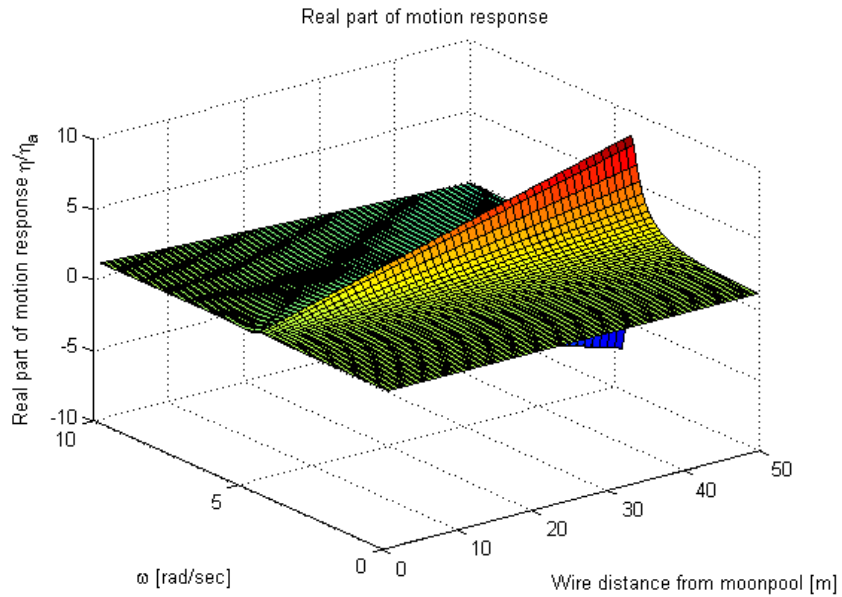


Figure 40 Real part of motion response along lifting wire

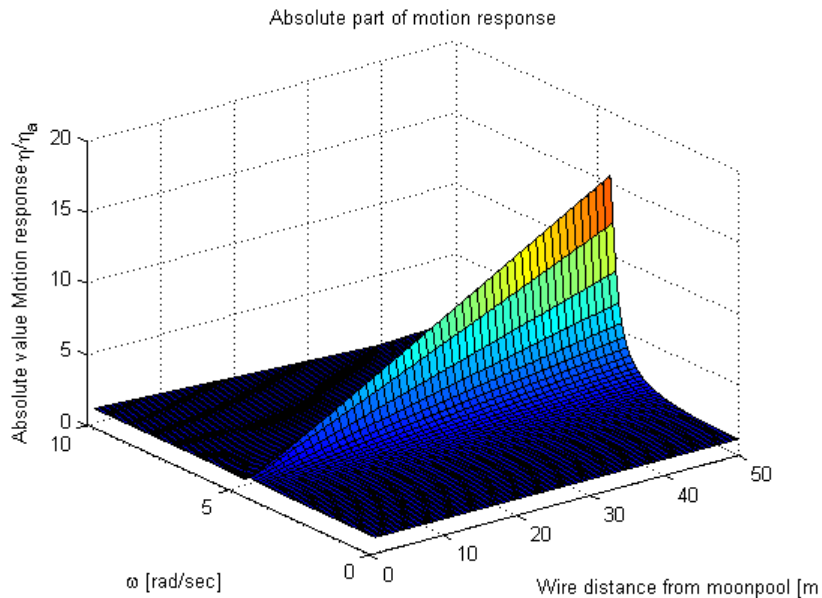


Figure 41 Absolute part of motion response along the lifting wire

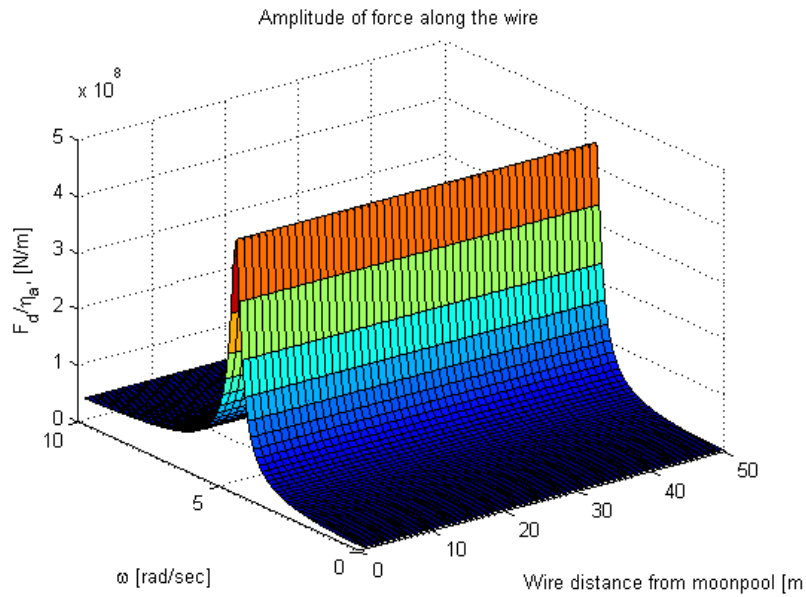


Figure 42 Force Amplitude along the lifting wire

Comparing Figure 40 and Figure 41 with Figure 39, we see that the system has a distinct eigenmode and eigenfrequency when ω is close to 4.8 [rad/s]. The most important result these curves show, is the shape of its respective eigenmode. Since the stiffness is relatively high ($E=210 \cdot 10^9$ Pa), the transient phase remains similar in space during loading. However, with decreased stiffness K of the wire, the force amplitude in Figure 42, doesn't have to be constant in space. This can be imagined in a transient lapse; If a wire with tension suddenly is cut in one end, it will experience a shock propagating with the velocity of sound in the material. In front of the shock, the tension will remain the same as before the cut, but behind the shock the wire will be relieved from tension.

These dynamics for higher order modes is especially important when evaluating different damping concepts. The concepts can be using Dyneema wire with rubber inserts (Jacobsen, 2009), and/or introducing damping in the hang-off structure on the vessel deck.



6.4 Differential equation in heave

The partial differential equations in chapter 6.2 and 6.3 are derived for simple 1-DOF oscillations. The main contribution to the movement of the template is caused by the heave oscillations of Skandi Acergy. As these heave oscillations will be irregular in time, a time domain analysis (chapter 6.6) is done to determine the movement of the template.

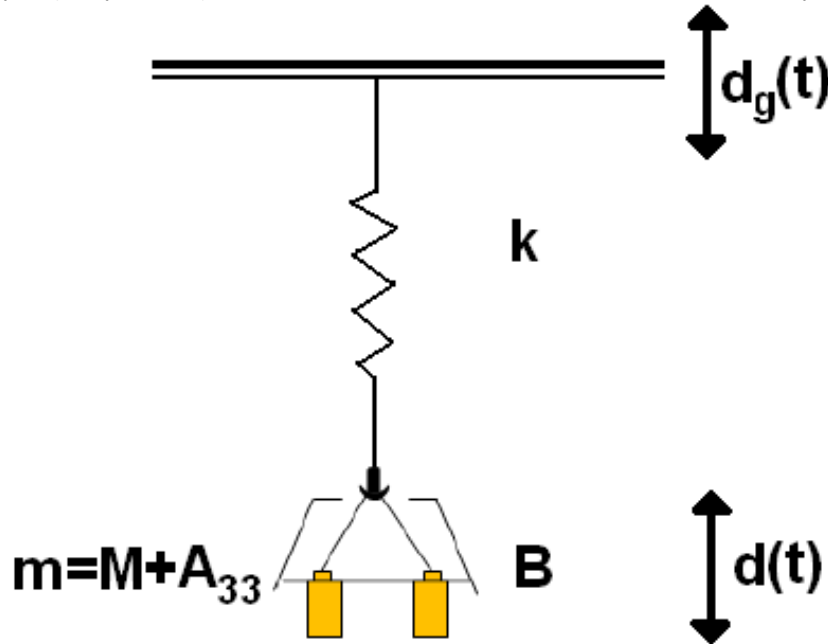


Figure 43 1-DOF system with prescribed displacement

Figure 43 shows the template with mass $m=M+A_{33}$ and damping B . The dynamic equilibrium equation for a 1-DOF system with prescribed displacements as a function of time $d_g(t)$, can be written as:

$$\begin{aligned}
 m\ddot{d} + B\dot{d} + kd &= 0 \\
 m\ddot{d} - m\ddot{d}_g + m\ddot{d}_g + B\dot{d} - B\dot{d}_g + B\dot{d}_g + kd - kd_g &= 0 \\
 m(\ddot{d} - \ddot{d}_g) + B(\dot{d} - \dot{d}_g) + k(d - d_g) &= -m\ddot{d}_g - B\dot{d}_g \\
 m\ddot{d}_{rel} + B\dot{d}_{rel} + kd_{rel} &= -m\ddot{d}_g - B\dot{d}_g = F(t)
 \end{aligned}
 \tag{6.34}$$

Where the right hand side: $-m\ddot{d}_g - B\dot{d}_g$ is the external forces caused by Skandi Acergy's response in heave. Solving this equation for $d_{rel} = d - d_g$ gives the template displacement. This is the differential equation to be solved by Newmark's β -method in chapter 6.6. But first the response of the vessel $d_g(t)$ needs to be determined.



6.5 Response Skandi Acergy

To simulate the response of Skandi Acergy in head sea, a sea state has to be described using the JONSWAP wavespectrum. The JONSWAP (Joint North Sea Wave Project) spectrum is often used to describe coastal waters where the fetch is limited. It is based on the ITTC spectrum and defined below:

$$S_n(\omega) = \frac{5}{32\pi} H_s^2 T_p \left(\frac{\omega_p}{\omega} \right)^5 e^{-\frac{5}{4} \left(\frac{\omega_p}{\omega} \right)^4} (1 - 0.287 \ln \gamma) \gamma^{\frac{(\frac{\omega}{\omega_p} - 1)^2}{2\sigma^2}} \quad (6.35)$$

Given a peak period T_p , a significant wave height H_s and γ value, the wavespectrum can be plotted as seen on Figure 44.

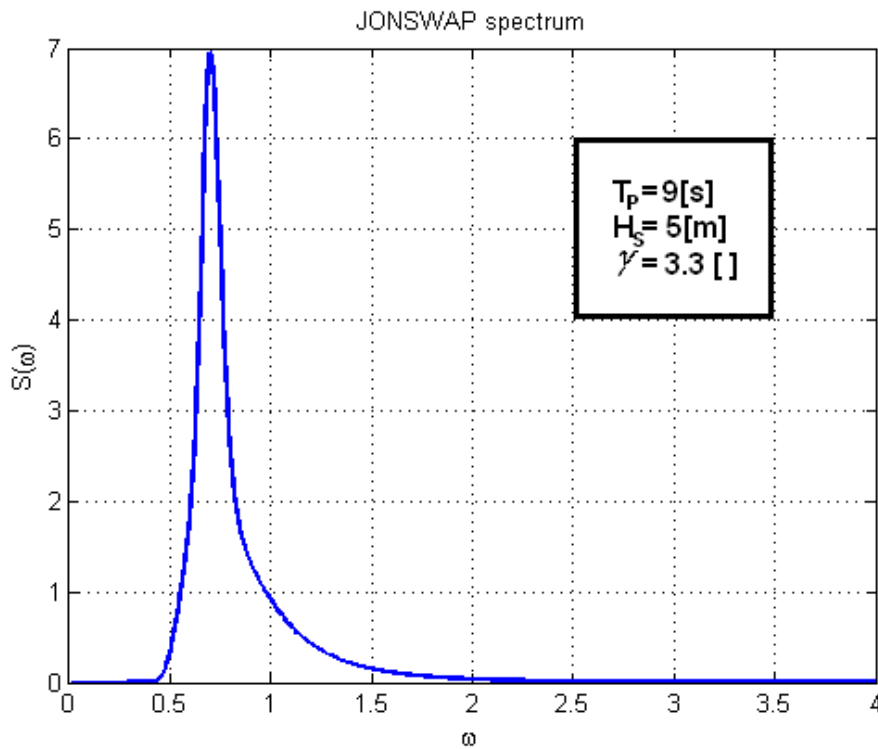


Figure 44 JONSWAP spectrum

When using the JONSWAP wavespectrum, it is important to choose the peak period T_p and significant wave height H_s wisely. According to (DNV Recommended practice H103, 2009) section 2.2.6.7 the JONSWAP spectrum is expected to be a reasonable model for:

$$3.6 < \frac{T_p}{\sqrt{H_s}} < 5 \quad (6.36)$$

Outside this interval, the wavespectrum should be used with caution which can be observed by Figure 110 in the appendix.

When the wavespectrum is known, some statistical parameters can also be determined based on the spectral moments. The following statistical wave values are calculated in the MATLAB code in the enclosed CD.



Zerocrossing period: $T_z = \frac{H_s \pi}{2\sqrt{m_2}}$

Mean period: $T_{m0} = 2\pi \sqrt{\frac{m_0}{m_1}}$

Mean period between wave crests: $T_{m24} = 2\pi \sqrt{\frac{m_2}{m_4}}$ (6.37)

Max. wave amplitude in 5 hours $H_{\max} = H_{m0} \sqrt{\frac{\ln N}{2}}$

Spectral moments: $m_n = \int_0^\infty \omega^n S(\omega) d\omega, \quad n = 0, 1, 2, \dots$

For the wavespectrum in Figure 44, the following values are obtained from the MATLAB code in the enclosed CD.

```
*****WAVE DATA*****
*****ALL UNITS IN M AND S*****
Given significant wave height (Hs)..... 5
Given peak period (Tp)..... 9
Given gamma value ..... 3.300000e+000
Calculated significant wave height (Hm0)..... 5.004133e+000
Biggest wave in 5 hours (Hmax)..... 9.906790e+000
Mean zero crossing period (Tz)..... 7.096015e+000
Zero crossing period (Tm0z)..... 7.101881e+000
Mean period (Tm0e)..... 7.539778e+000
Mean period between wave crests (Tm24)..... 4.887467e+000
*****END OF CALCULATIONS*****
>> |
```

Figure 45 Sea state characteristics from MATLAB

From Figure 45, we can see that the biggest wave during 5 hours will be 9.90 [m] and the mean period (T_{m0}) is 7.09 [s].



6.5.1 Surface elevation

To create stochastic waves from the wavespectrum, a summation of many wave elevations and wave frequencies is made by using equation (6.38). Each harmonic wave is randomly phase shifted with an angle between 0 and 2π .

$$\zeta(x,t) = \sum_{n=1}^N \sqrt{2S(\omega)\Delta\omega} \cos(\omega_n t + k_n x + \varepsilon_n) \quad (6.38)$$

A sum of cosine waves randomly phase shifted relative to each other, gives a stochastic sea state.

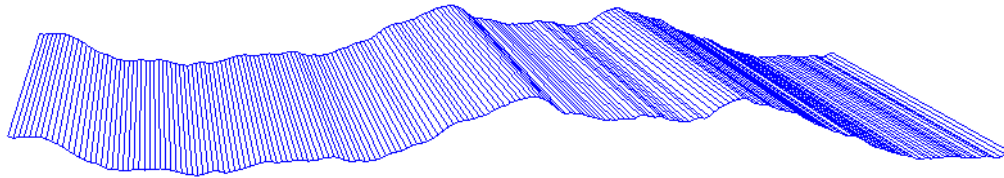


Figure 46 Irregular waves in GLview

For a time series of 100(s) in the time domain for a $H_s = 5(m)$ and $T_p = 9(s)$, the irregular sea state in Figure 50 can be created. To verify that the irregular sea generated by (6.38) is correct, a Fourier transformation (FFT) of the sea state can be made. As stated, the peak period $T_p = 9.0(s)$ gives a $\omega_p = 0.69(s)$ and is the dominating wave frequency in the analysis. This can be verified from the Fourier transformation (represented by a spectrogram) in Figure 47.

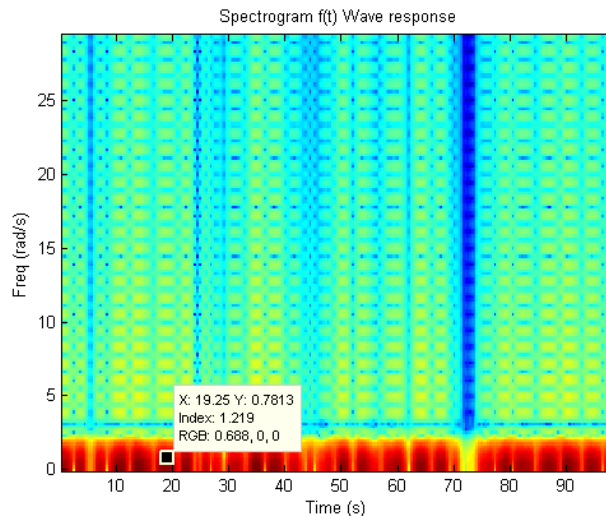


Figure 47 Fourier transformation of wave packet

From the Fourier transformation of the irregular sea, it can be observed that the dominating frequency (red color) is around 0.7 [rad/s]. Also higher frequency components close to 2 [rad/s] are present, but they are rare. From Figure 47, equation (6.38) seems to be valid and generates an irregular sea with the correct peak period T_p .



6.5.2 Vessel response in heave

The vessel response in heave is the main contribution to dynamic forces in the wire during the transit phase of the operation. According to (Faltinsen, 1990, p. 41) the movement of any offshore structure can be described by equation (6.39):

$$\mathbf{s} = (\eta_1 + z\eta_5 - y\eta_6)\mathbf{i} + (\eta_2 - z\eta_4 + x\eta_6)\mathbf{j} + (\eta_3 + y\eta_4 - x\eta_5)\mathbf{k} \quad (6.39)$$

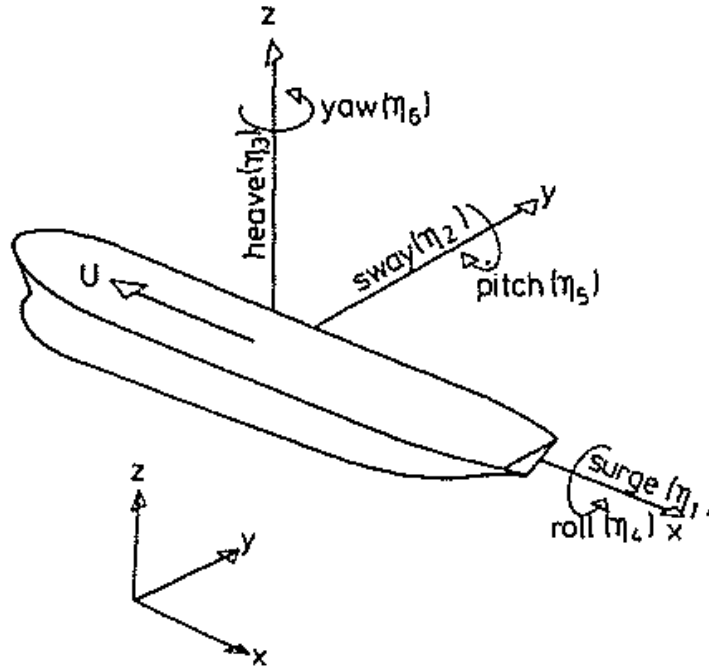


Figure 48 Ship degrees of freedom (Faltinsen)

Along the z-axis, this equation is reduced to:

$$\mathbf{s} = (\eta_3 + y\eta_4 - x\eta_5)\mathbf{k} \quad (6.40)$$

Since the moonpool is located in the centre of the ship ($y = 0$) and close to LCG ($x \approx 0$), only the heave motion η_3 contributes to vertical motion and is considered in the further calculations.

When the surface elevation is known, it is possible to determine the vessel response based on RAO (Response Amplitude Operators). RAO are also known as transfer functions and are mathematical representations, in terms of wave period, of the relation between the vessel response on a incident wave $\left| \frac{\eta_{\max}}{\zeta_a} \right|$. Transfer functions can be found experimentally or by using computer software (such as VeRes²). The transfer function for Skandi Acergy for zero surge motion, in heave is known from (Nesse, 2008)

² Vessel response computer program developed by MARINTEK

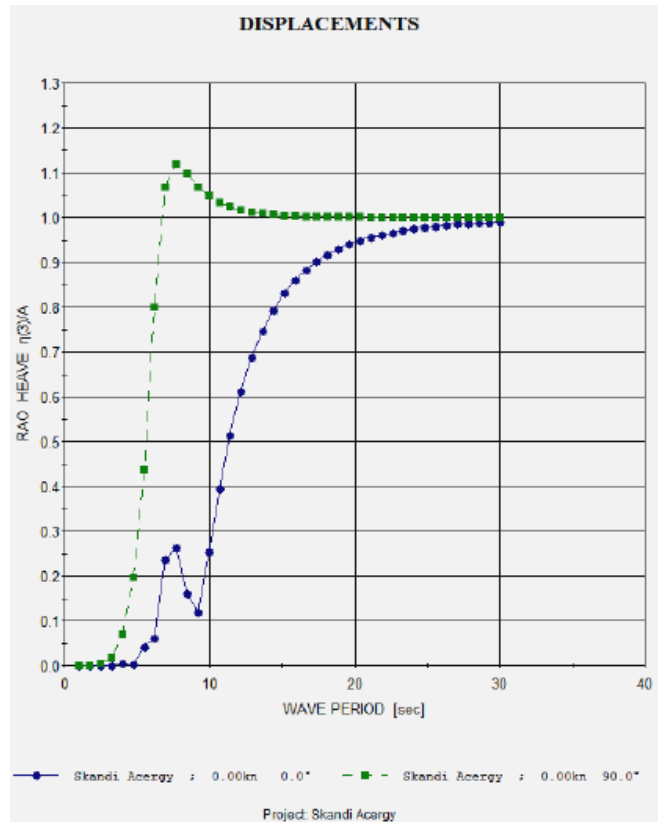


Figure 49 Transfer function Skandi Acergy in heave

This RAO approaches 1 as the wave period increases. According to theory, long waves will displace the vessel in heave corresponding to the incident wave amplitude. For short waves (or high frequency waves) the RAOs will go toward zero as large volume structure does not have time to react to the forces acting on it. The wave periods causing the peak values found from VeRes for 90 [deg] and 0 [deg] with zero incident velocity were both 7.69 [s].

When RAO data is known, this data can be used with the wavespectrum to calculate the response of the vessel.

According to (Faltinsen, 1990), the transfer function for heave is defined as:

$$|H(\omega_n)| = \frac{\eta_{3An}}{\zeta_{an}} \quad (6.41)$$

Where the terms can be rearranged to:

$$\begin{aligned} \eta_{3An} &= |H(\omega_n)| \cdot \zeta_{an} \\ \eta_{3An}^2 &= |H(\omega_n)|^2 \cdot \zeta_{an}^2 \end{aligned} \quad (6.42)$$

The relationship between wave amplitude ξ_{an} and the wavespectrum $S(\omega_n)$ is:



$$\frac{1}{2} \zeta_{an}^2 = S(\omega_n) \Delta \omega \quad (6.43)$$

For heave motion of the vessel η_{3An} , a similar heave-spectrum can be created using energy relations:

$$\frac{1}{2} \eta_{3an}^2 = S_{\eta_3}(\omega_n) \Delta \omega \quad (6.44)$$

$$\eta_{3an}^2 = 2 \cdot S_{\eta_3}(\omega_n) \Delta \omega = |H(\omega_n)|^2 \cdot \zeta_{an}^2 = |H(\omega_n)|^2 \cdot 2 \cdot S(\omega_n) \Delta \omega \quad (6.45)$$

Assuming a linear relationship between heave motion and wave amplitude, the heave motion of the vessel in irregular sea can be written as:

$$\begin{aligned} \eta_3 &= \sum_n \eta_{3An} \cos(\omega_n t + \varepsilon_{ship} + \varepsilon_{sea}) \\ &= \sum_n \sqrt{|H(\omega_n)|^2 \cdot 2 \cdot S(\omega_n) \Delta \omega} \cos(\omega_n t + \varepsilon_{ship} + \varepsilon_{sea}) \end{aligned} \quad (6.46)$$

Equation (6.46) for heave is implemented into the MATLAB code in the enclosed CD for incident head waves. By plotting the results from the theory presented above, graphs can be made to represent the time-history of the wave-vessel interaction.



From Figure 51 it can be observed that the maximum response for the vessel in heave for a 100[s] simulation is 0.6 [m] given head waves, $H_s = 5[m]$, $T_p = 9[s]$, $\gamma = 3.3$.

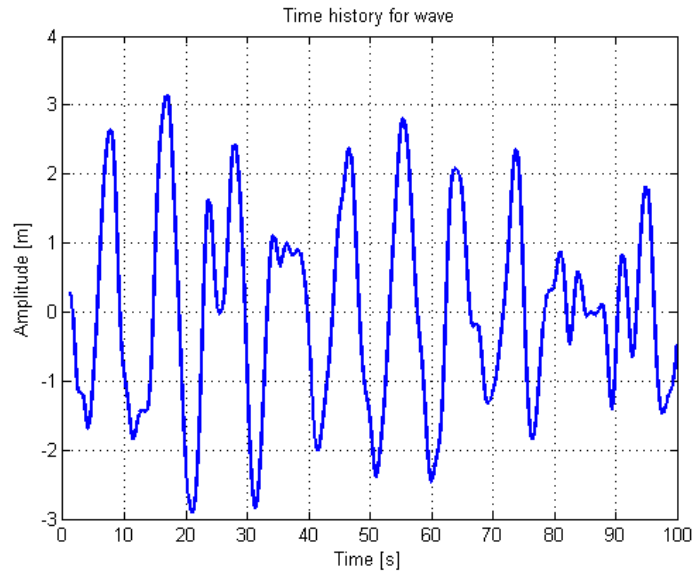


Figure 50 Time history of wave

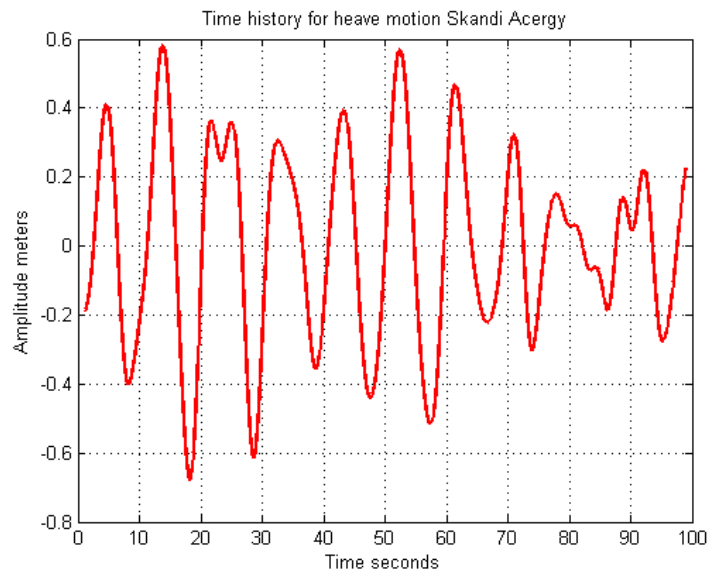


Figure 51 Time history for heave motion Skandi Acergy

Comparing Figure 51 with MOSES analysis done by Acergy (Saha, 2009), it can be concluded that implementing vessel RAO in heave for head seas, and by using a harmonic sum of waves to represent stochastic sea can provide a numerically cheap model as input in a time-integration scheme (6.6).



6.6 Newmark's method

Forced displacements are dynamic excitations important for ships and marine structures. In our case the vessel and template is subject to forced displacements caused by wave loads. Since the vessel is subject to irregular sea described by the JONSWAP wavespectrum, the differential equation can be solved numerically by using Newmark's method as indicated in (Hughes, 2008, pp. 490-500).

Generally the semidiscrete equation of motion can be written as:

$$\mathbf{M}\ddot{\mathbf{d}} + \mathbf{B}\dot{\mathbf{d}} + \mathbf{k}\mathbf{d} = \mathbf{F} \quad (6.47)$$

Where \mathbf{M} is the mass matrix, \mathbf{B} is the viscous damping matrix, \mathbf{K} is the stiffness matrix, \mathbf{F} is the vector of applied forces, $\ddot{\mathbf{d}}$, $\dot{\mathbf{d}}$ and \mathbf{d} are the acceleration, velocity and displacement respectively. To find the displacements $\mathbf{d} = \mathbf{d}(t)$ that fulfil equation(6.47), the following set of equations can be used.

$$\begin{aligned} \mathbf{M}\mathbf{a}_{n+1} + \mathbf{B}\mathbf{v}_{n+1} + \mathbf{k}\mathbf{d}_{n+1} &= \mathbf{F}_{n+1} \\ \mathbf{v}_{n+1} &= \mathbf{v}_n + \Delta t((1-\gamma)\mathbf{a}_n + \gamma\mathbf{a}_{n+1}) \\ \mathbf{d}_{n+1} &= \mathbf{d}_n + \Delta t\mathbf{v}_n + \frac{\Delta t^2}{2}((1-2\beta)\mathbf{a}_n + 2\beta\mathbf{a}_{n+1}) \end{aligned} \quad (6.48)$$

\mathbf{d}_n , \mathbf{v}_n , \mathbf{a}_n are the approximations of $\mathbf{d}(t_n)$, $\dot{\mathbf{d}}(t_n)$ and $\ddot{\mathbf{d}}(t_n)$. Equation (6.47) is the equation of motion in terms of the approximate solution, and (6.48) are finite difference formulas describing the evolution of the approximate solution. The parameters β and γ describe stability and accuracy of the algorithm under consideration. Usually average acceleration is used ($\beta = \frac{1}{4}, \gamma = \frac{1}{2}$) since it is unconditional stable, but there are also other possibilities.

Method	Type	β	γ	Stability condition
Average acceleration	Implicit	$\frac{1}{4}$	$\frac{1}{2}$	Unconditional Stable
Linear acceleration	Implicit	$\frac{1}{6}$	$\frac{1}{2}$	Conditional stable
Fox-Goodwin	Implicit	$\frac{1}{12}$	$\frac{1}{2}$	Conditional stable
Central difference	Explicit	0	$\frac{1}{2}$	Conditional stable

Table 6 Newmark's β family

There are several possible implementations, and the easiest one to implement in Matlab is considered below.



Defining predictors as:

$$\begin{aligned}\tilde{\mathbf{d}}_{n+1} &= \mathbf{d}_n + \Delta t \mathbf{v}_n + \frac{\Delta t^2}{2} (1 - 2\beta) \mathbf{a}_n \\ \tilde{\mathbf{v}}_{n+1} &= \mathbf{v}_n + (1 - \gamma) \Delta t \mathbf{a}_n\end{aligned}\quad (6.49)$$

And correctors as:

$$\begin{aligned}\mathbf{d}_{n+1} &= \tilde{\mathbf{d}}_{n+1} + \beta \Delta t^2 \mathbf{a}_{n+1} \\ \mathbf{v}_{n+1} &= \tilde{\mathbf{v}}_{n+1} + \gamma \Delta t \mathbf{a}_{n+1}\end{aligned}\quad (6.50)$$

The solution of equation (6.47) can be predicted as:

$$(\mathbf{M} + \gamma \Delta t \mathbf{C} + \beta \Delta t^2 \mathbf{K}) \mathbf{a}_{n+1} = \mathbf{F}_{n+1} - \mathbf{C} \tilde{\mathbf{v}}_{n+1} - \mathbf{K} \tilde{\mathbf{d}}_{n+1}\quad (6.51)$$

Using these predictors and correctors, and solving equation (6.51) for \mathbf{a}_{n+1} ; equation (6.48) can be solved numerically. This is done in the MATLAB code attached in the enclosed CD. The result of doing the time integration, gives Figure 52. As can be seen by the figure, the template motion and ship motion are almost exactly similar for a sea state of $H_s = 5[m]$, $T_p = 9[s]$, $\gamma = 3.3$ when using steel wire.

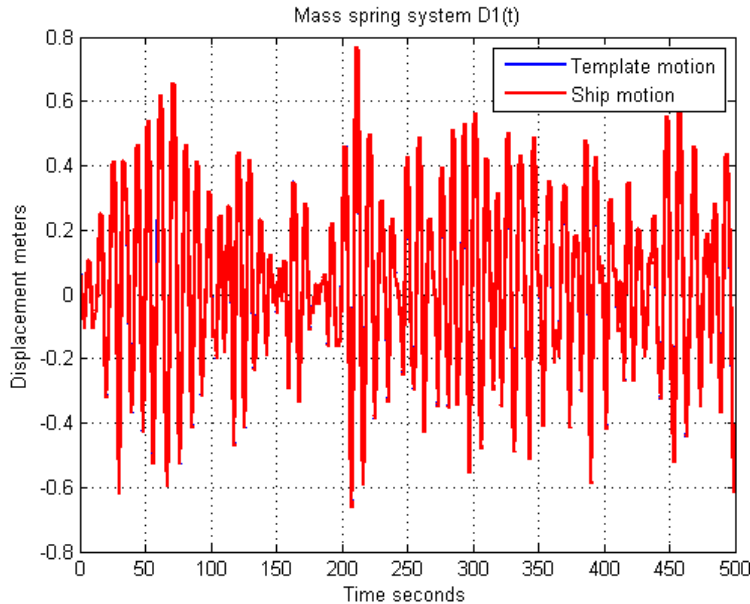
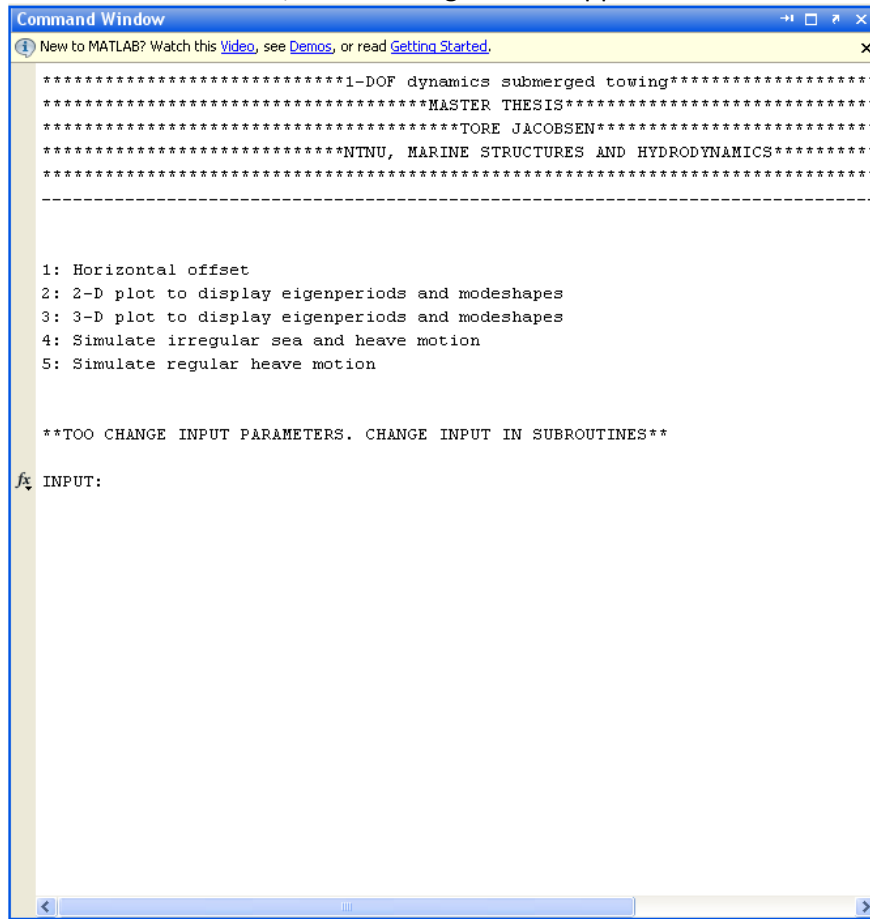


Figure 52 Steel mass spring system

The results of no relative difference between the template and ship motion was expected for steel wire and a fixed hangoff point in the moonpool. However using Newmark's method in analytical expressions is useful when introducing Dyneema fiber rope (Jacobsen, 2009) or a damped hangoff structure positioned above the moonpool.

6.7 MatLab model

The theory presented in chapter 6 is implemented in MATLAB. By running the MatLab script main.m in the command window, the following window appears.



```

Command Window
New to MATLAB? Watch this Video, see Demos, or read Getting Started.

*****1-DOF dynamics submerged towing*****
*****MASTER THESIS*****
*****TORE JACOBSEN*****
*****NTNU, MARINE STRUCTURES AND HYDRODYNAMICS*****
-----

1: Horizontal offset
2: 2-D plot to display eigenperiods and modeshapes
3: 3-D plot to display eigenperiods and modeshapes
4: Simulate irregular sea and heave motion
5: Simulate regular heave motion

**TOO CHANGE INPUT PARAMETERS. CHANGE INPUT IN SUBROUTINES**

fx INPUT:
  
```

Figure 53 MATLAB command window

By choosing an input number from 1 to 5, the different calculations presented in chapter 6 can be made. The input parameters in each calculation can be altered in the subroutines.

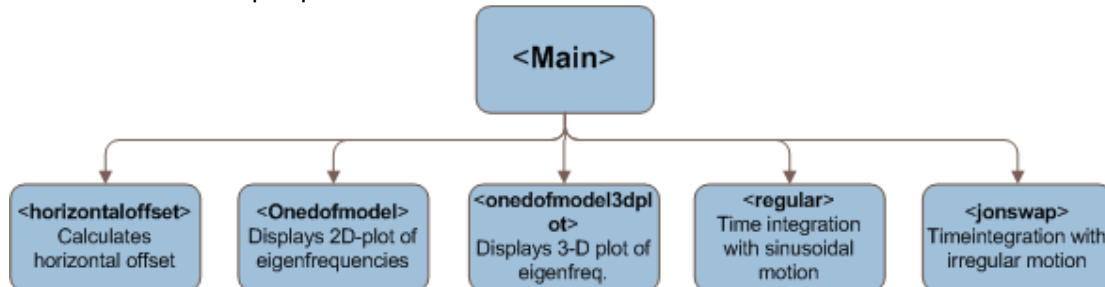


Figure 54 MATLAB flowchart



7 General description of SIMO

SIMO is a time domain simulation program developed by MARINTEK, for dynamic analysis of multibody systems. Long slender elements can be used to model the structural components of a subsea template (represented as a separate body), where each element is given distinct inertia, damping and added mass terms. Stiff connections between all slender elements are used which implies that all forces are calculated and directly transferred to the main body. The results from the program are presented as time traces, statistics and spectral analysis of all forces and motions of all bodies in the analyzed system.

SIMO is a modular and interactive computer program with batch processing options. Typical applications for SIMO are offshore crane operations, TLP installation, floating production systems and dynamic positioning systems.

7.1 Program BuildUp

According to the SIMOv3.6 user manual, the program is divided up into 6 separate modules.

- INPMOD- Input data manipulation
- OUTMOD- Output module
- STAMOD- Initial condition and static equilibrium
- DYNMOD- Dynamic response calculations
- S2XMOD- Export of time series
- PLOMOD- Plotting module

Each of the different modules communicate with each other by the layout diagram presented in Figure 55. A complete dynamic analysis must include the modules STAMOD and DYNMOD. Post processing or export of results is done by OUTMOD/S2XMOD, and graphic representations are possible by the use of the plotting program PLOMOD.

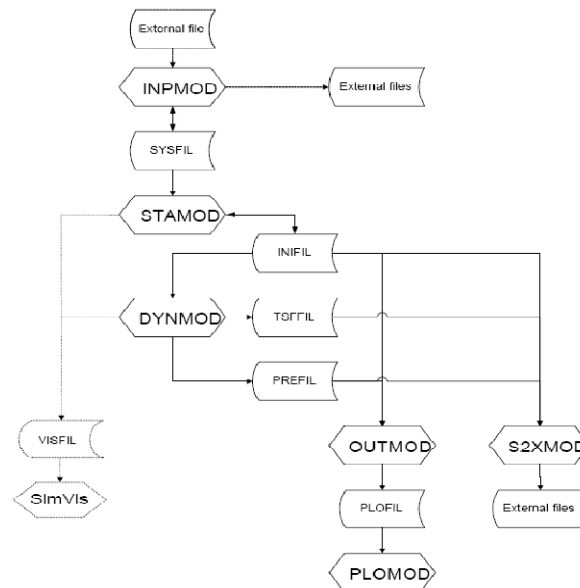


Figure 55 Layout of the SIMO program system (SIMO manual)

A brief description of the different modules in Figure 55 is made in chapter 8.5.



7.2 Fundamental hydrodynamic theory

SIMO uses strip theory for calculating potential coefficients (added mass and potential damping) and exciting hydrodynamic loads (Froude-Krylov and diffraction forces). In order to understand the simplifications and limitations made, a short description of potential theory and strip theory is presented.

7.2.1 Potential theory

Potential theory is based on the assumption that water is incompressible, inviscid, homogenous and irrotational. The velocity potential is a function of spatial coordinates; that is $\phi = \phi(x, y, z)$, or $\phi = \phi(r, \theta, z)$ and has no physical meaning itself, but combined with the assumption of irrotational flow it can be used to describe fluid velocity components.

$$u = \frac{\delta\phi}{\delta x}, \quad v = \frac{\delta\phi}{\delta y}, \quad w = \frac{\delta\phi}{\delta z} \quad (7.1)$$

Since the water is assumed incompressible, the velocity potential needs to satisfy the Laplace equation (7.2):

$$\nabla^2\phi = \frac{\partial^2\phi}{\partial x^2} + \frac{\partial^2\phi}{\partial y^2} + \frac{\partial^2\phi}{\partial z^2} = 0 \quad (7.2)$$

The pressure in the fluid can be found by using Bernoulli's equation:

$$\rho + \rho gz + \rho \frac{\delta\phi}{\delta t} + \frac{\rho}{2} |\Delta\phi|^2 = 0 \quad (7.3)$$

In addition the kinematic and dynamic free surface condition needs to be satisfied, meaning that a fluid particle stays on the free surface and the water pressure is equal to the constant atmospheric pressure on the free surface. Combining these two boundary conditions gives the linearized free surface condition on $z=0$:

$$\frac{\partial^2\phi}{\partial t^2} + g \frac{\delta\phi}{\delta z} = 0 \quad (7.4)$$

When a flow field is irrotational, thus allowing a velocity potential, there is a tremendous simplification: Instead of dealing with velocity components (u, v, w) as unknowns (hence requiring three equations for three unknowns), one can deal with the velocity potential as one unknown. When only the velocity potential needs to be determined, only one equation needs to be determined for the flow field which simplifies numerical efforts.



7.2.2 Strip theory

Strip theory is combined with two-dimensional added mass and damping coefficients by integrating these over a structures length to obtain an approximation for the three dimensional added mass and damping. The structure is divided into a finite number of strips, and as a rule of thumb, the minimum investigated wavelength should be at least five times longer than the distance between the strips. Also it is important to have the correct added mass and damping coefficients in order to correctly represent forces and moments acting on the body.

In strip theory, where added mass and damping and restoring forces are found, a structure is forced to oscillate with the wave excitation frequency in any rigid-body mode. This is described as subproblem B in (Faltinsen, 1990, p. 39). During a subsurface towing operation the forward velocity of the vessel influences the encounter frequency which is important to take into account regarding the frequency dependent added mass and damping coefficients. In Sea Loads of Ships and offshore structures (Faltinsen, 1990, p. 55) the frequency of encounter can be expressed as:

$$\omega_e = \omega_0 + \frac{\omega_0^2 U}{g} \cos \beta \quad (7.5)$$

This frequency is further described in chapter 8.6.2.

Moreover is important to beware of strip theory's limitations: Strip theory is based on potential theory, and is therefore a low Froude number theory. Consequently it should be used with caution for Froude numbers larger than 0.4. Also the theory is limited by the assumption of linearity between response and incident wave amplitude, excluding high sea states from its range of application. In addition, viscous effects are not accounted for (potential theory). Since the structural complexity and the possibility of vortex shedding and VIV of the subsea template, this may be an important source of errors (but can be represented by using correct values for quadratic damping coefficients).



7.3 SIMO theory

SIMO can be compared to a black box: numbers go in and results come out. To be able to understand, discuss and validate the results, it is important to understand the theory and which assumptions are made.

7.3.1 SIMO's objective

SIMO's main purpose is to solve equation (4.1) in (SIMO theory manual, 2008)

$$\mathbf{M}\ddot{\mathbf{x}} + \mathbf{C}\dot{\mathbf{x}} + \mathbf{D}_1\dot{\mathbf{x}} + \mathbf{D}_2\mathbf{f}(\dot{\mathbf{x}}) + \mathbf{K}(\mathbf{x})\mathbf{x} = \mathbf{q}(\mathbf{t}, \mathbf{x}, \dot{\mathbf{x}})$$

$$\begin{aligned}\mathbf{M} &= \mathbf{m} + \mathbf{A}(\omega) \\ \mathbf{A}(\omega) &= \mathbf{A}_\infty + \mathbf{a}(\omega) \\ \mathbf{A}_\infty &= \mathbf{A}(\omega = \infty) \\ \mathbf{C}(\omega) &= \mathbf{C}_\infty + \mathbf{c}(\omega) \\ \mathbf{C}_\infty &= \mathbf{C}(\omega = \infty) \equiv 0\end{aligned}\tag{7.6}$$

where:

- M** := frequency-dependent mass matrix
- m** := body mass matrix
- A** := frequency-dependent added-mass
- C** := frequency-dependent potential damping matrix
- D₁** := linear damping matrix
- D₂** := quadratic damping matrix
- f** := vector function where each element is given by $f_i = \dot{x}_i |\dot{x}_i|$
- K** := hydrostatic stiffness matrix
- x** := position vector
- q** := exciting force vector

The exciting force vector on the right-hand side of equation (7.6) is given by:

$$\mathbf{q}(\mathbf{t}, \mathbf{x}, \dot{\mathbf{x}}) = \mathbf{q}_{WI} + \mathbf{q}_{WA}^{(1)} + \mathbf{q}_{WA}^{(2)} + \mathbf{q}_{CU} + \mathbf{q}_{ext}\tag{7.7}$$

where:

- q_{WI}** := wind drag force
- q_{WA}⁽¹⁾** := 1.order wave excitation force
- q_{WA}⁽²⁾** := 2.order wave excitation force
- q_{CU}** := current drag force
- q_{ext}** := any other forces (wave drift damping, specified forces, station-keeping and coupling forces)



When the external forces have been determined in equation (7.6), and the structural mass matrix (\mathbf{M}) and stiffness matrix (\mathbf{K}) have been defined, the equation of motion can be solved by convolution integrals in the time domain with retardation functions, or alternatively by separation of motions. Separation of motions implies that the motions are separated into a high-frequency and low-frequency part. This means that the high-frequency motions are solved in the frequency domain (assumes linear responses of the structure to incident waves), and the low-frequency motions are solved in the time-domain. For a subsurface towing operation both approaches provide good solutions of the equation of motion.

As previously mentioned, SIMO's objective is to solve the equation of motion (equation(7.6)) and this is in principle the same equation which was presented in the simple analytic model in chapter 6.2. However SIMO is not limited to 1-DOF dynamics, and can therefore capture higher order dynamic effects. Also SIMO has a relative simple user interface, and it's operator is not required to directly manipulate the vectors and matrices in equation (7.6), but can follow the user manual (MARINTEK, Appendix A- System description file, 2007).

7.3.2 Environmental forces

The theory behind the environmental force models is described in chapter 3 of (MARINTEK, Theory Manual Version 3.6, 2001). The most commonly used environmental forces in SIMO are:

- Waves
- Current
- Wind

With the exception of wind, these are the environmental forces used in this thesis.

Waves

Linear wave potential theory is used where the incoming undisturbed wave field is determined by the wave potential for long-crested sinusoidal waves Φ_0 . According to Airy's theory, this wave potential can be expressed by (7.8):

$$\Phi_0 = \frac{\zeta_0 g}{\omega} C_1 \cos(\omega t - kx \cos \beta - ky \sin \beta + \phi_c) \quad (7.8)$$

where the coefficient C_1 is given by:

$$C_1 = \frac{\cosh k(z+d)}{\cosh kd} \quad (7.9)$$

k is the wavenumber and d is the water depth. From equation (7.8) velocities, accelerations, linearized dynamic pressure and surface elevation can be determined for a given time t .



As previously mentioned, to describe a sea state, different wavespectrum models can be modeled. The most common model for marine operations in the North Sea is the JONSWAP spectrum which in SIMO is defined as:

$$S_{\xi}(\omega) = \frac{5.061H_s^2g^2}{T_p^4\omega^5} (1 - 0.287\ln\gamma) \exp(-\beta(\frac{\omega_p}{\omega})^4) \gamma^{e(-\frac{(\omega/\omega_p-1)^2}{2\sigma^2})} \quad (7.10)$$

where:

α spectral paramter

ω_p peak frequency

γ peakedness parameter

β form parameter, default value $\beta = 1.25$

σ spectral parameter with default values

H_s significant wave height

T_p peak period

Also the Pierson-Moskowitz spectrum and other custom numerically defined spectra are available in SIMO.

When the wave spectrum has been defined, it can be used to calculate first and second order wave excitations forces. As previously mentioned exciting force vector on the right-hand side of equation (7.6) is given by:

$$\mathbf{q}(t, x, \dot{x}) = \mathbf{q}_{WI} + \mathbf{q}_{WA}^{(1)} + \mathbf{q}_{WA}^{(2)} + \mathbf{q}_{CU} + \mathbf{q}_{ext} \quad (7.11)$$

In SIMO the 1.order wave excitation force $\mathbf{q}_{WA}^{(1)}$ are described in the frequency domain as transfer functions between wave elevation and force.

$$\mathbf{q}_{WA}^{(1)}(\omega) = \mathbf{H}_H(\omega) \zeta_0(\omega) \quad (7.12)$$

where:

$H_H(\omega)$ hydrodynamic transfer function

$\zeta_0(\omega)$ harmonic wave component

The 2.order wave excitation force is based on assumptions regarding 2.order transfer functions (Newman method). The contributions to the 2.order wave forces originate from difference or sum frequencies resulting in mean and slowly-varying wave and drift forces. The Newman method is further described in chapter 5 of "Sea Loads on ships and offshore structures" by (Faltinsen, 1990).



Current

The current profile is defined in the wave zone by stretching the profile to the instantaneous water level. It can be described using the DNV current velocity profile or an explicitly defined profile. The expression for q_{cu} in (7.11) is defined as:

$$q_{cu}(\alpha, t) = C_1(\alpha)|u(t)| + C_2(\alpha)|u(t)|^2 \quad (7.13)$$

where:

C_1 = linear current force coefficient

C_2 = quadratic current force coefficient

u = relative velocity between low-frequency body velocity and current velocity

α = relative angle between direction of low-frequency body velocity and current velocity

7.4 Modeling capabilities

According to (MARINTEK, Appendix A- System description file, 2007) body types must be defined to represent various structures in SIMO.

Body type	Description
1	Large volume, total motion is simulated in time domain. 6 Degrees of Freedom
2	Large volume, separation of motions in frequency domain (high frequencies) motions and time domain (low frequencies). 6 degrees of freedom
3	Small volume, position dependent hydrodynamic coefficients are allowed, 3 translational degrees of freedom
4	As body type 1, but fixed of prescribed body position.

Table 7 SIMO body types

Body type 1 and 2, may be further defined as force models and can be represented by two types of elements each giving 6 D.O.F. forces on the body.

- Slender elements
- Fixed body elements

Only slender elements are used in this master thesis.



7.4.1 Slender elements

Slender elements have a large range of applications and are typically the most commonly used elements in SIMO. They may be used to model large spool pieces, jacket legs and templates where the modeled structure may consist of several slender elements. Each element is given specific properties like mass, rotation stiffness, hydrodynamic coefficients and geometric dimensions, and is divided into a specific number of strips (strip theory is described in chapter 7.2.2).

External loads on slender elements consist of buoyancy forces, wave forces and slamming forces. The resultant forces for each element, is the summation of force contribution from each strip, and total body forces is the sum of contributions from all elements.

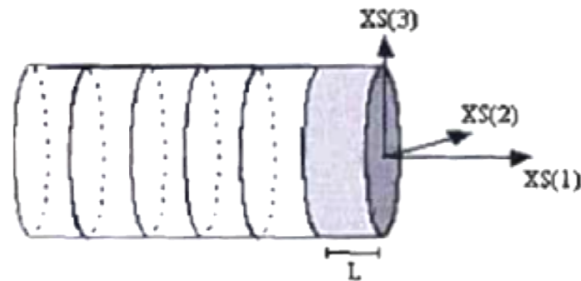


Figure 56 Slender element

Another element type in SIMO are “Fixed body elements”. These elements are similar to slender elements but have zero extension implying that concentrated forces are acting at a specified point. As for the slender element, the fixed body element is defined by hydrodynamic coefficients, volume and mass. These elements are often used when modeling vertical hydrodynamic coefficients for structures lowered through the splash zone.



7.4.2 Coupling forces

SIMO offers three main alternatives to represent coupling forces between bodies, where a simple wire coupling is the most common method. The simple wire coupling is modeled as a linear spring attaching two bodies. Since the position is known for each line end, the elongation and tension can be determined.

$$\Delta l = \frac{T}{k} \quad (7.14)$$

where:

Δl = elongation

T = wire tension

k = effective axial stiffness

The effective axial stiffness is given by:

$$\frac{1}{k} = \frac{l}{EA} + \frac{1}{k_0} \quad (7.15)$$

where:

E = modulus of elasticity

A = cross section area

l = unstretched wire length

$1/k_0$ = connection flexibility (crane flexibility)

To determine the tension in the wire coupling, the position of each line end and wire damping C_w needs to be calculated. When these are known, the wire tension can be calculated by (7.16).

$$F = \frac{C_w \Delta l}{l \Delta t} \quad (7.16)$$



8 SIMO modeling procedure

The transit phase of the subsurface towing operation is modeled in SIMO. Once a correct representation of the suspended load and towing configuration is made, parametric studies regarding towing velocities, wave conditions, sling setup and damping sources can be made.



Figure 57 Subsurface towing SIMVIS

Two bodies were modeled in SIMO: the ITS (modeled as slender elements) and the vessel (Skandi Acergy). Acergy Norway have provided an example system description file for a lifting operation with Skandi Acergy, which is altered to represent a subsurface towing operation of a template.



8.1 Environmental conditions

Waves

The environmental conditions defined in the system description file are regular cosines waves. In the system description file; “waveamp” defines the wave amplitude and “waveper” the waveperiod. “Dir” represents the wave direction and is set to 180(degrees) to represent head sea.

```

'*****
ENVIRONMENT DATA SPECIFICATION
'*****
'txenv (3)
regular wave conditions
H = xx T = xx
Heading: Head Sea
-----
REGULAR WAVE SPECIFICATION
-----
'chrewa
WR200645
'nregwa
1
wavamp wavper phase dir
  2.5    10.    0.   180.
-----

```

Figure 58 Wave Conditions System Description file

Syntax	Description
NREGWA	Number of regular waves
WAVEAMP	Wave amplitude [m]
WAVPER	Wave period [s]
PHASE	Phase angle according to theory manual [deg]
DIR	Wave propagation direction [deg]

Table 8 Environment data specification



Current

To simulate the horizontal translation of the vessel; current is implemented into the SIMO model. Depending on the analysis, the current is altered between 0 and 2.57 [m/s]. The current direction ('curdir') is set to 180 degrees (head current). Different values of current can also be specified at different water depths, but for simplicity a uniform current is used in this thesis.

```

-----
CURRENT SPECIFICATION
-----
'chcurr
CURDUM
'ncur
1
curvel curdir curlev
2.5 180. 0.
*****

```

Figure 59 Current Conditions System Description file

Syntax	Description
NCUR	Number of current levels
CURVEL	Current velocity [m/s]
CURDIR	Current direction [deg]
CURLEV	Global Z-coordinate of current level [m]

Table 9 Current specification

8.2 Skandi Acergy in SIMO

The ship is defined as body type 1 (see chapter 7.4), which is a large volume body where total motion is simulated in the time domain. The body has 6-Degrees of Freedom and different data groups are assigned to the body in accordance with (MARINTEK, Appendix A-System description file, 2007).

- Body location data
- Body mass data
- Time dependent mass
- Hydrostatic stiffness data
- First order wave force transfer function

Body location data

This is the position of the body's origin in the global coordinate system. This position may be modified in STAMOD.

```

-----
BODY LOCATION DATA
-----
'
XGLOB  YGLOB  ZGLOB  PHI  THETA  PSI
.0000E+00 .0000E+00 .0000E+00 .0000E+00 .0000E+00 .0000E+00
-----

```

Figure 60 Body Location Data System Description File

XGLOB, YGLOB and ZGLOB are the global coordinates of the origin of the body, and PHI, THETA and PSI are the Euler angles of rotation around the three axes respectively.

Syntax	Description
XGLOB, YGLOB, ZGLOB	Global coordinates of body origin [m]
PHI, THETA, PHI	Euler angles of rotation around axis [deg]

Table 10 Body location data



Body mass data

The body mass data identification line represents the centre of gravity, the body mass, inertia, and added mass.

```

=====
BODY MASS DATA
=====
TXMASS
Imported from 'm2782b.out
+ by solaas on moses.marintek.sintef.no - 15-Jan-2008 11:02:20
XCOG      YCOG      ZCOG
.1221E+00 .0000E+00 .5062E+01
.1221E+00 .0000E+00 .425E+01
=====
MASS COEFFICIENTS
=====
          RM      RIXX      RIYX      RIYY      RIZX      RIZY      RIZZ
1.69E+04 1.719E+05 2.091E+07 - .0000E+00 .2397E+08 .1062E+05 - .0000E+00 .2353E+08
1.69E+04 1.93E+06 0.00E+00 2.35E+07 8.78E+03 0.00E+00 2.31E+07
=====
ADDED MASS INFINITE
=====
          AMi1      AMi2      AMi3      AMi4      AMi5      AMi6
.3147E+03 .0000E+00 .7365E+03 .0000E+00 .8377E+05 .0000E+00
.0000E+00 .3797E+04 .0000E+00 -.1803E+05 .0000E+00 .8022E+04
.7355E+03 .0000E+00 .3346E+05 .0000E+00 .2296E+06 .0000E+00
.0000E+00 -.1799E+05 .0000E+00 .5269E+06 .0000E+00 .2462E+06
.8366E+05 .0000E+00 .2296E+06 .0000E+00 .3036E+08 .0000E+00
.0000E+00 .8071E+04 .0000E+00 .2477E+06 .0000E+00 .5327E+07
=====

```

Figure 61 Body Mass Data System Description File

Values for the centre of gravity and mass coefficients are obtained from previous analysis done by Acergy. The “ADDED MASS INFINITE” identification line represents that the added a mass matrix for infinite frequencies is specified.

Syntax	Description
XCOG, YCOG, ZCOG	Coordinates of centre of gravity (m)
RM	Mass (tonne)
RIXX, RIYX, RIYY, RIZX, RIZY, RIZZ	Mass moment of inertia about origin (tonne*m ²)
AMi1, AMi2, AMi3, AMi4, AMi5, AMi6	Added mass force in DOF i due to a unit acceleration in dof (1,2,3,4,5,6) [tonne, tonne*m, tonne*m ²]

Table 11 Body mass data



Time dependent mass

The data group “Time Dependent Mass” (TDM) allows the user to model the effects of a mass that can vary both in magnitude and in position. This can be useful in simulation of operations involving ballasting or de-ballasting, such as heavy-lift operations. Ballasting can be accurately modeled since free surface effects are accounted for. For Skandi Acergy, it is useful to have a ballast tank on the starboard side to maintain stability while using the 400 [Te] crane on deck. However since this crane is not used during this marine operation, the amount of ballast water is set to a minimum and neglected.

```

-----
TIME DEPENDent MASS
-----
CTDMTY NTTMD IHLA
POINT 4 0
XTDM YTDM ZTDM MAS0 MASMAX MASMIN MRATMAX MRATMIN
-38.15 -13 10 100 100 50
TIME FLOW
0 0
357 -0.403636
907 0.31111
1357 0
-----

```

Figure 62 Time Dependent Mass System Description File

The position of the time dependent mass, mass/volume flow rate is defined in accordance with (MARINTEK, Appendix A- System description file, 2007).

Syntax	Description
CTDMTY	Time dependent mass type (point mass or tank)
NTTMD	Number of time steps for which the mass/volume flow is given
IHLA	HLA control parameter. 1=imported data, 0=specified in description file
XTDM,YTDM,ZTDM	Position of time dependent mass in local system [m]
MAS0,MASMAX,MASMIN	Mass at initial time [tonne], maximum allowable mass [tonne], minimum allowable mass [tonne] respectively
MRATMAX, MRATMIN	Maximum/minimum allowable mass rate [tonne]

Table 12 Time dependent mass



Hydrostatic stiffness data

Hydrostatic stiffness and linear damping data of the vessel can be imported from a VERES analysis. Since potential damping for the vessel in roll is low, linear and quadratic damping is included to account for skin friction. The damping coefficients in roll are of great importance in beam sea conditions, but since our operation is in head sea; these can be neglected.

```

-----
STIFFNESS REFERENCE
-----
      XREF      YREF      ZREF      RPHI      RTHETA      RPSI
-----
      .0000E+00  .0000E+00  .0000E+00  .0000E+00  .0000E+00  .0000E+00
-----
LINEAR STIFFNESS MATRIX
-----
      KMATi1    KMATi2    KMATi3    KMATi4    KMATi5    KMATi6
-----
      0.0000E+06  .0000E+00  .0000E+00  .0000E+00  .0000E+00  .0000E+00
      .0000E+00  0.0000E+06  .0000E+00  .0000E+00  .0000E+00  .0000E+00
      .0000E+00  .0000E+00  .3308E+05  .0000E+00  .2093E+06  .0000E+00
      .0000E+00  .0000E+00  .0000E+00  .3990E+06  .0000E+00  .1057E+01
      .0000E+00  .0000E+00  .2093E+06  .0000E+00  .4405E+08  .0000E+00
      .0000E+00  .0000E+00  .0000E+00  .1057E+01  .0000E+00  0.0000E+10
-----
LINEAR DAMPING
-----
      TXDPL
Sum of damping from Wamit and Retardation function calculations
-----
      DLi1      DLi2      DLi3      DLi4      DLi5      DLi6
-----
      .0000E+00  .0000E+00  .0000E+00  .0000E+00  .0000E+00  .0000E+00
      .0000E+00  .1090E+01  .0000E+00  .0000E+00  .0000E+00  .0000E+00
      .0000E+00  .0000E+00  .0000E+00  .0000E+00  .0000E+00  .0000E+00
      .0000E+00  .0000E+00  .0000E+00  .5000E+05  .0000E+00  .0000E+00
      .0000E+00  .0000E+00  .0000E+00  .0000E+00  .0000E+00  .0000E+00
      .0000E+00  .0000E+00  .0000E+00  .0000E+00  .0000E+00  .5289E+04
-----

```

Figure 63 Hydrostatic Stiffness Data System Description File

Syntax	Description
XREF,YREF,ZREF	Global coordinates of body origin [m]
RPHI,RTHETA,RPSI	Euler angle of rotation about axis [deg]
KMATij	Restoring force in DOF i, due to a unit displacement in DOF j [N/m, N, Nm]
DLij	Linear damping forces in dof i due to a unit velocity in DOF j, [Ns/L, Ns, Nsm]

Table 13 Stiffness and damping reference



First order wave force transfer functions

To model the motion of the vessel, transfer functions (RAO) are needed. Using ordinary motion RAO's in SIMO make the analyses uncoupled. This means that the wave induced motion of the vessel is not influenced by the towed structure. In reality, the towed structure will restrict the vessel motion and tend to dampen the vessel motion. In order to enable coupled analyses, force transfer functions are defined.

```

=====
FIRST ORDER WAVE FORCE TRANSFER FUNCTION
=====
' TXFO1
Imported from '/local/moses/i/p550147/sysgen/m2782b.3
+ by solaas on moses.marintek.sintef.no - 15-Jan-2008 11:02:20
'   NFODIR   NFOFRE   IFOSYM   ITYPIN
    17       38         0         2
=====

```

Figure 64 Transfer Functions System Description File

Syntax	Description
NFODIR	Number of directions
NFOFRE	Number of frequencies
IFOSYM	Symmetry code. 0=No symmetry
ITYPIN	Code for which format the transfer functions are given in. 2=amplitude ratio and phase (deg).

Table 14 Wave force transfer function

In our case, the force transfer functions are defined for 17 directions (NFODIR), 38 frequencies (NFOFRE), with phase angels in radians (ITYPIN 2). The transfer function data is directly included in the system description file. An example excerpt of a transfer function is shown in Figure 65.

```

=====
SURGE FORCE TRANSFER FUNCTION
=====
'   IDIR   IFREQ   ampl   phase
    1       1   .4241E+03   .9521E+02
    1       2   .5465E+03   .9463E+02
    1       3   .7279E+03   .9413E+02
    1       4   .1007E+04   .9377E+02
    1       5   .1200E+04   .9367E+02
    1       6   .1437E+04   .9373E+02
    1       7   .1654E+04   .9405E+02
    1       8   .1765E+04   .9440E+02
    1       9   .1819E+04   .9465E+02
    1      10   .1871E+04   .9497E+02
    1      11   .1919E+04   .9539E+02
    1      12   .1962E+04   .9591E+02
    1      13   .1997E+04   .9658E+02
    1      14   .2023E+04   .9742E+02
    1      15   .2035E+04   .9849E+02
    1      16   .2031E+04   .9984E+02
    1      17   .2007E+04   .1015E+03
    1      18   .1999E+04   .1019E+03
    1      19   .1957E+04   .1037E+03
=====

```

Figure 65 Transfer function Example System Description File

Syntax	Description
IDIR	Direction number
IFREQ	Frequency number. Where each number relates to a predefined frequency
AMPL	Wave amplitude [m]
PHASE	Phase angle [deg]

Table 15 Transfer function input

8.3 GjØa ITS in SIMO

Slender elements can be used to model the structural components of the subsea template (represented as a separate body), where each element is given distinct inertia, damping and added mass terms. Stiff connections between all slender elements are used which means that all forces are calculated and directly transferred to the main body.

As an example; a suction anchor is considered. Since the suction anchors on the template are critical with respect to added mass and drag components, they are carefully modeled using slender elements to represent hydrodynamic components.

```

-----
SLENDER ELEMent
-----
'Suction      Anchor  1      in      XY      direction
      vol      mass      ifoadd  ivol     iwdhf     nstrip
      0.314    0         1       1       2         7
      xel1     yel1     zel1     xel2     yel2     zel2     xref     yref     zref
      9.87     6.25    -1.465  9.87     6.25    -8.465  9.87     0       -1.465
      C2X     C2Y     C2Z     C1X     C1Y     C1Z     AMX     AMY     AMZ
      0       0.725   0.725   0       0       0       29.70   29.70   29.70
  
```

Figure 66 Slender element of suction anchor system description file

Syntax	Description
Vol	Specific volume (cross section area) of element [m ²]
MASS	Distributed mass of element [tonne/m]
IFOADD	Parameter defining wave integration method. IFOADD=1 means the force is integrated to actual wave elevation
IVOL	Parameter for load types.
IWDHF	Include wave particle velocity and acceleration. IWDHF=2 means that velocity and acceleration is included
NSTRIP	Number of strips
xel1, yel1, zel1	x,y,z coordinates end point 1 [m]
xel2, yel2, zel2	x,y,z coordinates end point 2 [m]
xref, yref, zref	These coordinates are used to specify the orientation of the local XY-plane of the slender element.
C2X, C2Y, C2Z	Quadratic longitudinal drag coefficient (damping) [kN*s ² /m ³]
C1X, C1Y, C1Z	Linear longitudinal drag coefficient [kN*s/m ²]
AMX, AMY, AMZ	Longitudinal and transverse added mass coefficients [tonne/m]

Table 16 Slender element description

The coordinates of each slender element can easily be determined from technical drawings of the template; however the hydrodynamic coefficients are more tedious to decide. This is due to the fact that fixed values for quadratic drag coefficients are hard to determine (dependent on flow characteristics).



Linear longitudinal drag coefficients can be neglected since it is assumed that linear damping is low (no waves are generated by the template during towing). Quadratic drag coefficients are calculated from the force expression (8.1):

$$F_d = C_d \frac{1}{2} \rho A U_R^2 \quad (8.1)$$

The values for drag coefficients for a circular cylinder C_d are taken from hydrodynamic experimental reports prepared by (Øritsland, 1989). In Figure 67 one of these experimental results are shown. Since the diameter and incident fluid velocity of the suction anchors are relative large ($D=5[m]$), the flow is in the post-supercritical regime with $Re > 3 \times 10^6$. For the suction anchors C_d is approximated to be: $C_d=0.3$ for all 4 suction anchors. Assuming a stationary value for C_d is an approximation since shielding effects, vortex shedding and wake caused by the suction anchors will affect the flow regime around the structural components.

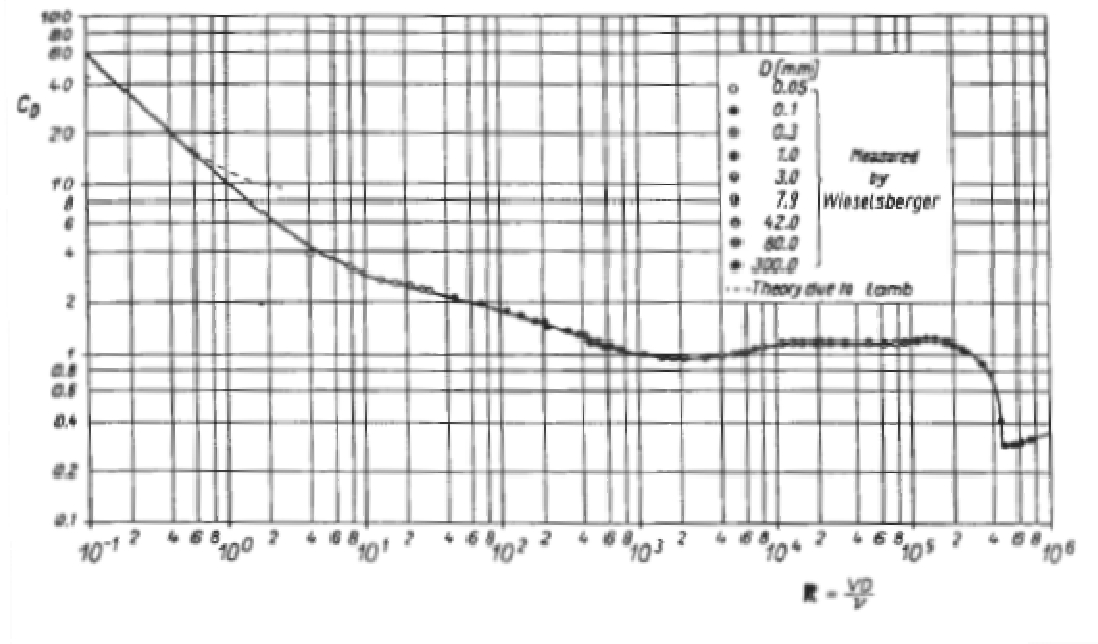


Figure 67 Drag coefficient for circular cylinders as function of Reynolds number (Øritsland,1989)

To calculate the quadratic drag coefficients C_{quad} (C_{2X}, C_{2Y}, C_{2Z}) equation (8.2) is used.

$$C_{quad} = C_d \frac{1}{2} \rho D \quad (8.2)$$

This is necessary for all slender elements in all directions.



By using experimental data for cylinders by (Øritsland, 1989), a very detailed model of the subsea template can be made which can be seen in Figure 68.



Figure 68 Template visualization in SIMVIS

From Figure 68, it can be seen that the volume of the suction anchors is not correctly visually represented. The reason for this is that volumes in SIMO represent buoyancy forces, and since the suction anchors are filled with water the correct buoyancy is mathematically modeled. This visualization problem is solved using a surface skin (*.wrl file) which is placed on top of the slender elements to represent a more sophisticated graphical visualization.



8.4 Rigging in SIMO

The lifting wire and rigging is represented by SIMO's "Simple and multiple wire couplings".

```

*****
      COUPLING      DATA
      Single crane lift
      -----
      CHCPL
      SLING1
      wire from plate to hook
      -----
      SIMPLE WIRE COUPLING
      ----- sling 1 ==
      sling 6x36IWRC, DIA 90mm,
      CHBDY1 XBDY YBDY ZBDY
      HOOK 0 0 0
      CHBDY2 XBDY YBDY ZBDY
      ITS 8.401 4.181 0.48
      EA Rlen Flexc Dampsw irect ehla
      6.12E+05 17.801 0.00E-03 1.00E+03 0 0 0
      IEMOCO FTIME RTENS
      0
*****

```

Figure 69 Simple wire coupling system description file

Two different wire types are used during the operation. The lifting wire has diameter $D=122$ [mm] and the slings have diameters $D=90$ [mm].

Syntax	Description
CHBDY1, CHBDY2	Identifier for body 1 and 2 respectively
XBDY1,YBDY1,ZBDY1	Coordinates of coupling connection point in body fixed coordinate system [m]
EA	Wire cross section stiffness [kN]
RLEN	Initial, un-stretched wire length [m]
FLEXC	Connection flexibility [m/kN]. This is used to model crane tip flexibility. In our case this is set to 0.
DAMPSW	Material damping [kN*s] See equation(7.16).
IREST	Flag for "Restoring coupling", only used in STAMOD
EHLA	HLA export flag for simplified wire. 0=no export
IEMOCO	Failure mode of coupling element, 0=no failure
FTIME	Earliest possible time of failure [s]
RTENS	Breaking strength [kN]

Table 17 Simple wire coupling system description file



8.5 Running SIMO

When the system description file is created, a static and dynamic analysis of the system can be simulated. The static analysis in STAMOD is done in order to find equilibrium positions and create an initial condition file. Moreover, the dynamic analysis is done in DYNMOD to calculate the response and forces acting on the system during environmental loads. The settings used in the analysis steps are attached to the CD in this report in the form of macrofiles:

- STA.mac
- DYN.mac
- OUT.mac
- S2X.mac

STAMOD

Using the pre-generated batch file, STA.MAC, the system description file is read. Equilibrium positions is calculated, and stored in the print file, prs.lis. An initial condition file INI.SAM is created and is further used in DYNMOD.

DYNMOD

By running the batch file, DYN.MAC, DYNMOD can read the initial condition file, and set the simulation and storage parameters necessary for a time domain simulation. Time step is set to $\partial t = 0.1$ and the number of subdivisions for each step is set to 30 for high accuracy. Only some results are stored to the file prd.lis, dependent on further export to S2XMOD.

Before initializing the dynamic analysis, 2000 time steps are chosen, giving a simulation length of 200[s]. The Runge-Kutta method is applied using constant averaged acceleration, and when the analysis is done, a visualization file vis.lidat is stored to be viewed in SimVIS.

OUTMOD

This module is used to export time series and generate plots from the results in DYNMOD. OUTMOD is run by using the pre-generated batch file OUT.mac. The results of interest are vessel movement, template movement and coupling forces. Also the deflection angle (horizontal offset) is plotted as a function of time. All the results from different analysis are on the CD attached to this report.

S2XMOD

This module is used to extract statistics of the time series found in the simulations and is helpful when extracting time series to MATLAB form. This is especially essential when accurately determining values from the time series.



Visualization/Post processing

Results from the static analysis (STAMOD) and the dynamic analysis (DYNMOD) are stored in the VISFIL, which is necessary for visualization in SimVis. All bodies modeled in SIMO and couplings are visualized in addition to stationary bodies such as the seafloor. A movie of the simulations can be seen in the enclosed CD.

In order to use SimVis a .svp-file needs to be made. This file (Gjoa ITS.svp) is the project file that contains the main input to SimVis (bodies to be visualized and data location). The vessel, template, free surface and seafloor are visualized by adding predefined texture files to represent the different bodies. These geometry files (.wrl files) are given by Acergy Norway and can be seen in Figure 70.

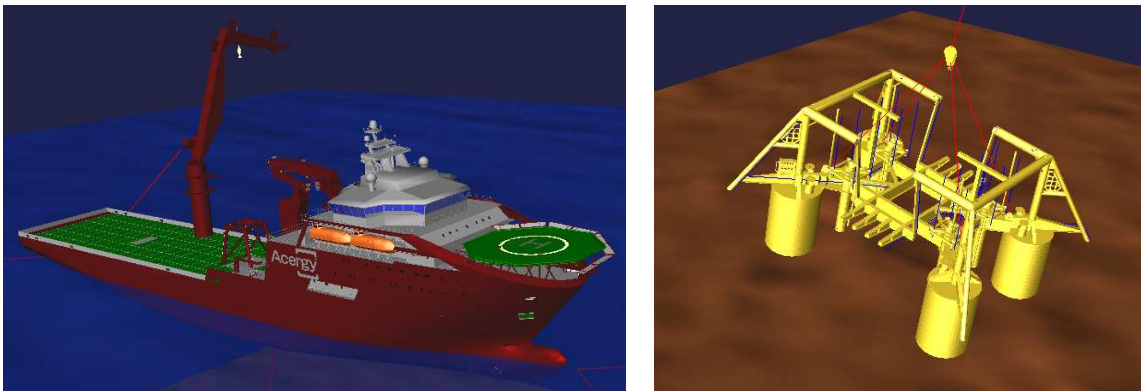


Figure 70 Visualization files

The lifting cable and slings are also simulated in SimVis, and numerical values are indicated by using inbuilt trend plots. Trend plots are defined for the lifting cable, and the 4 slings connecting the hook to the template. Hence, SimVis makes it possible to give a graphic representation of the time-domain simulation and at the same time provide real-time coupling forces. SimVis is therefore a nice tool to verify the simulation physics and dynamics of the operation.



8.6 Post processing in SIMO

In these analyses the only environmental conditions acting on the system is current, which represents the forward velocity of the vessel during the transit phase. The template is towed in the X-direction (longitudinal) in this analysis, meaning that it is towed in the direction indicated in Figure 71.

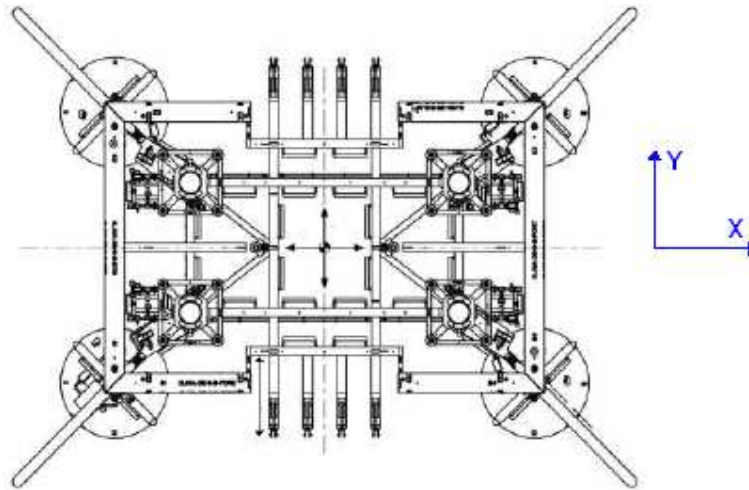


Figure 71 Template Aerial View (Acergy)

It is easy to change the towing configuration in SIMO, and also analyze a tow in the Y-direction (transverse). A tow in the Y-direction implies a greater uncertainty since the vortex shedding of the forward suction anchors influences the flow characteristics on the rear suction anchors. These viscous effects are hard to capture in SIMO, and therefore this towing configuration is avoided in this thesis.

Nevertheless, towing the template in the Y-direction is an interesting concept. Since the main contributors to drag is caused by the suction anchors, and the turbulent flow caused by the forward suction anchors reduce the drag on the rear anchors; one could easily conclude that this is the best solution with respect to drag forces. However it is also important to keep in mind that also the projected area of the template incident to the current increases, and hence increases the drag forces. It is thus important to do a detailed analysis, and/or a model experiment to decide which towing configuration is preferred. For the Gjøa ITS, this has been done by (Eilertsen, 2008) and the conclusion from this report is that towing the template in the X-direction is marginally better with regard to stability and hydrodynamic forces. Towing in the X-direction is therefore the towing configuration further examined in this thesis.



8.6.1 Exclusion of regular waves

For towing in the X-direction with no incident waves to the vessel, the following example plots can be made by extracting data from S2XMOD in SIMO.

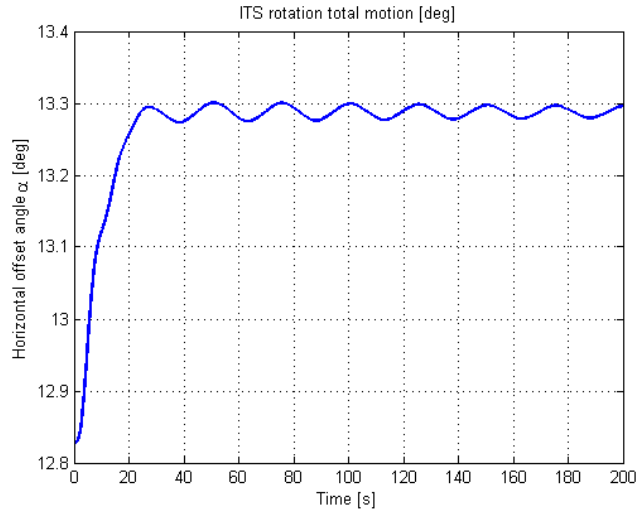


Figure 72 Horizontal offset angle for U=5[knots]

As can be seen in Figure 72 the offset angle α reaches a stationary values of 13.3 [deg] when the system reaches its equilibrium condition and imposed to a towing velocity U=5[knots].

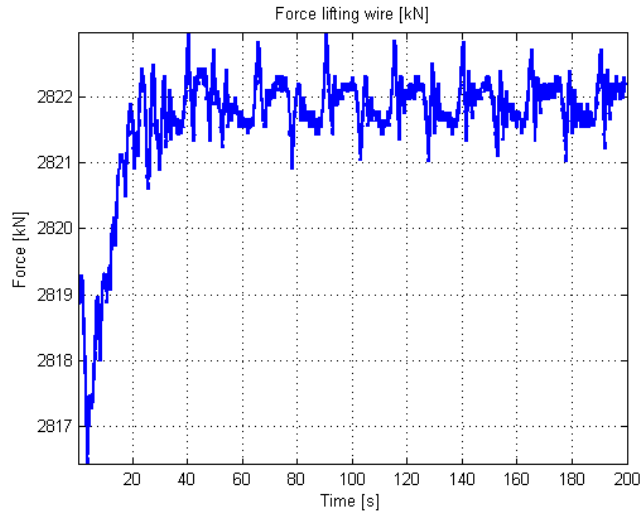


Figure 73 Hook total force lifting wire for U=5 [knots]

The total force in the hoisting cable reaches a value of 2822 [kN] when the system is subject to a uniform current with U=5[knots] and no waves. This means that the tension in the lifting wire increases with 225 [kN] compared to the systems static weight in water and these results are in accordance with experimental values obtained by (Eilertsen, 2008).



8.6.2 Inclusion of Regular Waves

The SIMO analysis can also be done with waves present. When using current for modeling the surge motion the ship, leaving the ship itself stationary: the wave frequency needs to be altered. This is because of the important frequency of encounter changes. According to (Faltinsen, 1990), the frequency of encounter can be written as:

$$\omega_e = \omega_0 + \frac{\omega_0^2 U}{g} \cos(\beta) \quad (8.3)$$

Where β is the general heading angle between the vessel and the wave propagation direction. In (8.3), $\beta = 0^\circ$ in head seas. $\beta = 90^\circ$ in beam seas and $\beta = 180^\circ$ in following seas.

Doing these calculations for different towing velocities U, and wave periods T_0 gives Table 18.

	U=0[knots]	U=1[knots]	U=2[knots]	U=3[knots]	U=4[knots]	U=5[knots]
T_o=9 [s]	T _e =9.00 [s]	T _e = 8.68 [s]	T _e = 8.39 [s]	T _e = 8.11 [s]	T _e = 7.85 [s]	T _e = 7.60 [s]
T_o=10 [s]	T _e =10.00 [s]	T _e = 9.68 [s]	T _e = 9.38 [s]	T _e = 9.10 [s] [s]	T _e = 8.83 [s]	T _e = 8.58 [s]
T_o=11 [s]	T _e =11.00 [s]	T _e = 10.68 [s]	T _e = 10.38 [s]	T _e = 10.10 [s]	T _e = 9.82 [s]	T _e = 9.56 [s]
T_o=12 [s]	T _e =12.00 [s] [s]	T _e = 11.68 [s]	T _e = 11.38 [s]	T _e = 11.09 [s]	T _e = 10.81 [s]	T _e = 10.55 [s]

Table 18 Period of encounter

Using the data in Table 18, analysis can be done for varying wave periods T_0 , towing velocities U and wave heights (3[m], 5[m]). The results from all 30 SIMO analyses are attached on the CD and represent the time-history for:

- Vessel ZG translation Total motion (m)
- Vessel XL rotation Total motion (deg)
- Vessel YL rotation Total motion (deg)
- ITS XG translation Total motion (m)
- ITS YG translation Total motion (m)
- ITS ZG translation Total motion (m)
- ITS XL rotation Total motion (deg)
- ITS YL rotation Total motion (deg)
- ITS ZG rotation Total motion (deg)
- Lifting wire Total force (kN)
- Sling 1,2,3,4 Total force (kN)
- Moonpool translation XG (m)
- Moonpool translation YG (m)
- Moonpool translation ZG (m)

As previously mentioned, the forces in the lifting wire are of interest. For a more detailed analysis, the following properties are extracted from the lifting wire forces for further processing.



- Maximum force in wire F_{max}
- Average force in wire F_{avg}
- Force amplitude in wire F_{amp}

Maximum force in wire F_{max}

The maximum force in the wire represents the magnitude of the static+dynamic load. Finding the maximum force in the wire is important when evaluating the necessary dimensions of the wires needed for the operation. Also the maximum force in lifting wire is important to determine if the operation is safe with respect to the ultimate limit strength of the hangoff structure.

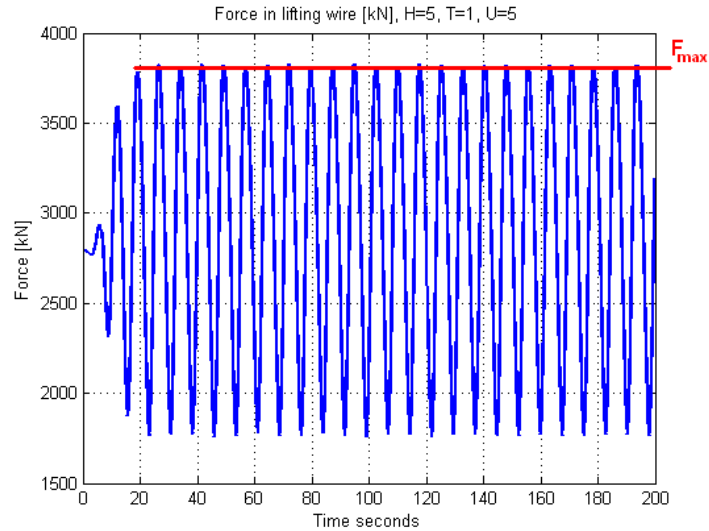


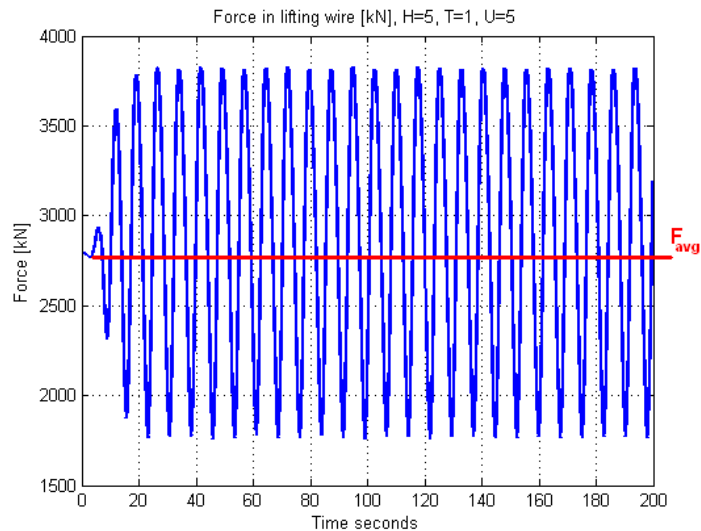
Figure 74 Maximum force in lifting wire

The maximum force is found by extracting the largest value from the data samples, after removing “outliers”. Outliers are data samples that deviate significantly from the majority of data samples. Chauvenet’s (Taylor, 1997, pp. 166-169) criterion states: “If the expected number of measurements is at least as deviant as the suspect measurement is less than one-half, then the suspect measurement should be rejected.” Chauvenet’s criterion should be used if longer (3-hous simulations with irregular sea) is done.

Average force in lifting wire F_{avg}

The average force in the lifting wire represents the static force + average dynamic force in the wire and is useful in fatigue calculations. The average force is found by adding all data samples and dividing by the number of data samples in the analysis (‘mean’ function in Matlab).

$$F_{avg} = \sum F_t / n_{data} \quad (8.4)$$



The average force for all the runs are assembled in graphs, showing how the average force changes with different towing velocities.



Force amplitude in wire F_{amp}

The force amplitude F_{amp} in the lifting wire is important for the dynamic loads acting in the wires. These values are of great significance since large dynamic loads implicate a greater possibility of fatigue in the system.

The force amplitude is calculated from time-domain results where 3 of greatest and smallest values is extracted and divided by sum of these values.

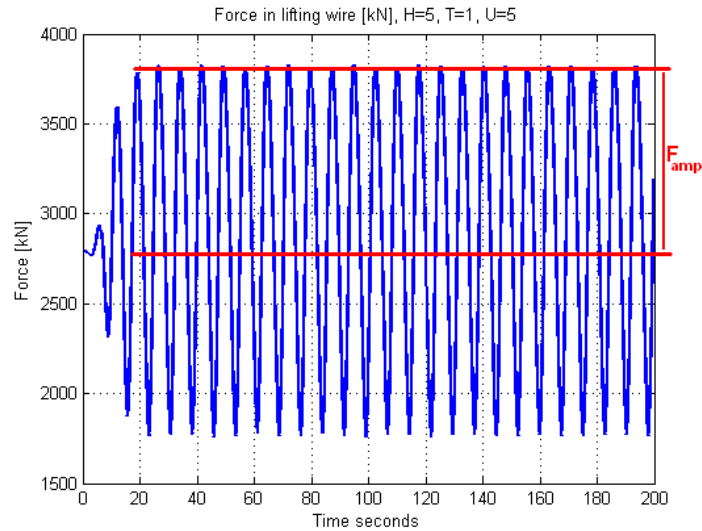


Figure 75 Force amplitude in lifting wire

$$F_{amp} = \frac{F_{max} - F_{min}}{2} = \frac{(F_{max1} + F_{max2} + F_{max3}) - (F_{min1} + F_{min2} + F_{min3})}{6} \quad (8.5)$$

If the force amplitude is larger than the average force in lifting wire F_{avg} , snatch loads may occur.



All results from the time-domain analyses in SIMO are attached to the CD. Since numerous analyses for different sea states have been done, only the extreme conditions namely when the vessel is subject to wave heights $H=5[m]$, and wave period $T=9[s]$ and $T=12[s]$ is further presented in this report in order to reduce the number of plots.

For a towing velocity of $U=5[knots]$, the following figures can be made:

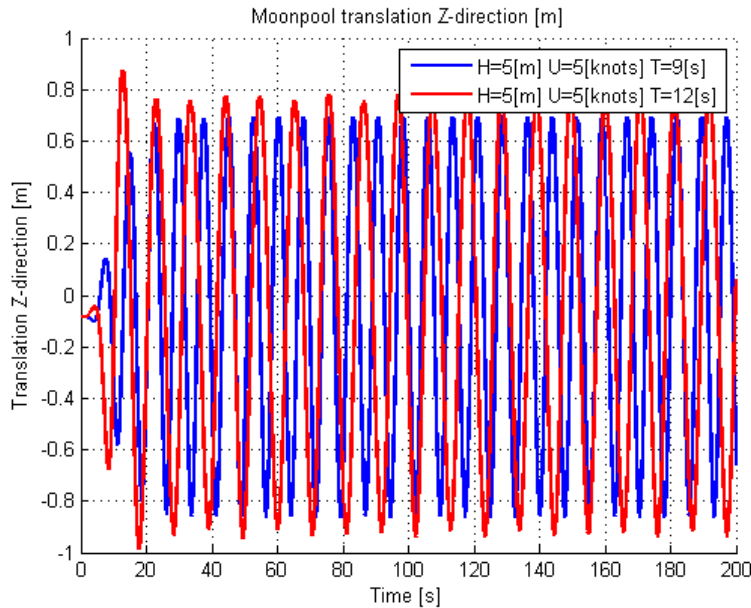


Figure 76 Moonpool translation vertical direction

It can be seen that the amplitude of the moonpool translation is similar for both wave periods, however the forces acting in the lifting wire differ due to the increased frequency of oscillation (Figure 77).

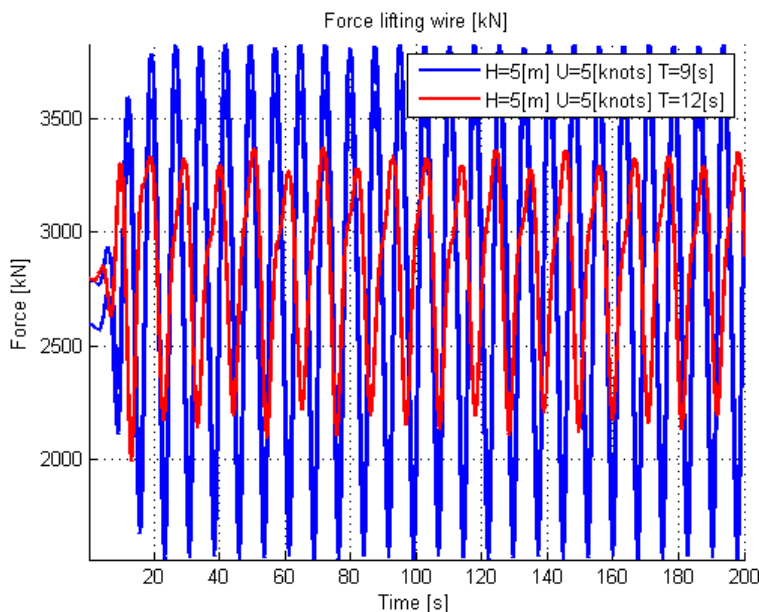


Figure 77 Forces in lifting wire

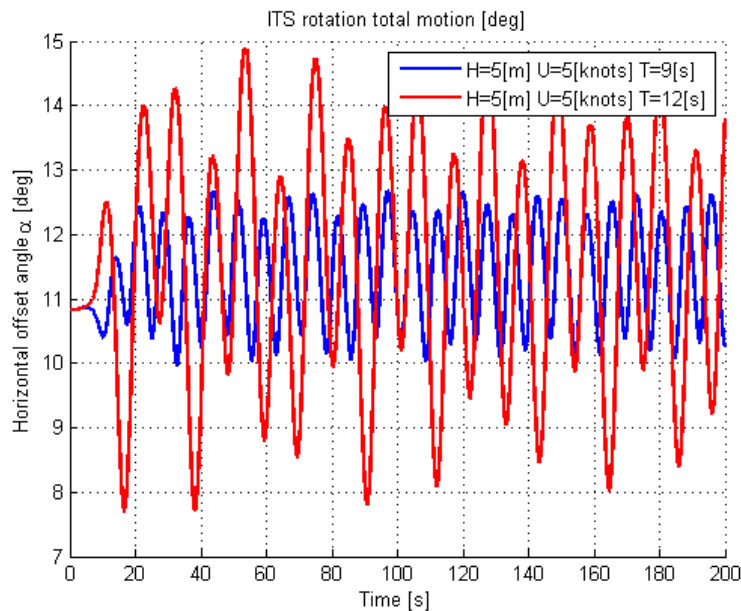


Figure 78 Horizontal offset angle

At a towing velocity $U=5$ [knots], a wave period of $T=9$ [s] is the worst condition with respect to lifting wire forces. However, a wave period of $T=12$ [s] is worst with respect to horizontal offset angles. This can be verified by observing the transfer functions for the vessel in heave and pitch direction.

From Figure 78 it can also be observed that the horizontal offset angle is a function of time. In chapter 2.3, it was stated that the maximum allowable offset angle was: $\alpha_{max} = 10$ [deg]. This is exceeded for both cases and towing in 5 [knots] is therefore not feasible for regular waves with $H = 5$ [m].



For a more detailed analysis of tension in the lifting wire for varying towing velocities, the following figures can be made.

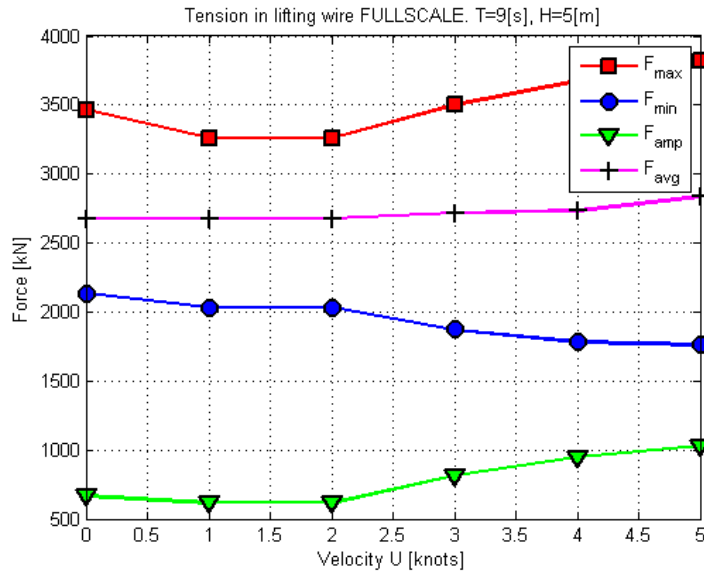


Figure 79 SIMO Tension in lifting wire, Regular waves analysis, T=9[s], H=5[m]

With a incident wave period of T=9[s], the maximum force F_{max} increases almost linearly in Figure 79, while the minimum force F_{min} decreases linearly. Introducing the dynamic amplification term (DAF), and safe working load (SWL) described in (DNV Recommended practice H103, 2009, p. 40):

$$DAF = \frac{F_{total}}{F_{static}} = \frac{F_{static} + F_{dyn}}{F_{static}} = \frac{SWL}{F_{static}} \quad (8.6)$$

The DAF for a towing velocity of 0[knots] and 5[knots] is increased from 1.33 and 1.44 respectively.

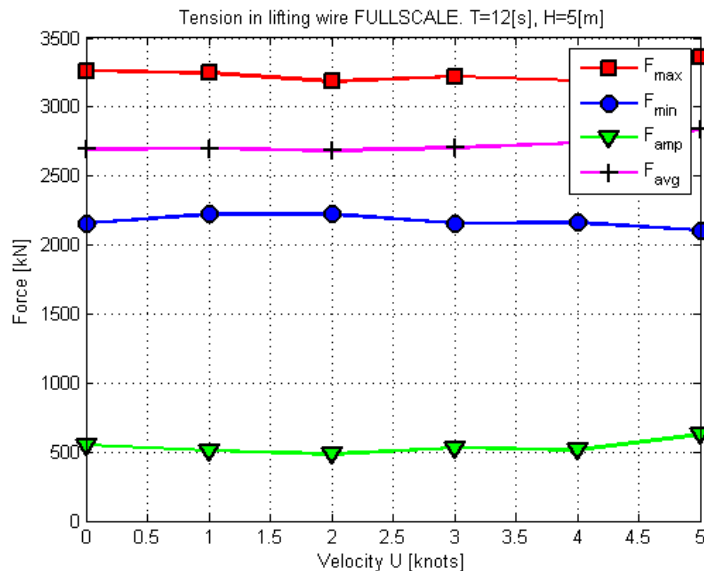


Figure 80 SIMO Tension in lifting wire, Regular waves analysis, T=12[s], H=5[m]



Moreover for a longer wave period, $T=12[s]$ in Figure 80, it can be seen that the maximum force in the lifting wire F_{max} doesn't change much, and the force amplitude F_{amp} barely rises with increased towing velocity. The maximum towing velocity is the worst condition for the system with respect to dynamic loads.

Based on the fact that the estimate of the template's natural period (chapter 6.3) is $T_0 \approx 1 [s]$, and that the maximum moonpool acceleration in heave for Skandi Acergy with zero forward velocity in head sea is achieved for $T = 9[s]$ (Saha, 2009), it can be concluded that a wave period of $T=9[s]$ is the limiting wave period with respect to dynamic forces in the lifting wire. Analyses with wave periods below $T=9[s]$ is of limited interest since these wave conditions are relatively rare (Figure 110 Scatter diagram North Sea).

Plots of the maximum, average and amplitude of the horizontal offset angle α could also be made, but is neglected in order to reduce the number of plots. This is also done since in a more detailed analysis a clump weight is introduced to limit the horizontal offset (chapter 13 Recommendations for further work), and these results will therefore be of limited interest.

To verify the results from SIMO, an experiment is conducted (chapter 9).



9 Experiment

To verify the hand calculation models derived in the previous chapters, an experimental investigation is done. An experiment is useful because it is possible to use dimensionless numbers and convert measurements made on small physical models to equivalent values for full-sized situations.

The experiment planned in this thesis adds to the experimental data measured by (Eilertsen, 2008). This is with the exception that a forced oscillator is used to model the moonpool movement in the Z-direction.

The following parameters are examined in this experiment, either by measurements, observations or both:

1. Dynamic forces in the main lifting wire
2. Motions of the template
3. Horizontal offset angle α
4. Detect possible vortex induced vibration and slack in wires

To limit experimental scope, 12 test cases representing different regular wave conditions is done. All test cases were done 3 times to limit precision errors (9.4.2).

To identify the data file-names of the test cases, Table 19 below can be used.

Testcases			
	U=0[knots]=0.0[m/s]	U=3[knots]=1.54[m/s]	U=5[knots]=2.57[m/s]
Wave period T₀=9[s]	$H_3T_9U_0$	$H_3T_9U_3$	$H_3T_9U_5$
	$H_5T_9U_0$	$H_5T_9U_3$	$H_5T_9U_5$
Wave period T₀=12[s]	$H_3T_{12}U_0$	$H_3T_{12}U_3$	$H_3T_{12}U_5$
	$H_5T_{12}U_0$	$H_5T_{12}U_3$	$H_5T_{12}U_5$

Table 19 Test cases

The test case identities in the table above, is equal to the experimental data filenames on the attached CD.



9.1 Model relationships

(Journèe & Massie, 2006) state that in order to scale experimental data to full size values, some form of similarity between model and the full size template is required. These forms of similarity can be:

- **Dynamic similarity:** Forces and accelerations in the model must be proportional to full scale measurements.
- **Kinematic similarity:** Velocities in the model must be proportional to those in full-scale. This means that the real flow and model-flow will have geometrically similar motions in model and full scale.
- **Geometric similarity:** The model must have physical dimensions which are uniformly proportional to those of the prototype. This means that all linear dimensions must have the same scaling ratio:

$$\lambda = L_f / L_M \quad (9.1)$$

Various forces are represented to different scales, and are therefore of importance to represent all model forces with the same relative importance as in full scale.

The two most common scaling laws are known as Reynolds Scaling and Froude scaling. Reynolds scaling is desirable for our case because inertia and viscous forces are of dominating interest, though according to (Journèe & Massie, 2006) demanding equality in Reynold's numbers for full and model scale, implies that:

$$\lambda_T \approx \lambda_L^2. \quad (9.2)$$

This means that the time scale is the square of the length scale and time would pass quite rapidly in a model test. Reynold scaling is therefore often impractical and Froude scaling is thus used in this thesis.

Froude scaling is based on requiring that the square root of the ratio between inertia or pressure forces and gravity forces is constant.

$$F_N = \sqrt{\frac{\text{inertia of pressure forces}}{\text{gravity forces}}} = \sqrt{\frac{\lambda_\rho \lambda_U^2 \lambda_L^2}{\lambda_\rho \lambda_L^3 \lambda_g}} = \sqrt{\frac{U}{gL}} \quad (9.3)$$

Since it is impossible to change the acceleration of gravity for a model, $\lambda_g = 1$. It can moreover be shown that:

$$\lambda_T = \sqrt{\lambda_L} \quad (9.4)$$

Equation (9.4) is the main benefit of Froude scaling compared to Reynold scaling..



The following Froude scaling table can therefore be derived:

Physical Parameter	Unit	Full Scale	Model Scale
Length:	[m]	L_F	$L_M = L_F / \lambda$
Structural mass:	[kg]	m_F	$m_M = F_F \cdot \rho_M / \lambda^3 \cdot \rho_F$
Force:	[N]	F_F	$F_M = F_F \cdot \rho_M / \lambda^3 \cdot \rho_F$
Moment:	[Nm]	M_F	$M_M = M_F \cdot \rho_M / \lambda^4 \cdot \rho_F$
Acceleration:	[m/s ²]	a_F	$a_F = a_G$
Time:	[s]	t_F	$t_M = t_F / \sqrt{\lambda}$
Pressure:	[N/m ²]	p_F	$p_M = \rho_M \cdot p_F / \lambda \cdot \rho_F$
Young's modulus	[N/m ²]	E_F	$E_M = E_F / \lambda$
Angular frequency	[rad/s]	ω_F	$\omega_M = \omega_F \sqrt{\lambda}$
Spring stiffness	[N/m]	k_F	$k_M = \rho_M \cdot k_F / \rho_F \cdot \lambda^2$
Work	[Nm]	W_F	$W_M = \rho_M \cdot W_F / \rho_F \cdot \lambda^4$
Linear viscous damping	[N/(m/s)]	c_F	$C_M = \rho_M \cdot c_F / \rho_F \cdot \lambda^{2.5}$

Table 20 Froude scaling table

9.2 Equipment

The experimental facility used in this model test is the Marine Cybernetics Laboratory at NTNU. Dynamic tension forces in the lifting wire are generated by an oscillator and measured by a force ring.

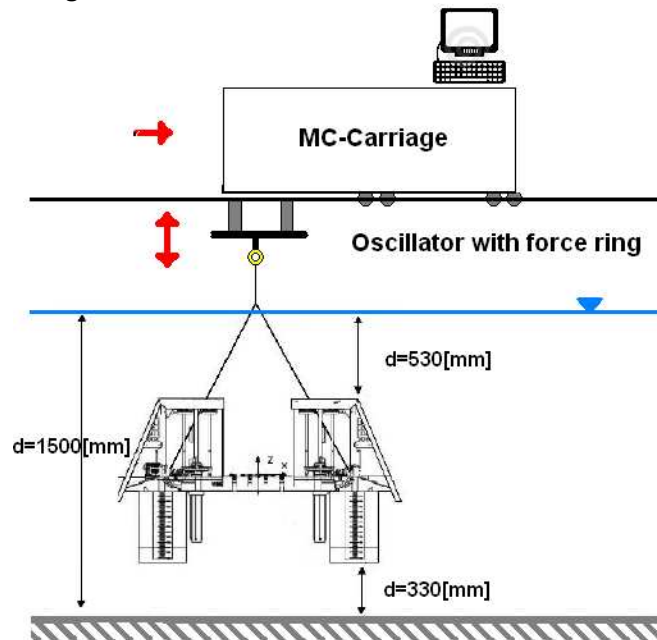


Figure 81 Experimental setup



9.2.1 Gjøa ITS model

Numerous tests have been done with the Gjøa ITS model by Acergy before. Prior to the experiment, control measurements of the model are needed. The results of these control measurements are presented in Table 21 below. The data is based on experimental reports by (Eilertsen, 2008) and (Solaas, 2008).

Parameter	Full scale	Model scale	λ
Total length [m]	28.665	1.150	24.92
Total breadth [m]	22.127	0.880	25.14
Total height [m]	15.972	0.640	24.95
Length top frame [m]	19.048	0.760	25.06
Breadth top frame [m]	12.520	0.490	25.55
Height suction anchors [m]	7.000	0.280	25.00
Diameter suction anchors [m]	5.000	0.200	25.00
Diameter top frame [m]	0.914	0.036	25.38
Weight in air [N]	2943000	177.8	25.49
Weight in water [N]	2631699	150.5	25.95
Inertia moment roll [Kg m ²]	1.223*10 ⁷	1.345	24.65
Inertia moment pitch [Kg m ²]	2.312*10 ⁷	2.424	24.88
Inertia moment yaw [Kg m ²]	2.686*10 ⁷	2.965	24.63

Table 21 Main dimensions ITS model

From Table 21 it can be observed that the scale factor deviates from the ideal scale-factor $\lambda = 25$ on some parameters, but this is acceptable.



Figure 82 Gjøa ITS model



9.2.2 Test basin

MARINTEK states that the Marine Cybernetics Laboratory is the newest test basin at the Marine Technology Centre. As the name indicates, the facility is especially suited for tests of marine control systems, due to the relatively small size and advanced instrumentation package. It is also suitable for more specialized hydrodynamic tests, mainly due to the advanced towing carriage, which has capability for precise movement in 6 degrees of freedom. For this experiment a heave oscillator representing the moonpools vertical translation is used.

Test basin capacities

- Tank Dimensions: $L \times B \times D = 40\text{m} \times 6.45\text{m} \times 1.5\text{m}$
- Wave generator: $H_s = 0.3\text{m}$, $T=0.6-1.5\text{s}$ (irregular waves)
- Carriage : towing velocity 2 m/s, 5 (6) DOFs forced motions
- Current generation: 0-0.15m/s
- Computer system for control, data recording and analysis
- Typical scaling ratios: $\lambda = 50-150$
- Typical ship model lengths: 1-3m



Figure 83 Marine Cybernetics laboratory



9.2.3 Oscillator

The moonpools vertical harmonic translation (Z-direction) and period is extracted from SIMO (S2XMOD) and implemented into a heave generator to represent the vessel. The results from these analysis is shown in the table below where the ζ_x and T_x is wave amplitude and wave period, and the subscript x denote wave height.

MOONPOOL TRANSLATION FULL SCALE			
	U=0[knots]=0.0[m/s]	U=3[knots]=1.54[m/s]	U=5[knots]=2.57[m/s]
Wave period T₀=9[s]	$\zeta_3 = 0.35[m]$	$\zeta_3 = 0.44[m]$	$\zeta_3 = 0.44[m]$
	$T_3 = 9.1[s]$	$T_3 = 8.2[s]$	$T_3 = 7.6[s]$
	$\zeta_5 = 0.59[m]$	$\zeta_5 = 0.74[m]$	$\zeta_5 = 0.72[m]$
	$T_5 = 9.1[s]$	$T_5 = 8.1[s]$	$T_5 = 7.8[s]$
Wave period T₀=12[s]	$\zeta_3 = 0.73[m]$	$\zeta_3 = 0.56[m]$	$\zeta_3 = 0.51[m]$
	$T_3 = 11.7[s]$	$T_3 = 11.1[s]$	$T_3 = 10.5[s]$
	$\zeta_5 = 1.23[m]$	$\zeta_5 = 1.05[m]$	$\zeta_5 = 1.05[m]$
	$T_5 = 12.1[s]$	$T_5 = 10.9[s]$	$T_5 = 10.9[s]$

Table 22 Vertical translation (Z-direction) of moonpool full scale

These results from SIMO analysis is tabulated in Table 22 above, and are in accordance with the transfer function for head sea in heave (Figure 49). Using a scale factor $\lambda = 25$, and the parameter relationships in Table 21, these results in Table 22 above can be transferred to model scale in the table below:

MOONPOOL TRANSLATION MODEL SCALE			
	U=0[knots]=0.0[m/s]	U=0.6[knots]=0.308[m/s]	U=1[knots]=0.514[m/s]
Wave period T₀=1.8[s]	$\zeta_3 = 1.4[cm]$	$\zeta_3 = 1.76[cm]$	$\zeta_3 = 1.76[cm]$
	$T_3 = 1.82[s]$	$T_3 = 1.64[s]$	$T_3 = 1.52[s]$
	$\zeta_5 = 2.36[cm]$	$\zeta_5 = 2.96[cm]$	$\zeta_5 = 2.88[cm]$
	$T_5 = 1.82[s]$	$T_5 = 1.62[s]$	$T_5 = 1.56[s]$
Wave period T₀=2.4[s]	$\zeta_3 = 2.92[cm]$	$\zeta_3 = 2.24[cm]$	$\zeta_3 = 2.04[cm]$
	$T_3 = 2.34[s]$	$T_3 = 2.22[s]$	$T_3 = 2.1[s]$
	$\zeta_5 = 4.92[cm]$	$\zeta_5 = 4.20[cm]$	$\zeta_5 = 3.52[cm]$
	$T_5 = 2.42[s]$	$T_5 = 2.18[s]$	$T_5 = 2.08[s]$

Table 23 Vertical translation (Z-direction) for oscillator model scale $\lambda = 25$

The results from Table 23 is implemented into a MatLab file that writes a .ascii file that can be read by the oscillator to represent the vessel translation in full scale.



9.2.4 Towlines and slings

The axial wire stiffness for the lifting wire is found from the stiffness relationship:

$$K = \frac{EA}{L} \quad (9.5)$$

It is known from Acergy that the stiffness of the full scale main wire with length $L = 40[m]$ is $K_f = 28100[kN/m]$. By using the Froude scaling law for springs from Table 20:

$$k_M = \frac{\rho_M \cdot k_F}{\rho_F \cdot \lambda^2} \quad (9.6)$$

and scaling the full scale value to model scale; the equivalent model wire stiffness necessary can be calculated to be: $k_{eq} = 41.73[kN/m]$. Since the stiffness of the present model wire is $k_M = 1000[kN/m]$ a spring needs to be introduced in the extension of the model wire if exact similarity is required.

The spring stiffness K_s is computed from the equivalent wire stiffness K_{eq} and wire stiffness k_M by using the spring in series relation:

$$\frac{1}{K_{eq}} = \left[\frac{1}{K_M} + \frac{1}{K_S} \right] \quad (9.7)$$

Solving (9.7) gives $K_s \approx 43 [kN/m]$ which is the spring stiffness necessary to model the full-scale system. However as this spring is very stiff, it is not included in the experimental setup.

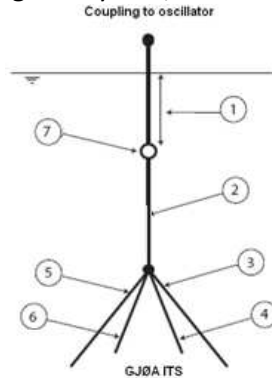


Figure 84 Model rigging

MODEL RIGGING SETUP			
Pos.nr.	Type	Length [mm]	Stiffness K [kN/m]
1	Oscillator	--	∞
2	Wire	370	1000
3	Wire	720	515
4	Wire	720	515
5	Wire	720	515
6	Wire	720	515
7	Force ring	--	∞

Table 24 Model rigging setup



9.2.5 The force ring

The force ring is a made of metal, and has three strain gauges glued to the rod, which enables the forces to be measured in three directions (x,y,z). The strain gauges are built up of compact windings that register the elongation (and change in electrical resistance) of the strain gauge, which then can be transformed to force signals. The force ring load capacities in vertical and horizontal directions are 1400 and 350 [N] respectively.

9.3 Experimental results

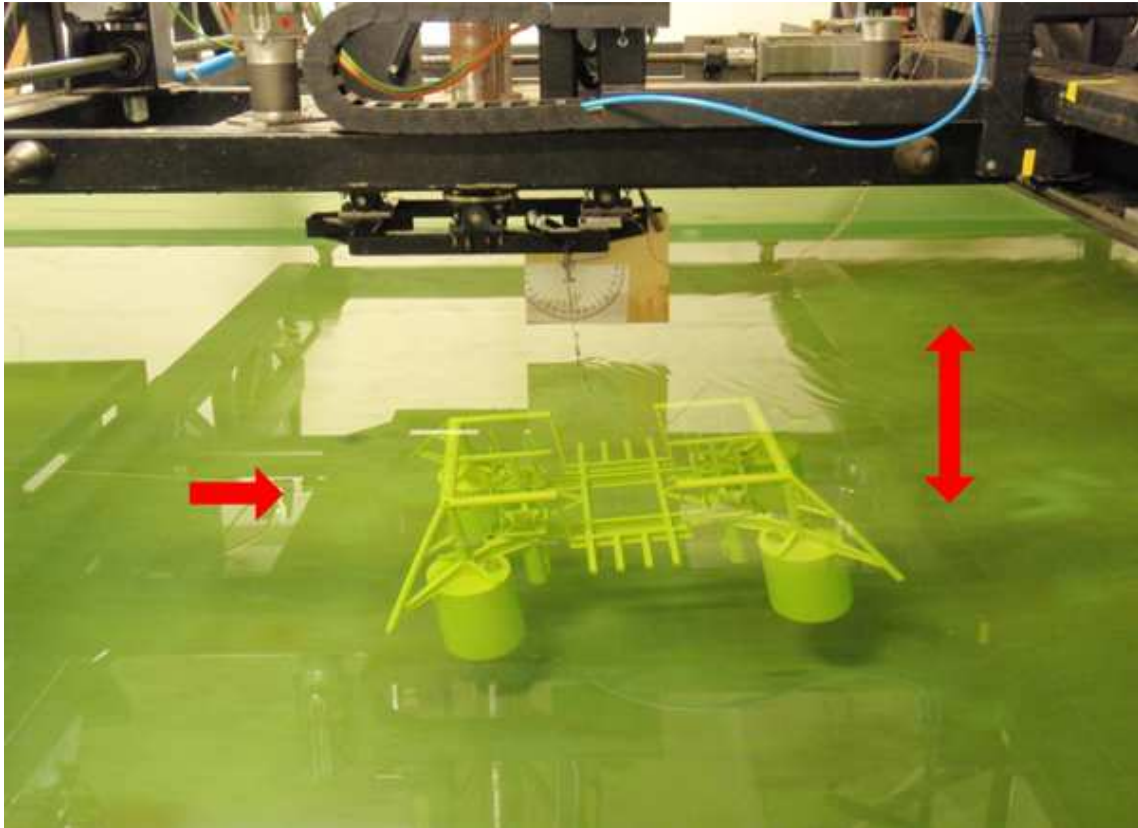


Figure 85 Experiment picture

During the experiment, forces were measured in the lifting wire. Plots of the forces, spectrograms and the horizontal offset angles can be seen in chapter 15. Lifting wire forces are scaled to full size values by using a scale factor of $\lambda = 25.00$.

Each time-history plot of lifting wire force is transferred to a power spectral density plot by using Welch's averaged modified periodogram method of spectral estimation. The power spectral density is calculated in units of power per radians per sample, and can be a nice analytical estimation of measured experimental noise. Measured noise can arise from sources like vibrations in the tow carriage, vortex induced vibrations (4.4) and lurching in the oscillator.



A sample force signal and spectrogram can be seen in Figure 86 below.

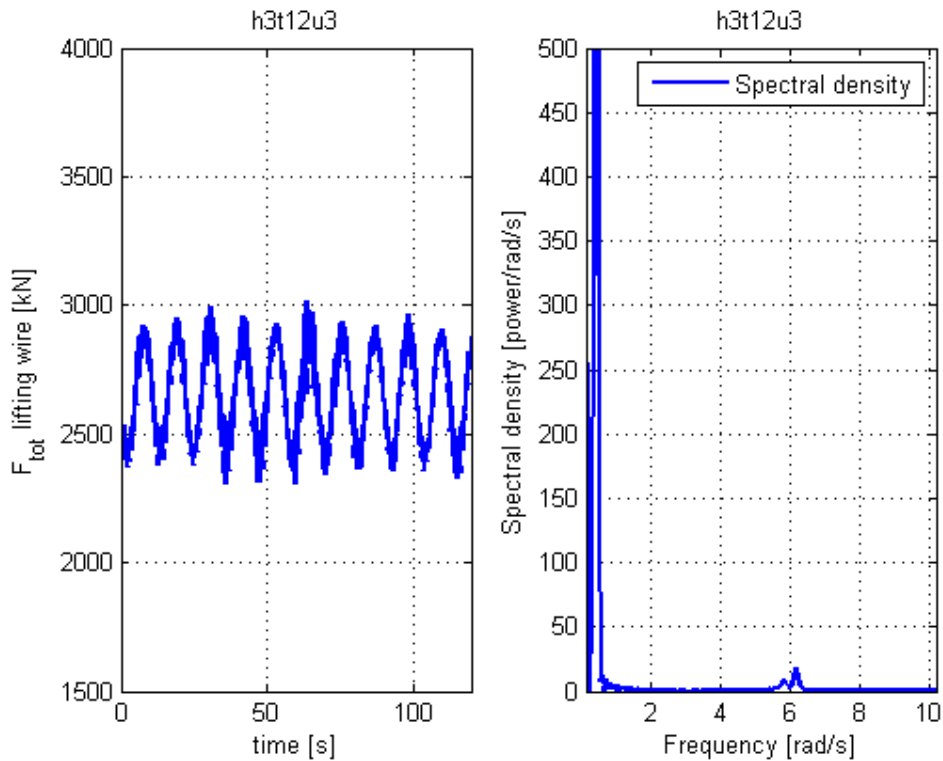


Figure 86 Sample force spectrogram

From Figure 86, it can be observed that the spectral density is localized at $\omega = \frac{2\pi}{12} = 0.52[\text{rad} / \text{s}]$ which is correct. Some signal noise is present at $\omega \approx 6[\text{rad} / \text{s}]$ but this is insignificant. This signal noise can be filtered by using a bandpass filter (e.g. a Butterworth filter which is attached to the CD). This noise is most likely caused by carriage vibrations, since it's not present when the forward velocity of the carriage is zero.

The horizontal offset angle F_z can be calculated from the force time-history.

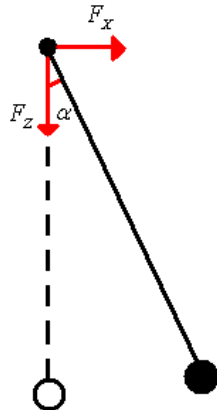


Figure 87 Horizontal offset-angle



Where:

$$\alpha = \arctan\left(\frac{F_x}{F_z}\right) \quad (9.8)$$

All offset angles are shown in Figure 106 and Figure 108 in the appendix. A sample plot is shown in Figure 88 below.

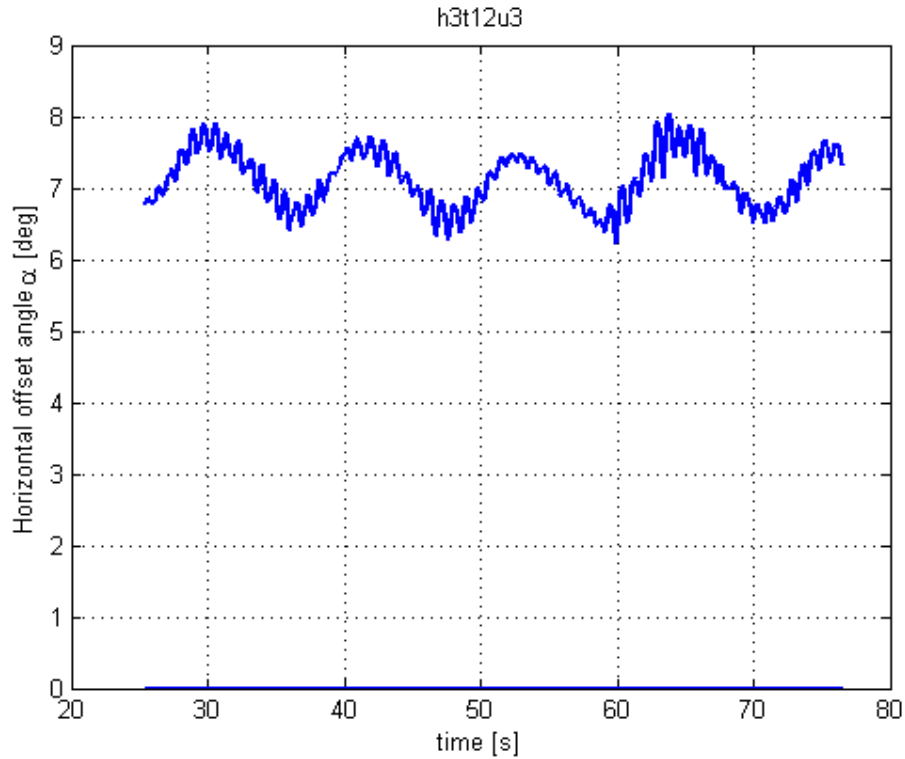


Figure 88 Horizontal offset angle H=3[m] , T=12[s], U=3[knots]

From the figure it can be observed that the horizontal offset angle changes with time. This motion is important to quantify and compare with SIMO as the risk for the wire touching the moonpool edge is imminent.



9.4 Error analysis

According to (Steen & Aarsnes, 2008), the goal of an error analysis is to give a quantitative measure of how reliable a measured or calculated value is. The word error is used for the difference between a measurement result and the true value, and is common to separate into bias and precision errors. Precision errors are scatters in the results, which may be found by comparing the results from repeated tests while bias errors are systematic errors (e.g. incorrectly calibration of force sensors). These types of errors are further described below.

9.4.1 Bias errors

Bias errors are systematic errors that are not revealed by repetition of the experiment. Usually there is no straight forward way of quantifying bias errors, but it is known that the most important source of bias errors is usually calibration errors. It is therefore necessary with good calibration procedures in a model experiment.

In these experiments, the Reynolds numbers for the subsurface towing operation in full scale and model scale differ. These differences in Reynolds numbers means that the drag coefficients are not equal, thus resulting in that the drag forces do not scale satisfactory according to λ . To achieve correct drag forces, the geometrical dimensions of the template model should ideally be adjusted, but this is impossible.

The limiting water depth in the Marine Cybernetics lab is also a limiting factor which influences bias errors. Due to bottom-shielding effects the added mass of the structure is not correctly represented. Also the damping coefficients of the template (linear damping) are affected by the generation of waves on the water surface. This effect is small, but can be observed in the video data in the appendix.

9.4.2 Precision errors

Precision errors are scatters in the results found by comparing the results of repeated measurements. These types of errors can be calculated from repeated measurements, and it is usually assumed that measured values infinitely many times will follow a Gaussian distribution. However, due to the relative simplicity of this experiment, precision errors are not considered as a major error source.



10 Model tests vs. numerical calculations

The most important qualities of physical models and numerical models are shown in Table 25.

Qualities	Physical models	Numerical models
Representation	Very good	Limited by available theories and computer power
Accuracy	Good	Good within validity limits
Scale effects	Yes	No
Reliability	Very good	Risk of human errors
Credibility	Very good	Prima facie not good
Flexibility	Not good	Good
Execution	Long	Low with standard programs
Cost	High	Development cost high

Table 25 Model test vs. numerical models (Aage, 1992)

The quantities in Table 25 will depend on the actual case, the complexity of the problem and how appropriate the test facility and numerical calculations are. However, the main essence in this table is that in a successful model test, one can be quite sure that all important physical phenomena are properly covered. The main problems with model tests are the lack of flexibility in changing design conditions, costs and scale effects. Also the test facilities may impose problems which were mentioned in 9.4.

Numerical models can provide good accuracy and flexibility and as the calculations evolve, model testing for routine verification becomes smaller. It is known that calculations are slowly taking over routine work, but the need for verification of numerical methods means that model tests still are as important as they were 30 years ago.

To evaluate the accurateness of model tests compared to numerical calculations, they can be benchmarked. As previously shown, two different types of analysis are done in this master thesis:

- Exclusion of regular waves
- Inclusion of regular waves



10.1 Exclusion of regular waves

As previously mentioned, in this analysis the only environmental conditions acting on the system are current, which represents the horizontal translation of the vessel during the transit phase. The template is towed in the X-direction (longitudinal), meaning that it is towed in the direction indicated in Figure 89.

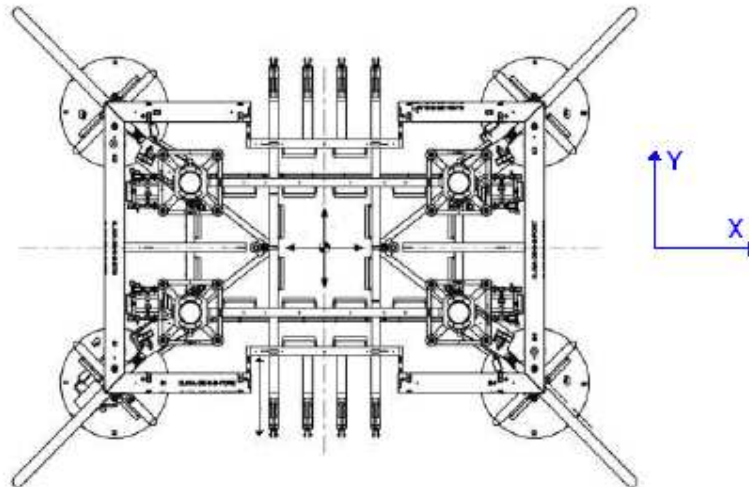


Figure 89 Template Aerial View (Acergy)

The SIMO analyses results for force in lifting wire with varying towing velocities can be summarized in Table 26.

Towing velocity [knots]	Force in lifting wire [kN]	Horizontal offset [deg]
0	2679	0.0
1	2680	0.5
2	2683	2.0
3	2694	4.5
4	2728	8.2
5	2804	13.0

Table 26 Results from SIMO with exclusion of waves

Comparing the results from SIMO with previously acquired experimental results on the Gjøa ITS from (Eilertsen, 2008), it can be observed in Figure 90 that both the SIMO model and the experimental results correlate, and the maximum deviation in lifting wire tension is only 3%. Assuming that experimental results for lifting wire tension are correct (Figure 90), the SIMO result under-predict the drag forces, while the hand calculations over-predict the forces. However, this deviation is acceptable since added mass and damping forces are the most important parameter in this analysis.

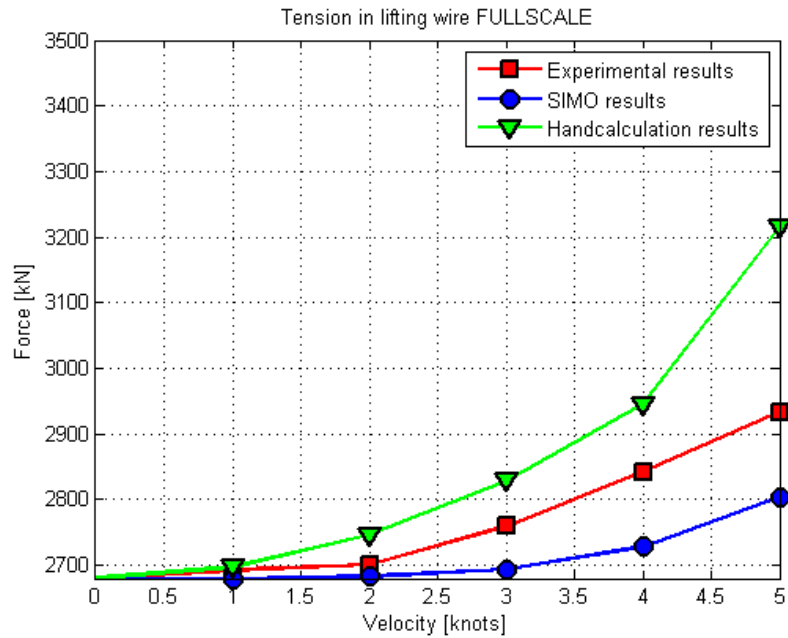


Figure 90 Tension lifting wire Experiment vs. SIMO with no waves

Even better results are obtained for the horizontal offset angle α in Figure 91 below. The hand calculation model under predicts the horizontal offset angle in its calculations.

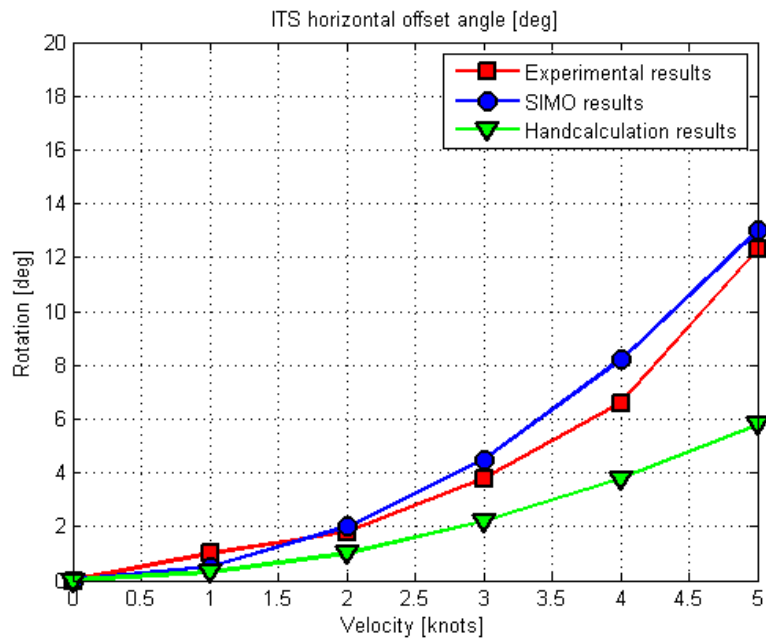


Figure 91 Horizontal offset Experiment vs. SIMO with no waves



10.2 Inclusion of regular waves

A sample comparison for the forces in the towing wire for experimental results, SIMO results and hand calculations for a sample wave condition can be seen in Figure 92 below.

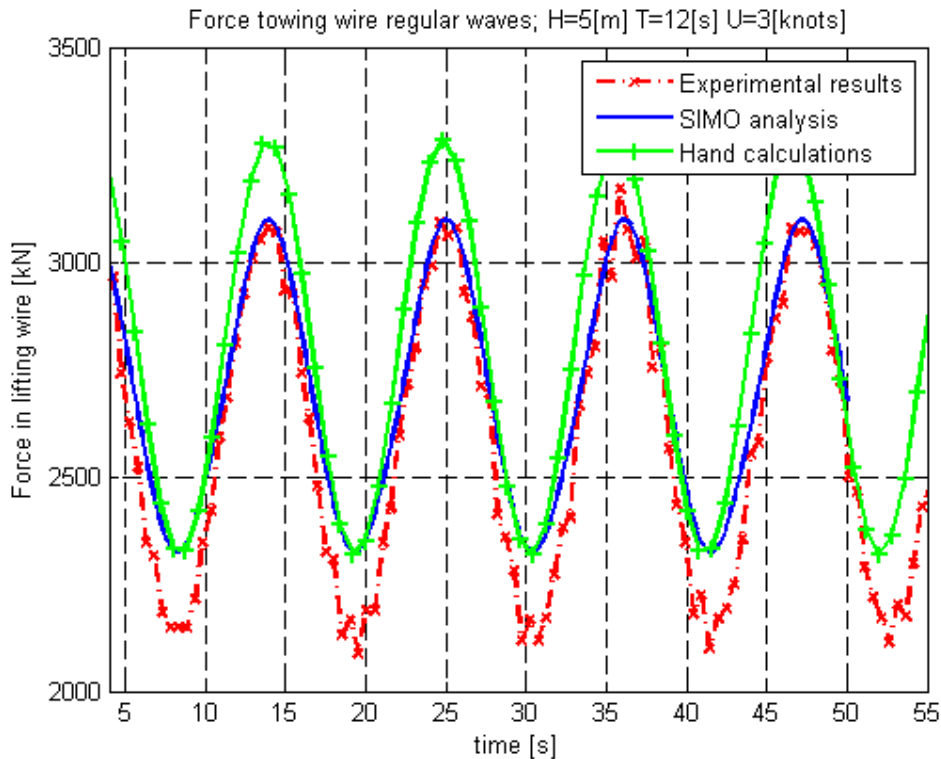


Figure 92 Experiment vs. SIMO vs. hand calculations for sample analysis

From the figure it can be observed that all three methods provide good approximations for the amplitude of the exciting force in the lifting wire. Especially the SIMO analysis results and the experimental results show a nice agreement. However, the experimental results under-predict the minimum force in the lifting wire, compared to SIMO. This deviation is most likely caused by the influence of bottom proximity effects of the added mass in heave A_{33} . These effects were an issue due to the limited water depth (1.5[m]) of the test basin. Another possible reason for this deviation is that the SIMO model over-predicts the quasistatic drag forces and under-predict the dynamic forces. This can be evaluated by towing the structure with no forced excitations (as in 10.1) and measuring the drag forces and comparing them with SIMO results. For this case the hydrodynamic drag force for the SIMO model was in accordance with experimental results (≈ 50 kN deviation), thus implying that the deviation in dynamic forces is primarily caused by bottom proximity effects.



Bottom proximity effects are according to (Faltinsen, 1990, p. 54) present when an oscillating cylinder comes close to the free-surface, a wall or another body. The results of these effects are that the cylinder will experience a greater added mass (Figure 93).

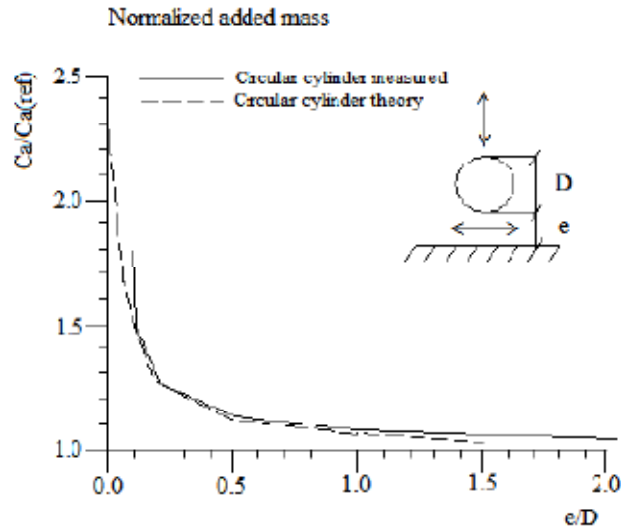


Figure 93 Normalized added mass for oscillating circular cylinder((Faltinsen,1990)

The hand calculations in Figure 92 also show good agreements with the SIMO analysis and experimental results. As previously mentioned, these results originate from a time integration of the equation of motion in heave where constant conservative values for added mass A_{33} and damping B_{33} were assumed. The static wire forces in the lifting wire caused by drag forces were directly added to the solution causing a phase difference of the equilibrium.

It can therefore be concluded that in this case, hand calculations overestimate the force in the lifting wire (caused by conservative estimates of added mass and damping), and under predict the wire tension. These results are undesirable since the minimum wire tension is of importance when evaluating the possibility for slack in the wire, and hand calculations should therefore only serve as a preliminary study of wire tension.



Also the horizontal offset angle α can be compared from SIMO and experimental results. From Figure 94, it can be seen that the experimental results yield lower minimum horizontal offset angle values, but generally both methods show good agreements for the maximum horizontal offset angle. The fact that there is a deviation of the minimum offset angle is again most likely due to bottom proximity effects. However, this is acceptable since the parameter of particular interest is the maximum horizontal offset angle α .

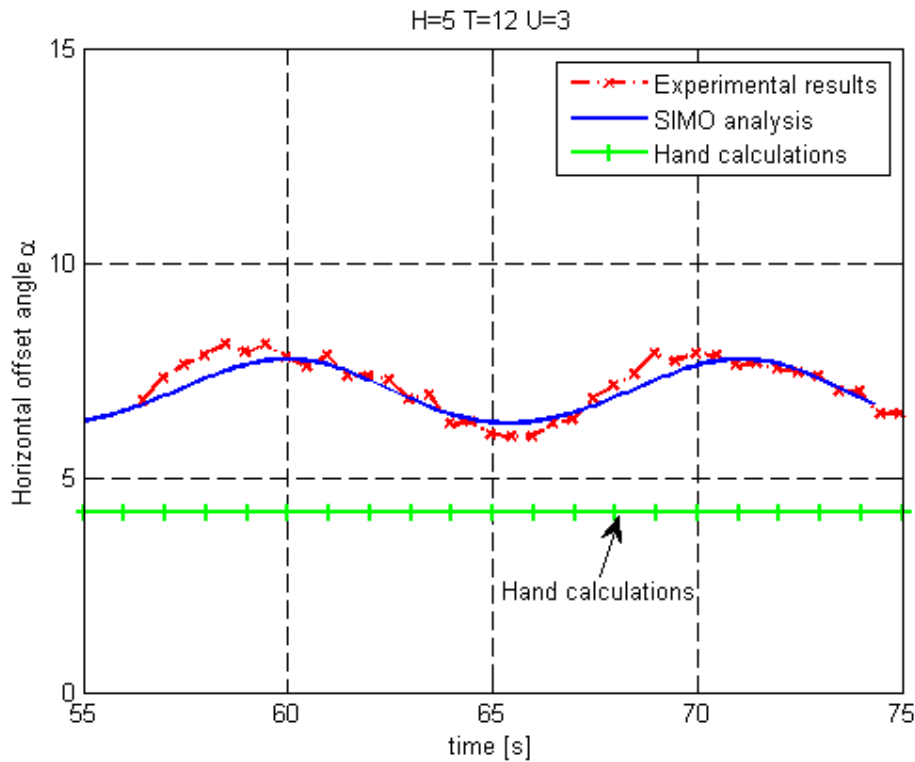


Figure 94 Sample horizontal offset angle SIMO vs. Experiment vs. Hand calculations

A summary of all the results from the hand calculations, SIMO and experimental tests are presented in Figure 95, Figure 96 and Figure 97. Only regular waves $H=5[m]$ are considered as these provide the maximum dynamic forces and offset angles. Also only the maximum horizontal offset angle is considered.

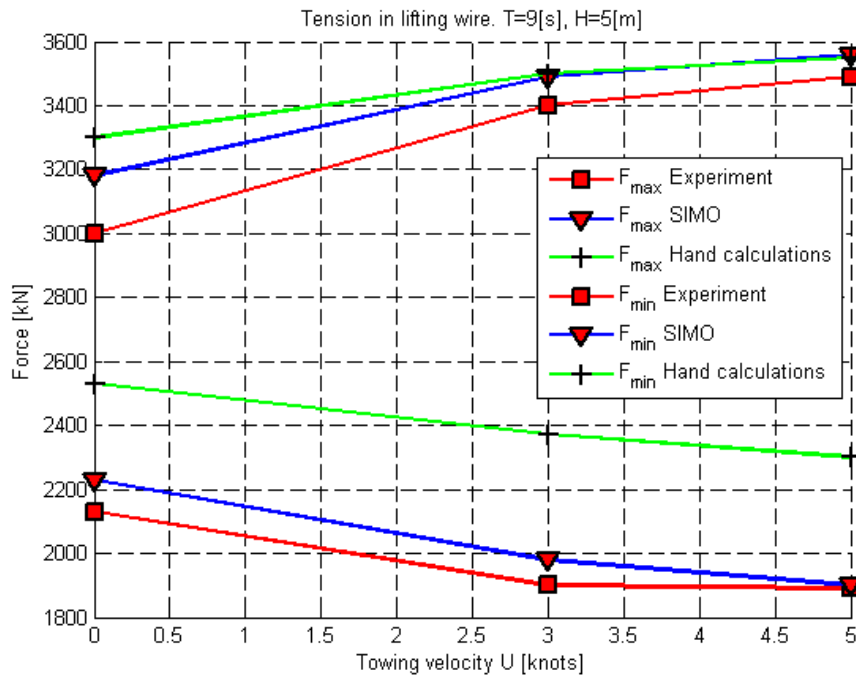


Figure 95 Comparison tension in lifting wire, Regular Waves, T=9[s], H=5[m]

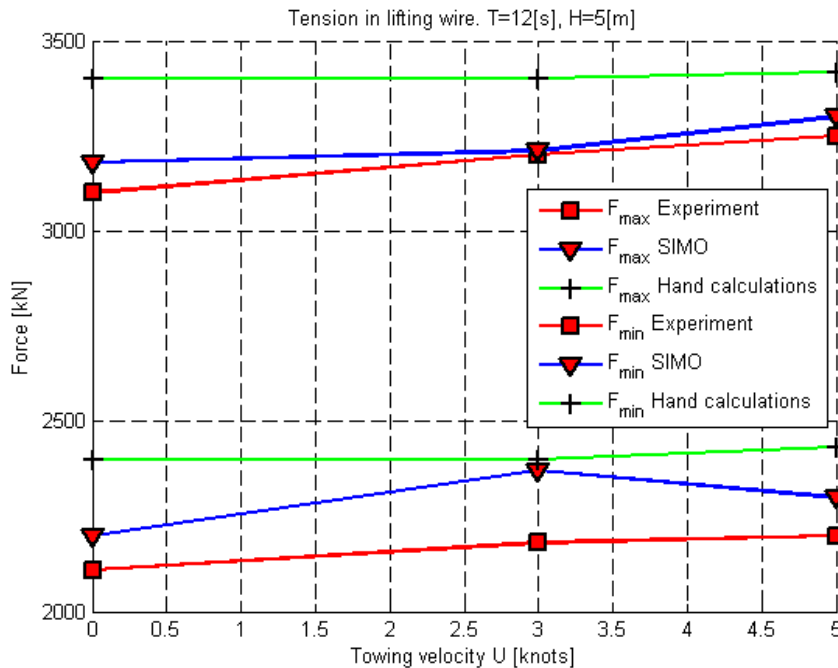


Figure 96 Comparison tension in lifting wire, Regular waves, T=12[s], H=5[m]

The maximum and minimum tension obtained with SIMO is in accordance with experimental values (maximum 10% deviation) for all test cases. However, hand calculations differ up to 15% from experimental values. This is the same pattern that could be observed in the sample comparison plot in Figure 92, meaning that the hand calculations over predicts the force and the experimental values are influenced by bottom proximity.



The results for the maximum observed horizontal offset angle α , can be observed by Figure 97. Since the hand calculations under predicted the horizontal offset angle, these results are neglected to reduce the number of plots.

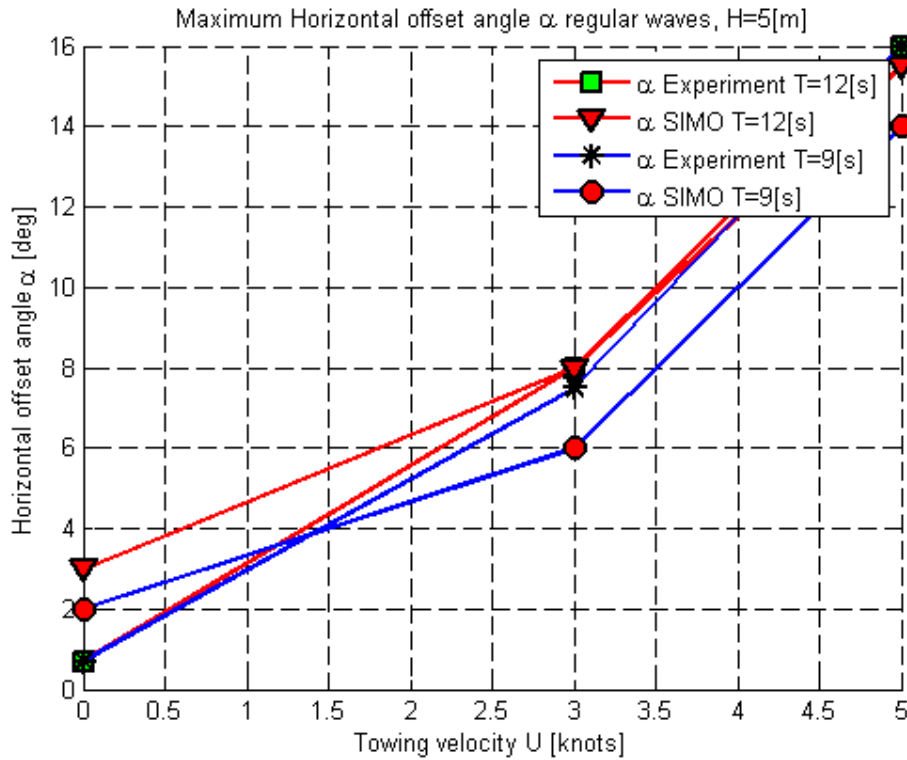


Figure 97 Comparison horizontal offset angle, Regular waves, H=5[m]

These figures show good accordance between experimental values and SIMO results for lifting wire tension and offset angle α for regular waves. This means that the SIMO model provides good results and can be further used in more detailed hydrodynamic analysis including stochastic wave conditions.



11 Parametric study

As previously mentioned, the SIMO model developed in chapter 8 provides good results for drag forces and dynamic forces. This model can then be further developed to check the dynamic behavior of the system when an active/passive heave compensated system is introduced in the moonpool hangoff structure.

During subsurface towing, regular waves will not be present and the results of this thesis can only serve as a calibration source for a numerical SIMO model. When calibration is done, irregular waves can be modeled by using a double peaked Torsethaugen wavespectrum, and wave headings from 15 [deg] to 180 [deg] head sea.

In marine operations, there are two ways to predict extreme value statistics. These two ways are based on a short time approach or a long term approach. In the short time approach the extreme wave height is estimated as the most probable largest wave during a certain period of time given a stationary wave condition. In practice a stationary condition means that the wavespectrum, mean wind velocity and towing velocity is constant. Normally, a 3 hour duration of a stationary sea is assumed. By using a significant wave height $H_s = 5[m]$, tow velocity $U=5[knots]$ and peak period $T_p = 9[s]$ ³, the following output can be produced for a 3[hour] simulation in SIMO.

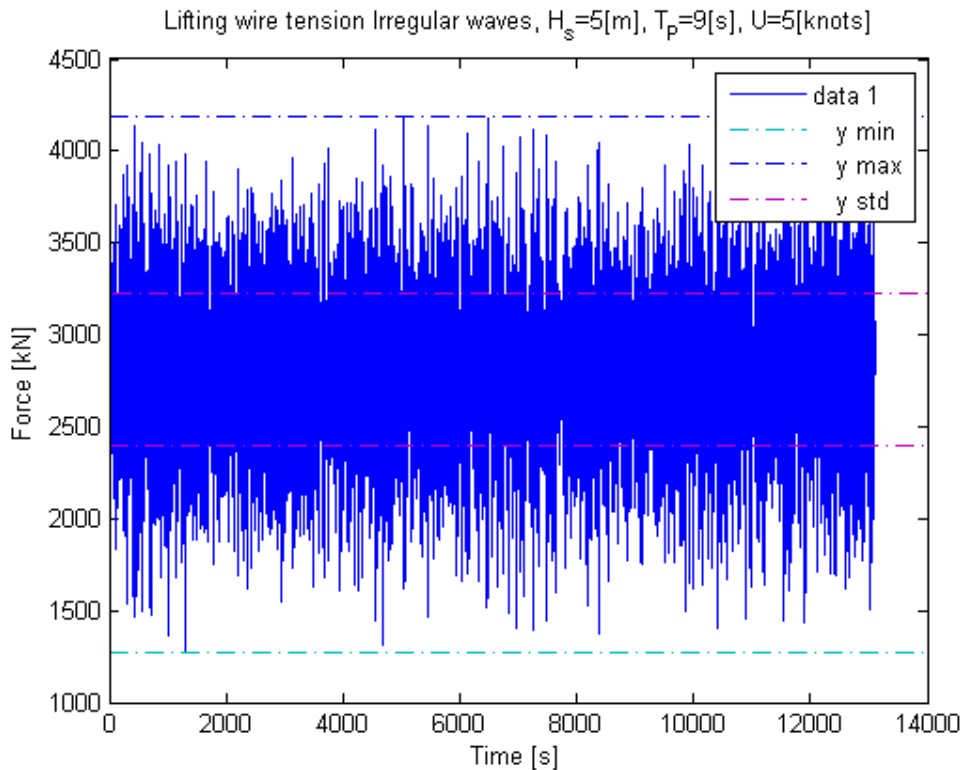


Figure 98 Tension in lifting wire, Irregular waves, $H_s=5[m]$, $T_p=9[s]$, $U=5[knots]$

³ Reduced to $T_p = 7.60[s]$ because of Table 18-Period of encounter



From Figure 98, the following results can be observed:

$$F_{max} = 4186[kN]$$

$$F_{min} = 1275[kN]$$

$$\sigma = 411[kN]$$

Where the large standard deviation, σ , indicates that the data points are relative far from the static force (mean force). These data can serve as a preparatory basis when deciding the limit state (fatigue and ultimate limit states) of the required hangoff structure. The horizontal offset angle α can also be plotted as a function of time for a 3[hour] simulation:

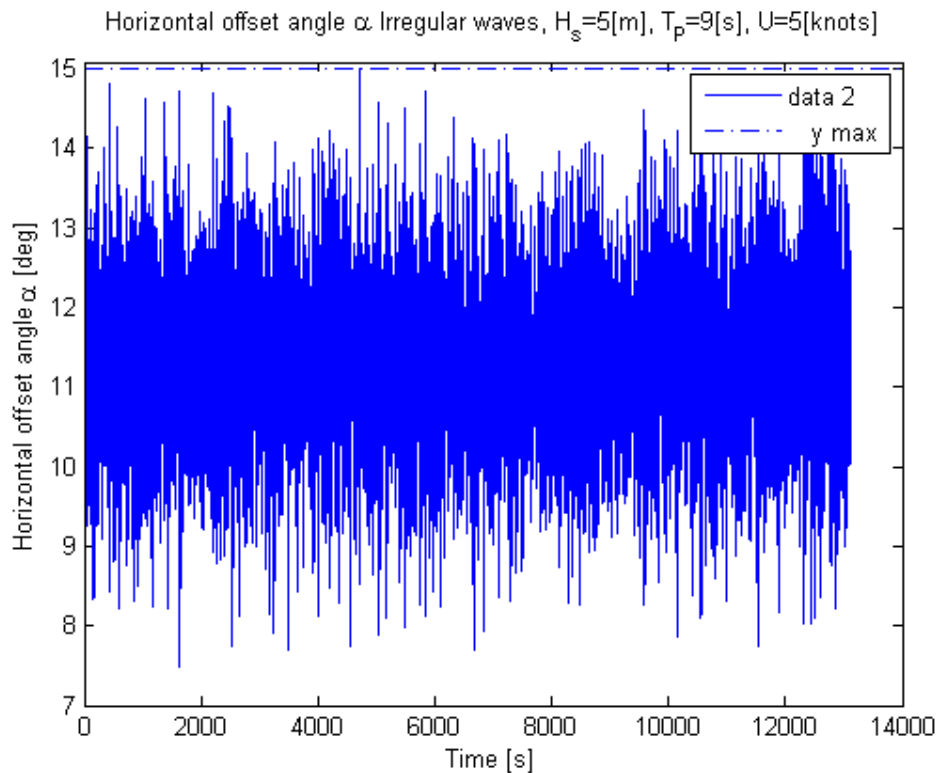


Figure 99 Horizontal offset angle, Irregular waves, $H_s=5[m]$, $T_p=9[s]$, $U=5[knots]$

From Figure 99 above, the maximum offset angle is $\alpha = 14.99[deg]$ which again exceeds the design criteria ($\alpha=10$) defined in Table 1. This means that the template's horizontal translation needs to be controlled external measures (e.g. clump weights) for adequate results regarding horizontal offset. This is further discussed in Recommendations for further work in chapter 13.



By reducing the towing velocity from $U=5$ [knots] to $U=3$ [knots], additional 3 hour simulations can be made.

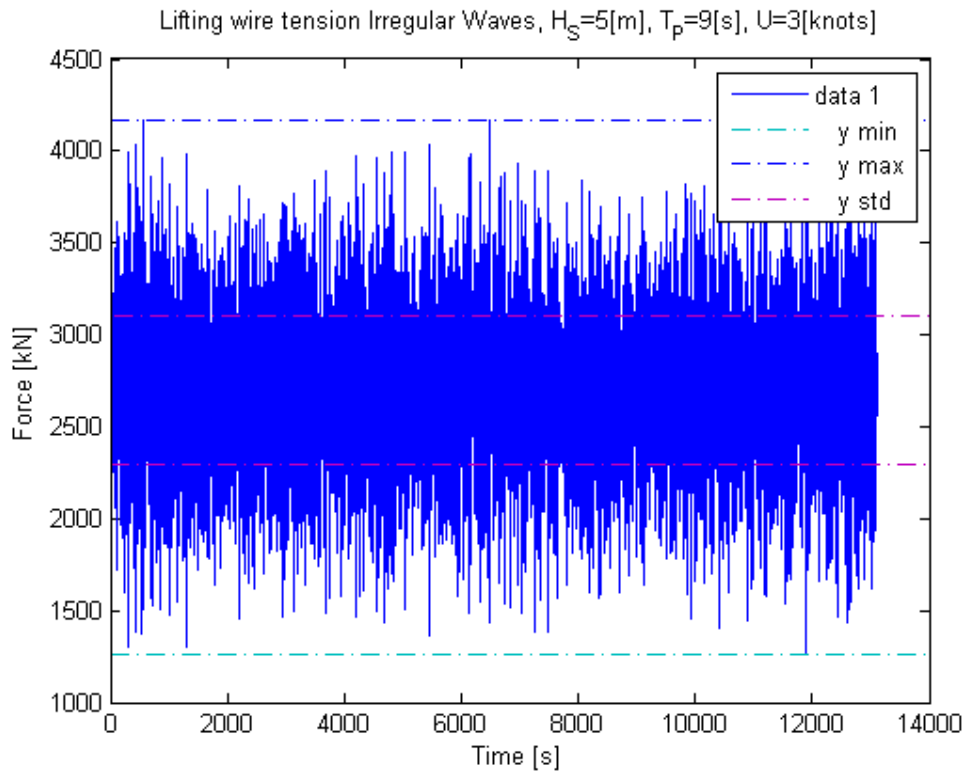


Figure 100 Tension in lifting wire, Irregular waves, $H_s=5$ [m], $T_p=9$ [s], $U=3$ [knots]

From Figure 100, the following results can be observed:

$$F_{max} = 4169[kN]$$

$$F_{min} = 1263[kN]$$

$$\sigma = 424[kN]$$

This is almost the same forces as for a towing velocity of $U=5$ [knots], however the horizontal offset angle changes dramatically (Figure 101).

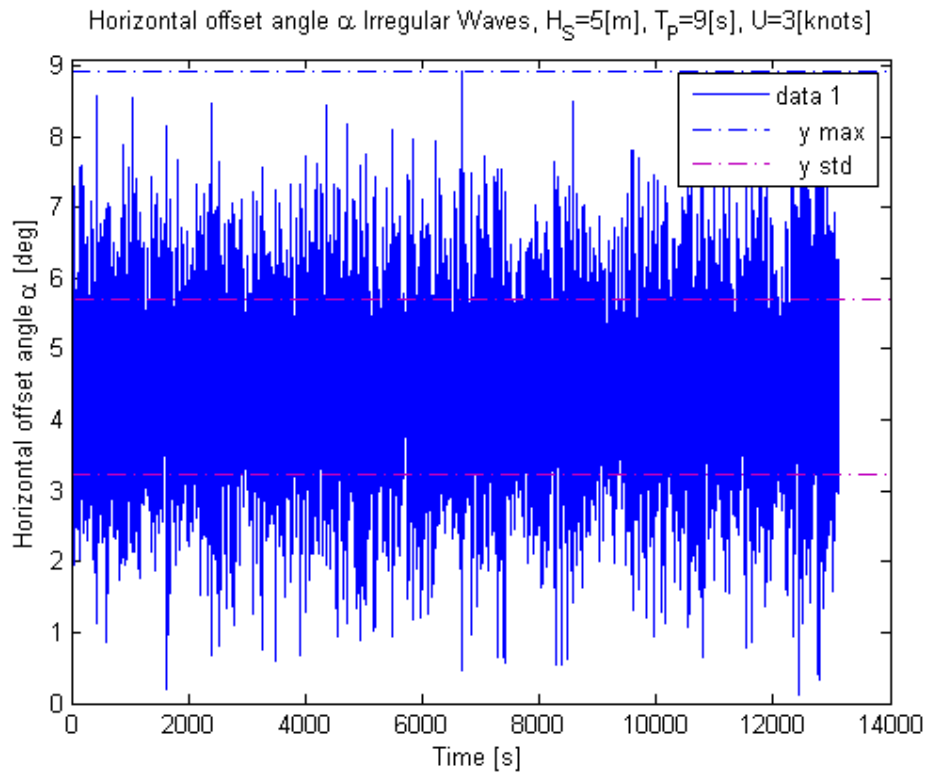


Figure 101 Horizontal offset angle, Irregular waves, $H_s=5[m]$, $T_p=9[s]$, $U=3[knots]$

From Figure 101 it can be seen that the maximum horizontal offset angle is $\alpha = 8.9 [deg]$ which is acceptable with respect to design criteria. Subsurface towing with towing velocity $U=3[knots]$ is therefore feasible for the Gjøa ITS template.



12 Conclusion

The main purpose of this master thesis was to study the basic dynamics occurring during subsurface towing of a template. Since the template is towed with wire running through the moonpool of a vessel, the most significant contribution to dynamic forces is the heave motion of the vessel. Based on RAO data of the vessel, the heave motion of Skandi Acergy could be simulated in a given time interval. Also using time integration, the dynamic forces and displacements could be determined.

Hand calculation models for the dynamic forces/horizontal offset occurring in a 1-DOF system were derived based on force equilibrium interpretations on infinitesimal wire segments. Drag forces for varying towing velocities were calculated using Morison's equation and estimated values for projected areas. These drag forces were then assumed quasistatic and super positioned to the dynamic forces in the lifting wire for a 1-DOF system.

A coupled time domain analysis for the system was then established in SIMO. The vessel was modeled as a 6-DOF large volume body where the total motion was simulated by the use of transfer functions in the time-domain. The template was modeled by using 79 slender elements, representing different structural elements (e.g. suction anchors, HEB beams). Hydrodynamic coefficients were estimated based on hydrodynamic reports for simple bodies from model test experiments (Øritsland, 1989).

In order to benchmark the accuracy of the hand calculations and SIMO model, a simplified experimental study was performed at the Marine Cybernetics lab at NTNU. The purpose of the experiment was to measure forces and horizontal offset angle α with the vertical plane when towing the template with prescribed vertical oscillations (representing the vessel's translation in head sea). Since the depth of the test basin was limited (1.5 [m]), some bottom proximity effects were observed.

Comparing values obtained from the 3. Different procedures show good accordance between hand calculations, SIMO and experimental values. Especially the SIMO analysis and the experimental results show a nice agreement, while the hand calculations model overestimate the force in the lifting wire (caused by conservative estimates of added mass and damping), and under-predict the wire tension. The minimum wire tension is of importance when evaluating the possibility for wire slack, and hand calculations should therefore only serve as a preliminary basis of wire tension. However, hand calculations are less time consuming and could be used in the first stages of feasibility studies for subsurface towing operations.

Since the SIMO model shows good agreements with measured experimental values, it can be further developed to investigate worst case stochastic sea states, and different rigging setups (inclusion of clump weights to reduce horizontal offset). In this master thesis, two 3 hour stochastic sea state simulations with a double peaked Torsethaugen wavespectrum with $H_s = 5[m]$ and $T_p = 9[s]$ were done. The results from this analysis is that a towing velocity of 5[knots] is feasible with respect to minimum and maximum dynamic tension in the lifting wire, but not with respect to the horizontal offset angle. Clever solutions for controlling the



dynamic loads and especially the horizontal offset angle are therefore needed in further work. However, for a towing velocity of $U=3$ [knots], subsurface towing of the Gjøa ITS is feasible with respect to dynamic loads and horizontal offset.

13 Recommendations for further work

Further work with respect to this master thesis should emphasize on dynamic analyses with introduced damping couplings in SIMO to represent a dynamically damped hangoff structure and/or using dynamic fiber rope with rubber inserts instead of steel in the lifting wire. DAF (dynamic amplification factors) for different setups should be compared to determine the optimal towing configuration.

A better towing configuration with clump weights should be designed and analyzed in SIMO as seen in Figure 102. These should be added to the towing configuration to reduce the horizontal offset angle α , and reduce the projected area of the structure (thereby reduce drag forces). Also a parametric study for introducing clump weights should be done with different clump weight configurations, and if time allows compared to experimental values.

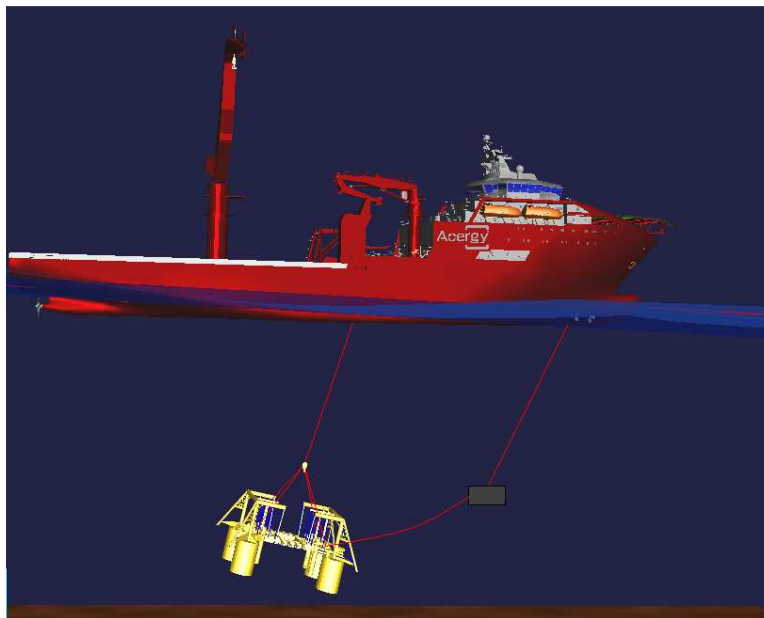


Figure 102 Towing with clump weights

Additional concepts for subsurface towing could also be evaluated. Dynamic and static loads could be reduced by using buoys attached to the lifting pad eyes of the template. This concept is shown in Figure 103 below where two yellow buoys have been added to the system. The buoys should be made of iron and filled with air and contain a ROV operable valve for releasing air.

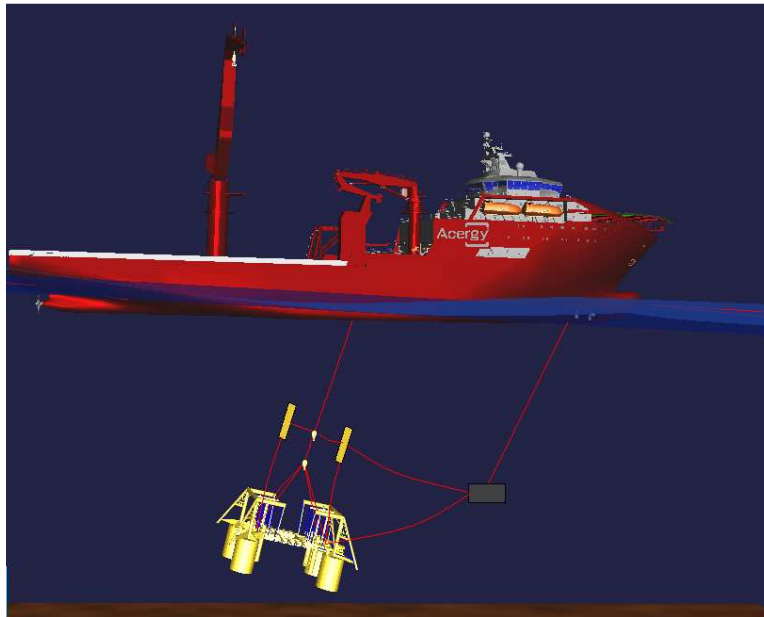


Figure 103 Towing with clump weights and buoyancy buoys

A major drawback with subsurface towing is the induced dynamic loads. These result in fatigue problems on lifting pad eyes/sheaves and hangoff structure. Fatigue problems are limiting factors experienced by contractors in previous operations and detailed accumulated fatigue calculations should therefore be made to determine the operational limits of an operation.

Additional time-domain simulations should also be done in SIMO for varying wave headings, and environmental parameters. Limits regarding survival conditions (while waiting on weather) with respect to dynamic loads and fatigue should also be investigated. “Worst case” scenarios should be quantified, for the transit phase of the operation, and for survival conditions. The results from these analyses should be summarized in an internal “recommended practice” guideline for Acergy Norway and used when planning a subsurface towing operation of a subsea structure.

The core of this “Recommended practice” should be based on statistical values as maximum expected forces/motions in the lifting wire and estimated by curve fittings to a Weibull distribution of the peaks of the time series. In order to calculate curve fittings:

- Time series from SIMO should serve as basis
- All local extreme values should be extracted from the time series
- The extreme values should then be sorted, and used as a basis for the observed cumulative probability distribution. This theoretical cumulative distribution should then be based on a Weibull fit.

Finally, the theoretical extreme value should be established based on a certain operational duration (dependent on project). The expected maximum value should then be used as the reported design value.



14 Bibliography

- Acergy Norway. (2007). *Dynamic testing of fibre rope with inserts*. Det Norske Veritas.
- C.M.Larsen. (2007). TMR4180 Marin Dynamikk. In C. M. Larsen. Tapir.
- Dietz, P., T, L., Scwarzer, T., & Wächter, M. (2009). *Problems related to the design of multi layer drums for synthetic and hybrid ropes*. OIPEEC conference.
- DNV Recommended practice H103. (2009). *Modelling and analysis of marine operations*. Det Norske Veritas.
- Eilertsen, A. D. (2008). *Hydrodynamic forces on a template during tow-out in submerged condition*. Trondheim: NTNU.
- (1999). *Engineers Design Guide, Deep water fibre mooring*. Oilfield Publications limited.
- Faltinsen, O. M. (1990). *Sea loads on ships and offshore structures*. Trondheim: Cambridge ocean technology series.
- Feng, C. (1968). *The measurement of vortex-induced effects in flow past stationary and oscillating circular D-section members*. Columbia: MSc. Thesis University of Columbia.
- Hughes, T. J. (2008). *The finite element method- Linear Static and Dynamic Finite Element Analysis*. Stanford University: Dover publications.
- Jacobsen, T. (2009). *Submerged towing of subsea template Project Thesis*. Trondheim: NTNU, Acergy.
- John D. Anderson, J. (2007). *Fundamentals of Aerodynamics*. McGraw-Hill.
- Johnsgard, H., & Gramnaes, J. (2007). *The Pencil Buoy Method- A subsurface Transportation and Installation Method*. Texas. USA: Offshore Technology Conference.
- Journèe, J., & Massie, W. (2006). *Offshore hydromechanics*. Delft: Delft University of Technology.
- (2006). Separation of variables. In E. Kreyzig, *Advanced engineering mathematics* (p. 540). Wiley International.
- L.R.M, M. (2006). *Internal waves: Dead-water*. Retrieved from Department of physical oceanography: http://www.nioz.nl/nioz_nl/281c18dbf72fc51c599b4f49dddc1143.php
- Langen, I., & Sigbjörnsson, R. (1979). Dynamisk Analyse av konstruksjoner. In *Dynamisk Analyse av konstruksjoner* (pp. 266-294). Tapir.
- Lienhard, J. (1966). *Synopsis on Lift, Drag and Vortex Frequency; Data for Rigid cylinders*. Washington: Washington State University, Research Division.



Lotsberg, I. O. (2004). *Risk assessment of loss of structural integrity of a floating platform due to gross errors*. Marine Structures 17 551-573.

MARINTEK. (2007). *Appendix A- System description file*. Trondheim: Marintek.

MARINTEK. (2010, January 20). *SIMO*. Retrieved from <http://www.sintef.no/Home/Marine/MARINTEK/Software-developed-at-MARINTEK/SIMO/>

MARINTEK. (2001). *Theory Manual Version 3.6*. Trondheim: MARINTEK.

Melville, K. W. (2009). Ocean waves: Surface and internal waves. *Lecture notes from course at Scripps Institution of Oceanography, UC San Diego*.

Nesse, V. (2008). *Use of Computer Software in Studying Marine Operations: Effect on Bottom Proximity*. Trondheim: NTNU.

Nielsen, F. G. (2007). *Lecture notes in marine operations*. NTNU.

Pedlosky, J. (2008). *Waves in the ocean and Atmosphere- Introduction to wave dynamics*. Boston: Springer.

Saha, M. (2009, September 11). Maximum heave motion statistics at centre of Moonpool of Skandi Acergy. Stavanger, Norway: Acergy.

SIMO theory manual. (2008). *SIMO- Theory Manual Version 3.6 rev1*. Trondheim: MARINTEK.

Solaas, F. (2008). *Hydrodynamic data for the GJØA ITS installation. Forced oscillation model tests of ITS*. Trondheim: MARINTEK- Norwegian Marine Technology Research institute.

Steen, S., & Aarsnes, J. V. (2008). Experimental methods in Marine Hydrodynamics. *Lecture notes*.

Taylor, J. R. (1997). *A introduction to Error analysis*. University science books.

Ulstein, T. (2006). *Wet Tow of Subsea Templates- Tyrihans*. Stavanger: Subsea 7.

Young's modulus for different materials. (2007). Retrieved December 12, 2009, from Engineering toolbox: http://www.engineeringtoolbox.com/young-modulus-d_417.html

Øritsland, O. (1989). *A summary of subsea module hydrodynamic data*. Trondheim: Marintek.
Aage, C. (1992). *Relevance of Model Testing in Irregular Seas and Current*.

Aarset, K., & Sinclair, D. (2007). *Wet-tow installation: an alternative to conventional heavy-lift methods*. Subsea 7.



NTNU
Norwegian University of Science and
Technology
Department of Marine Technology



15 Appendix

Regular waves H=3[m] results from experiment

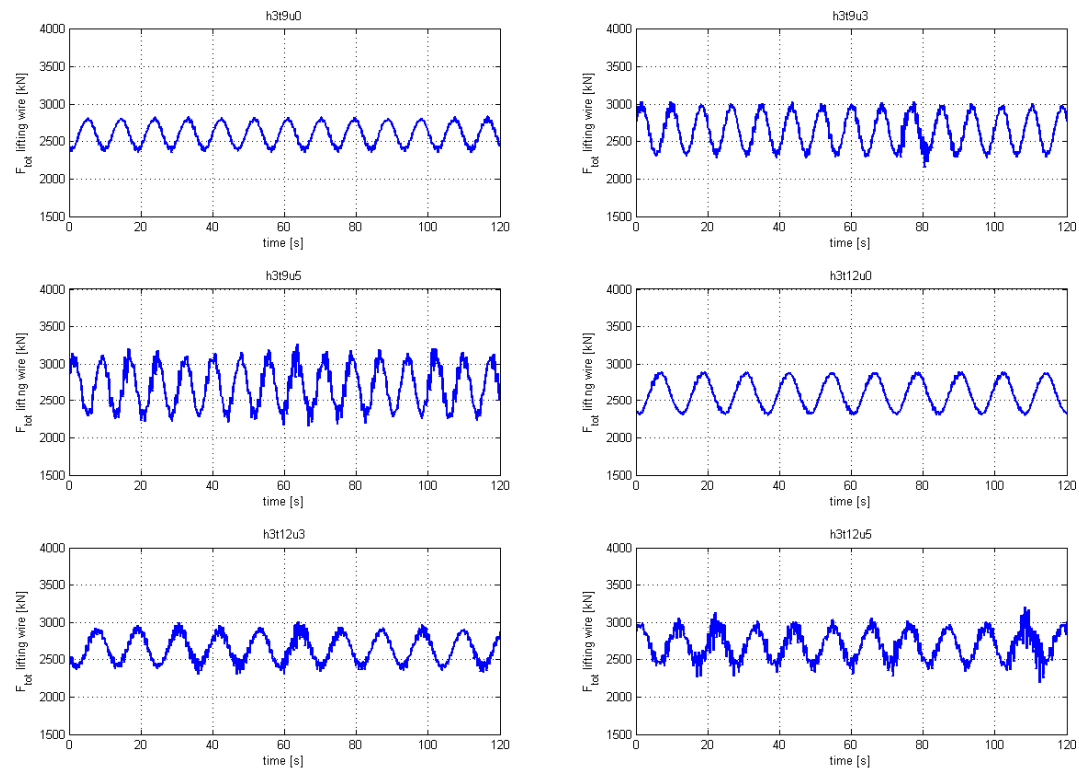


Figure 104 Force in lifting wire (Experiment) fullscale H=3[m]

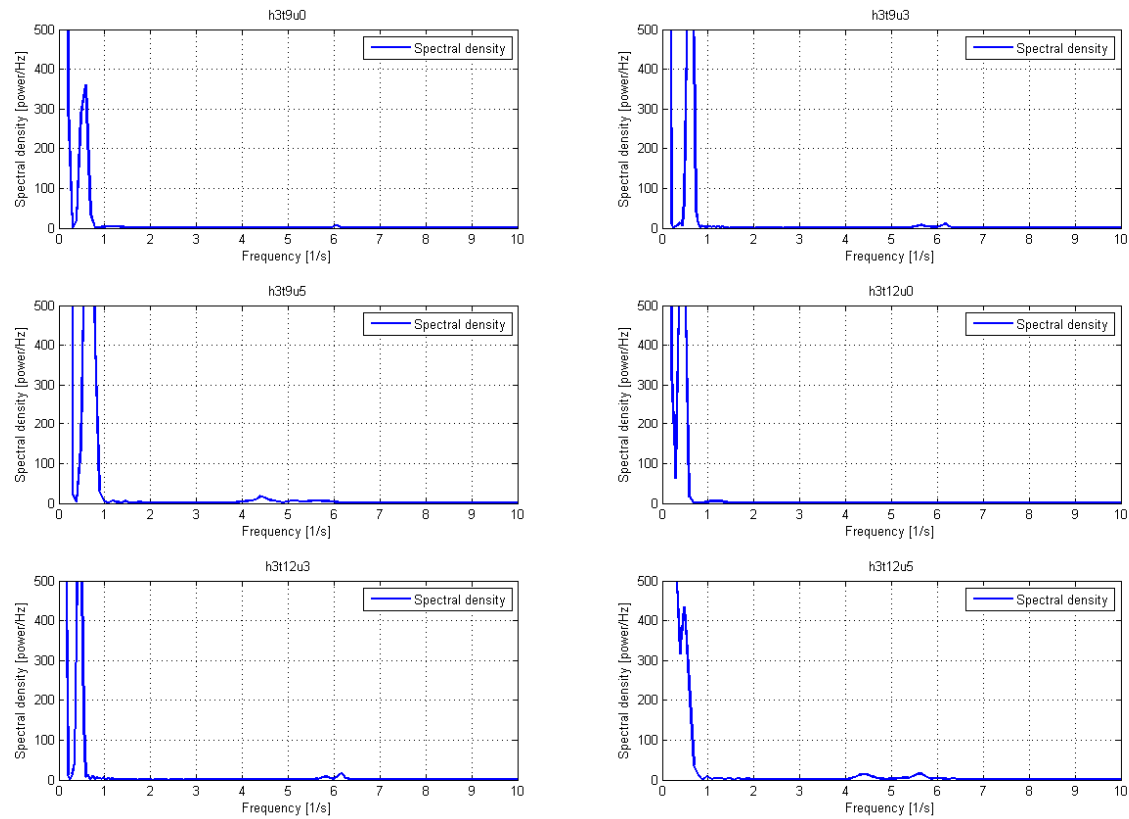


Figure 105 Spectrogram force signal (Experiment) H=3[m]

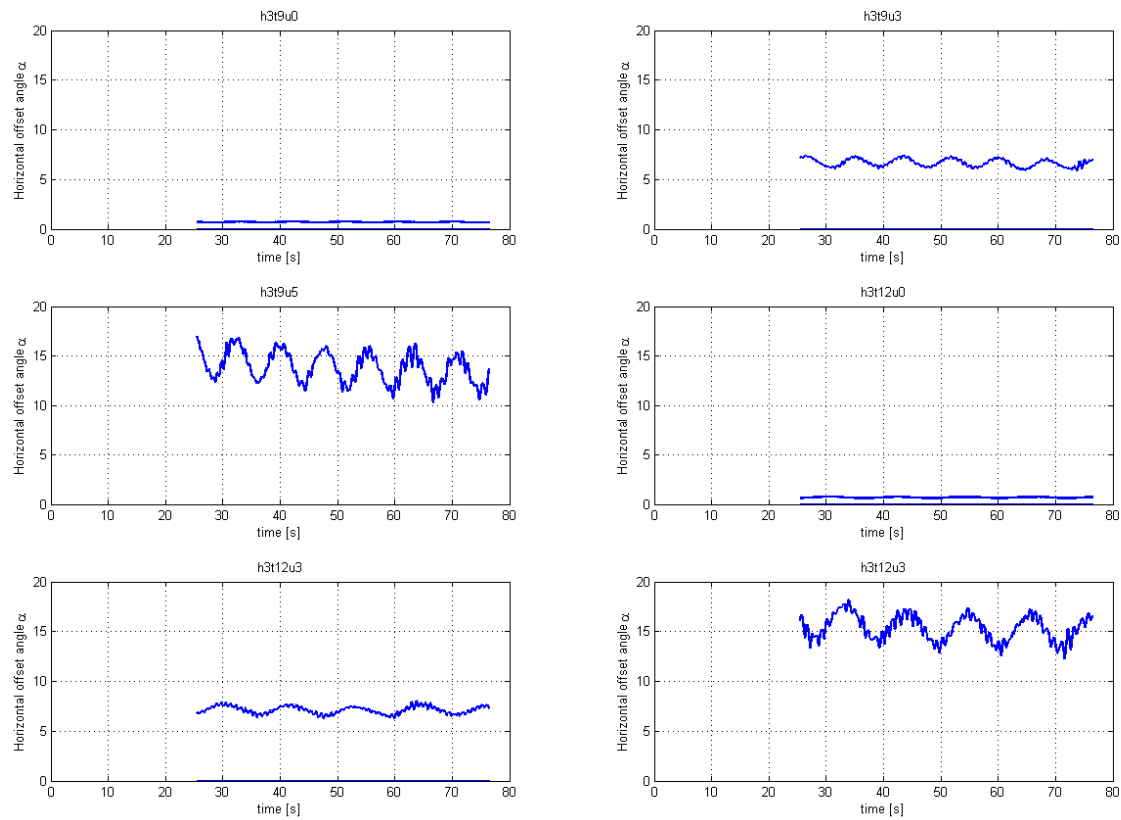


Figure 106 Horizontal offset angle (Experiment) H=3[m]



Regular waves H=5[m] results from experiment

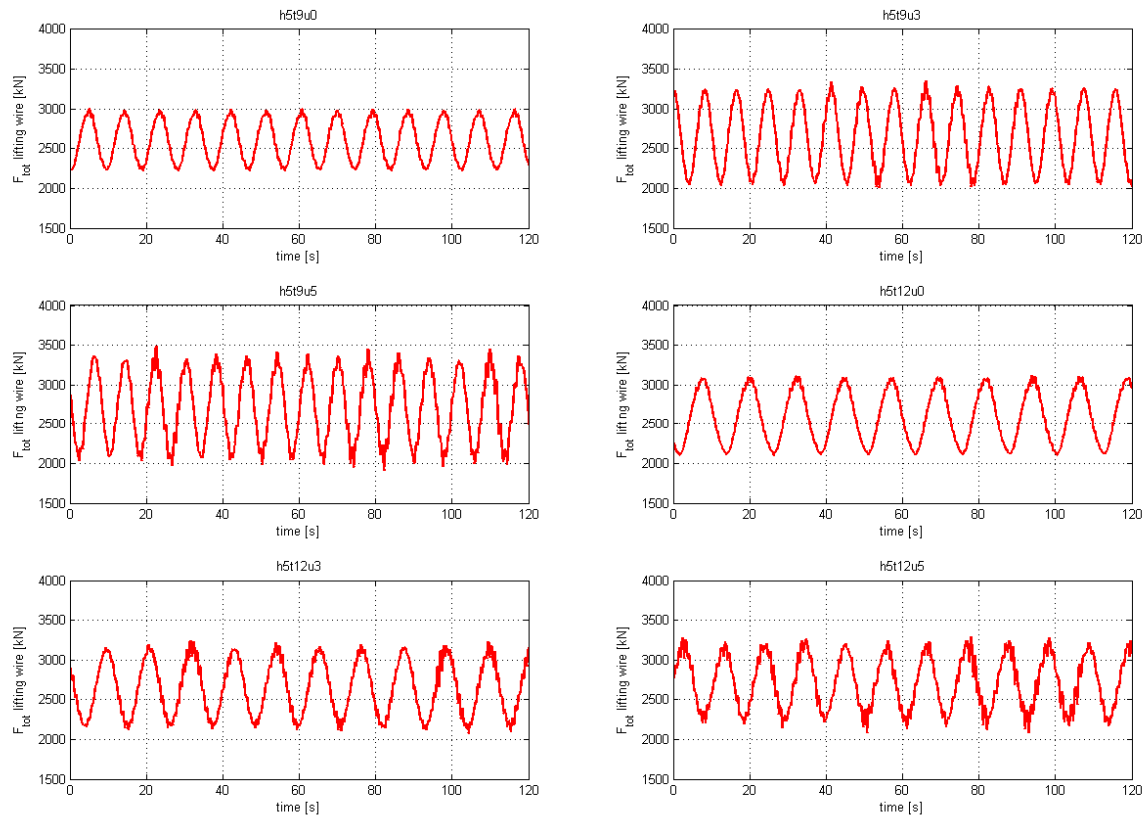


Figure 107 Force in lifting wire (Experiment) fullscale H=5[m]

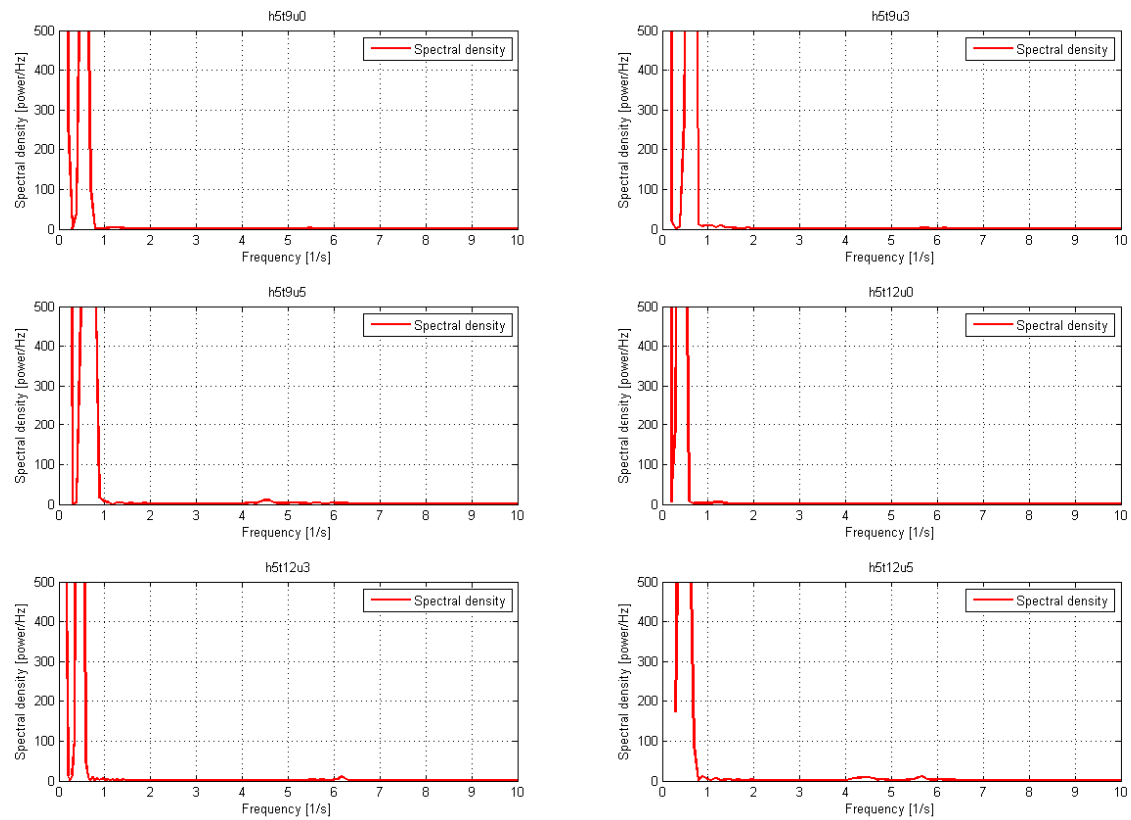


Figure 108 Spectrogram force signal (Experiment) H=5[m]

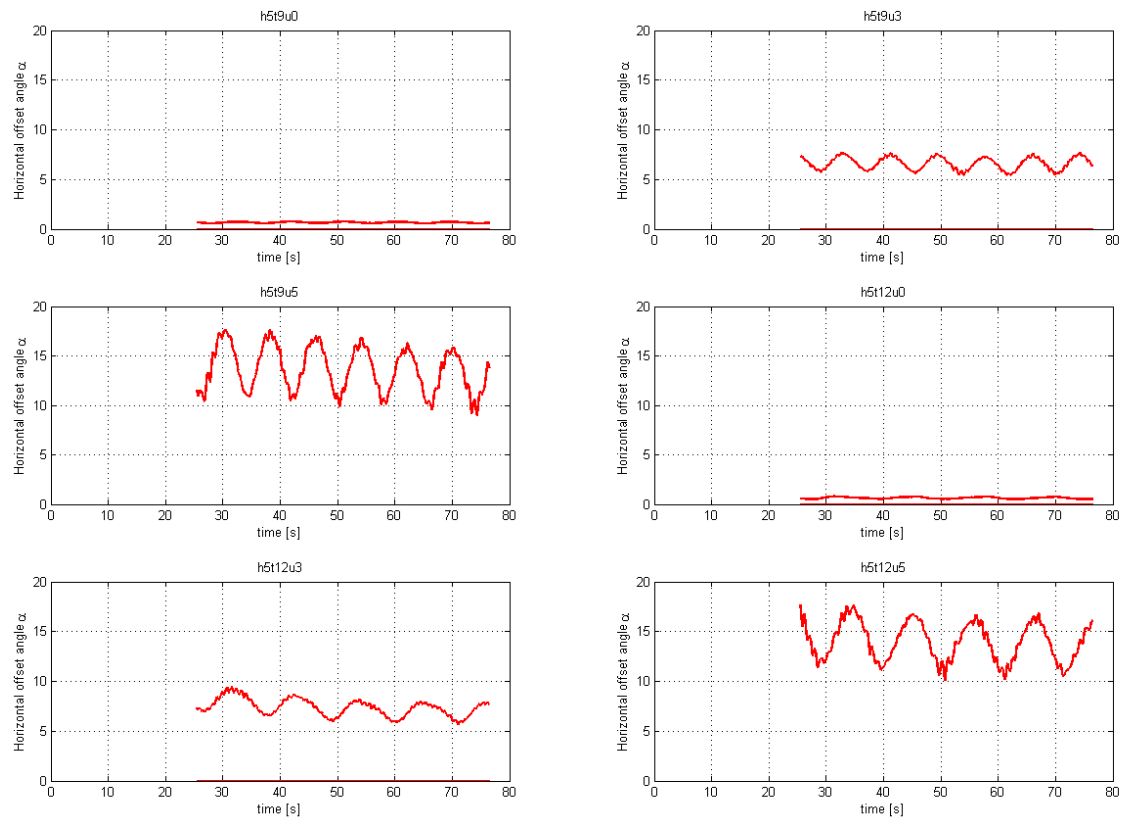


Figure 109 Horizontal offset angle (Experiment) H=5[m]



Scatter diagram (data from Faltinsen 1999)

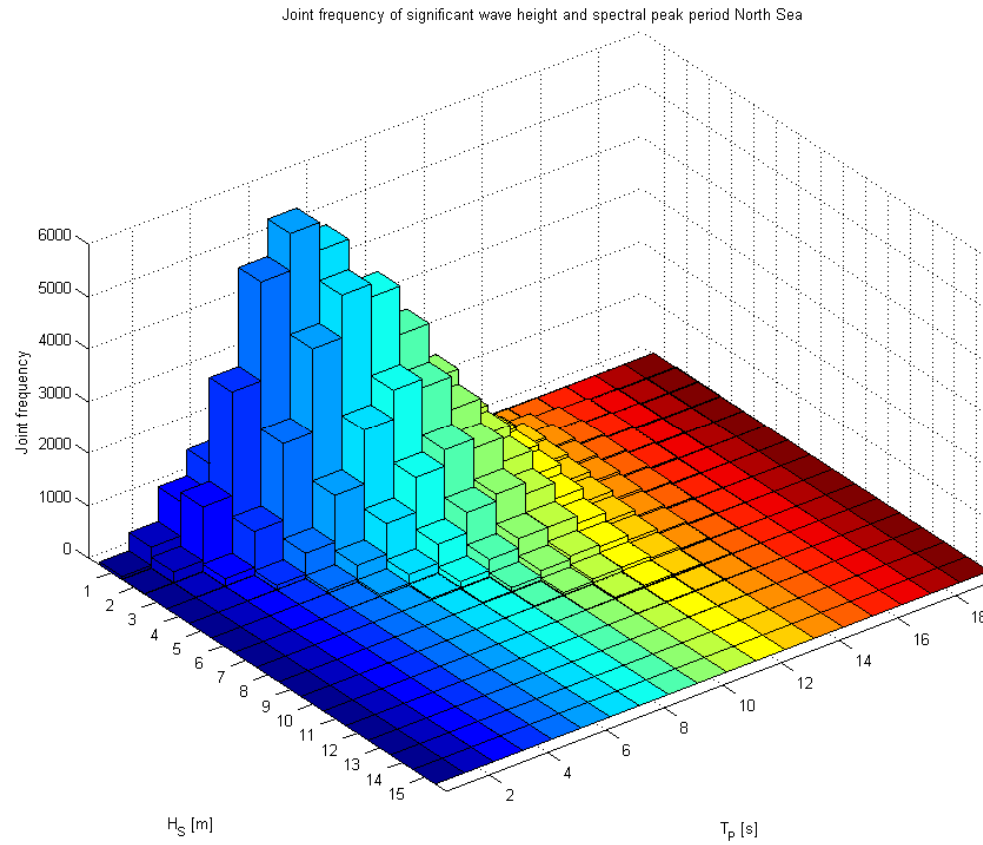


Figure 110 Scatter diagram North Sea



Conceptual hangoff structure

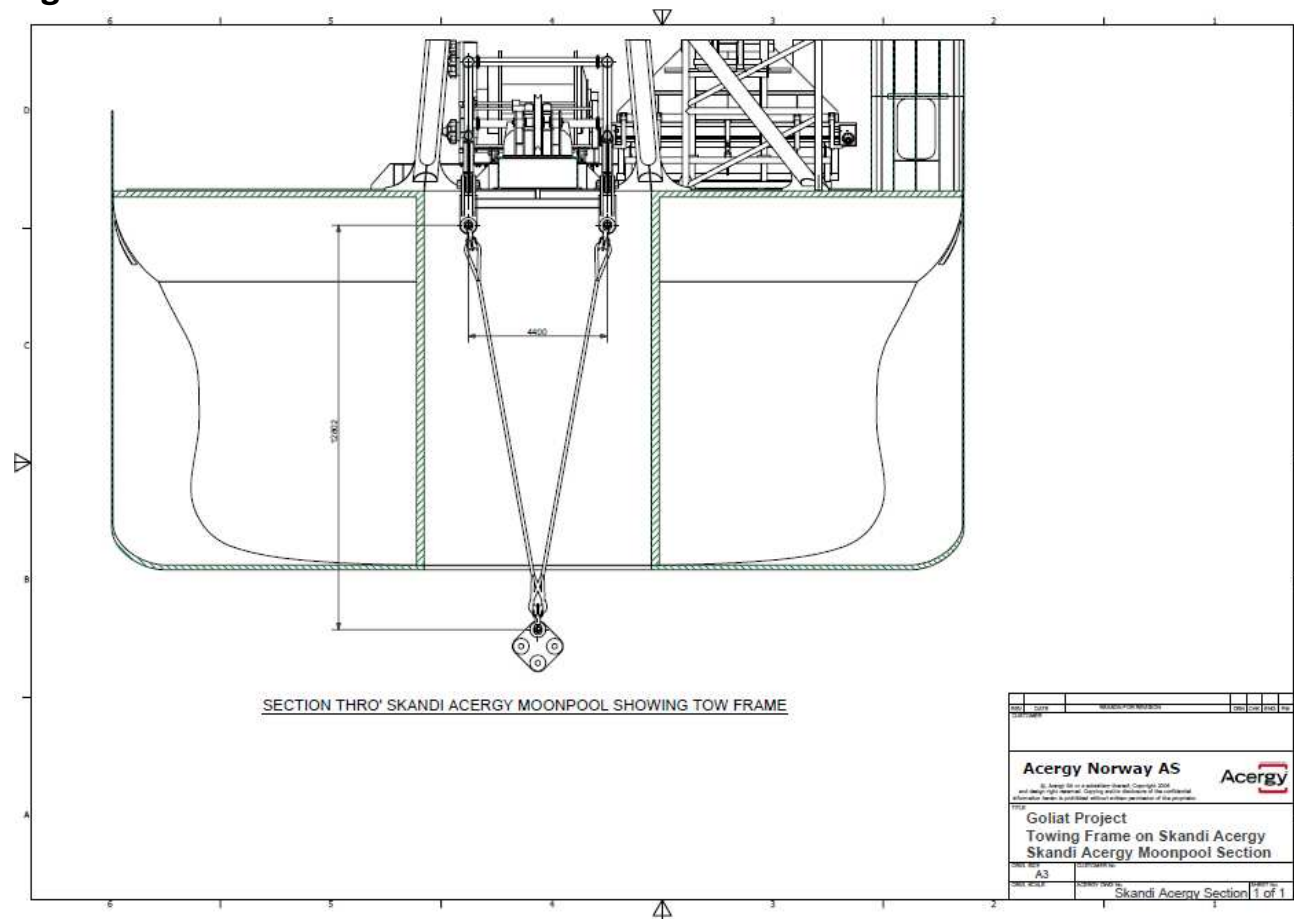


Figure 111 Conceptual hangoff structure



NTNU
Norwegian University of Science and
Technology
Department of Marine Technology

SIMVIS images

